Polyelectrolyte Complex Stabilized Supercritical CO_2 Foam Systems Used for Hydraulic Fracturing Applications

By

Rudhra Anandan

Submitted to the graduate degree program in Chemical and Petroleum Engineering and the Graduate Faculty of the University of Kansas in partial fulfillment of the requirements for the degree of Master of Science in Petroleum Engineering.

Chairperson: Dr. Reza Barati

Dr. Stephen Johnson

Dr. Shapour Vossoughi

Date Defended:

The thesis committee for Rudhra Anandan certifies that this is the approved version of the following thesis:

Polyelectrolyte Complex Stabilized Supercritical CO_2 Foam Systems Used for Hydraulic Fracturing Applications

_____

Chairperson: Dr. Reza Barati

Date Approved:

Abstract

The objective of this research is to develop polyelectrolyte complex nanoparticles capable of stabilizing surfactant-generated supercritical CO_2 foam systems prepared for hydraulic fracturing applications.

The polyelectrolyte pH, polycation/polyanion ratios and surfactant/PECNP ratios were optimized in order to generate stable polyelectrolyte complex nanoparticles by maximizing the absolute zeta potential of the resulting nanoparticle.

Next, high pressure, high temperature rheometer tests were conducted to study the bulk rheology of foam systems of varying surfactant/PECNP ratios for different foam qualities. The effect of shear, foam quality and presence of PECNP on the rheology of the foam was understood. Surfactant-PECNP generated $scCO_2$ foam showed better rheological properties than surfactant generated $scCO_2$ foam. The viscosity of the foam system increased with increase in foam quality. The same $scCO_2$ foam systems used in rheology experiments were tested for durability and stability in a view cell experiment both in the presence and the absence of crude oil. The foam lamellae were stabilized due to reduced dynamic movement of surfactant micelles caused by electrostatic interactions with PECNPs, this imparted high durability and stability to $scCO_2$ foam. The PECNP-surfactant generated foam proved to be more stable and durable compared to surfactant generated $scCO_2$ foam and foam stability increased with increase in foam quality. Supercritical CO_2 foam systems showed less durability in view cell test with crude oil, due to quick drainage of foam in presence of crude oil, which is favorable for improving the post fracture cleanup efficiency.

Based on the rheology and view cell test, the most optimized surfactant-PECNP ratio was found. Further, this ratio of surfactant-PECNP was used to generate $scCO_2$ foam for dynamic fluid loss and clean up experiments.

Dynamic fluid loss experiments were performed in the high pressure, high temperature foam setup. Supercritical CO_2 foam generated by surfactant had low fluid loss, thus low fluid loss coefficient. The fluid loss was even further reduced in case of $scCO_2$ foam generated by optimal surfactant/PECNP ratio.

Sand pack tests using crude oil from the Mississippian limestone play were performed to understand the post-fracture cleanup of CO_2 foam. Surfactant-generated $scCO_2$ foam showed promising cleanup efficiency. However, further increase in cleanup efficiency was observed by using the most optimal surfactant-PECNP generated $scCO_2$ foam.

Through this research, an optimal surfactant-PENCP generated $scCO_2$ foam system was developed for fluid loss control, rheological measurements, and to improve post fracture cleanup in hydraulic fracturing.

Acknowledgments

I would like to express my gratitude to my advisor Dr. Reza Barati for his insight, motivation and guidance throughout this research. He has spent patient hours in his office and lab, untangling my contorted questions. Dr. Barati has also been a constant source of support throughout the ups and downs of this project. I am deeply indebted to him.

I greatly appreciate the time and support extended by my thesis committee members Dr. Stephen Johnson and Dr. Shapour Vossoughi.

I would like to thank Mr. Zach Kessler and Mr. Scott Ramskill for their help and support in installing the experimental setup. I would like to extend my appreciation to the National Science Foundation EPSCoR Research Infrastructure Improvement Program: Track -2 Focused EPSCoR Collaboration award (OIA- 1632892) for partially funding this project and Harcos Chemicals Inc for supporting this project with a supply of their state-of-the-art surfactants. I would like to thank the Department of Chemical and Petroleum Engineering and the Tertiary Oil Recovery Program (TORP) at the University of Kansas for providing help and support.

Prasanth Vivekanandan and Anirudh Narasimman put up with my harassment without complaint and my arguments with them have been a source of entertainment. My deep appreciation is extended to all my friends who helped me maneuver my student life and made KU a great place to be in.

I dedicate this thesis to my mother, father and sister who instilled a love for engineering in me. Words are not enough to thank them so I will not try.

Table of Contents

List of Figures

List of Tables

Chapter 1. Introduction

Hydraulic fracturing has been used for reservoir stimulation to enhance hydrocarbon recovery from unconventional reservoirs like coal beds, tight sands and shale formations. Technological advances such as horizontal drilling made hydraulic fracturing a widespread technique to extract hydrocarbon especially natural gas from unconventional formations. Hydraulic fracturing is a water intensive process. The need for alternative fracturing fluid has increased due to limited availability and cost of using fresh water as well as increasingly stringent government regulations on use and disposal of fresh water. Based on the prediction of Environmental Protection Agency on 2011, 70 to 140 billion gallons of water are needed annually for hydraulic fracturing in the US (EPA, 2011).

Fracturing fluid is an essential component of hydraulic fracturing, it must have high enough viscosity to suspend and transport proppant into the fracture, low fluid loss and good clean up efficiency to increase productivity. Productivity of the well is affected due to damage to fracture conductivity caused by more viscous fluids such as cross linked gel (Barati and Liang, 2014; Barati et al., 2009). To minimize damage, less viscous fluids such as slickwater are used commonly in shale gas hydraulic fracturing, but, 30 to 90% of injected water can remain in the formation, which causes capillary pressure shifts and formation damage, resulting in less water recovery and negative impact on production (Penny et al., 2006; Barati et al., 2009; Economides and Nolte, 2000; Makhanov et al, 2012; Sharma and Agrawal, 2013). In this research, $scCO_2$ foam is used as fracturing fluid to address the above issues.

The objective of this research is to improve the performance of $scCO_2$ foam systems prepared using viscoelastic surfactants by applying polyelectrolyte complex nanoparticles (PECNP) for hydraulic fracturing applications.

In this work, optimized pH of polyethylenimine and optimized mass ratio of polyethylenimine to dextran sulfate were determined based on minimizing particle size and maximizing absolute zeta potential. Next, the effects of varying foam quality and addition of PECNPs to viscoelastic surfactant on rheological properties were studied. Following the rheological measurements, the stability and durability of $scCO_2$ foam were studied in the view cell test. Dynamic fluid loss tests were performed next to study the effect of addition of PECNP to viscoelastic surfactants on fluid loss control of $scCO_2$ foam. Lastly, post fracture clean-up of $scCO_2$ foam was studied and compared with brine by performing sand pack tests.

Chapter 2 contains the literature review of foam fracturing fluids, fluid loss control and post fracture clean up. The role of surfactants and polyelectrolytes complex nanoparticle in improving the performance of $scCO_2$ foam was also reviewed in this section.

Summary of the materials and procedures used to perform experiments reported in this research are in chapter 3.

The results of tests performed in this research are presented and discussed in chapter 4. Optimized pH of polyethylenimine and optimized mass ratio of polyethylenimine to dextran sulfate are reported and summarized in this chapter. The results of the rheology and view cell tests are summarized and were used to find the optimized ratio of surfactant- PECNP system that was used in dynamic fluid loss and sand pack tests. Results of dynamic fluid loss tests and clean up study performed using sand pack tests are summarized.

Chapter 5 provides conclusion based on the results discussed in previous chapter.

Chapter 2. Literature Review

2.1 Hydraulic Fracturing

Hydraulic fracturing is a stimulation technique to increase rock permeability through creation of fractures to increase in-place hydrocarbon flow (Kohshour et al., 2016). It is the most commonly used technique for stimulating oil and gas wells in unconventional reservoirs like tight sands, coal beds and shale formation. Due to increase in rock permeability after the fracturing process, it contributes significantly to accessing the previously unrecoverable reserves and to increase production in already existing reservoirs.

2.1.1 History

The first hydraulic fracturing job was conducted based on the study of relationship between well performance and treatment pressure conducted by Floyd Farris of Stanolind oil and gas. It was conducted at the Hugoton gas field in Grant county of Kansas in 1947 (Charlez, 1997). Commercial treatments were first performed by Haliburton oil well cementing company in 1949 in Archer county, Texas and Stephens County, Oklahoma (Montgomery and Smith, 2010).

Extensive research by geologists on unconventional reservoirs made them aware that there were huge volumes of gas saturated sandstones with permeability generally less than 0.1 md (Law and Spencer, 1993). This potential for hydrocarbon extraction from low permeability reservoirs led to massive hydraulic fracturing (high volume hydraulic fracturing) in hard rock formations in the US like Green River Basin, Piceance Basin (Chancellor, 1977), San Juan Basin and the Denver Basin (Fast & Holman G, 1977). Due to its success, hydraulic fracturing spread quickly to western Canada, Netherlands and North Sea (Detlef, 1989).

As the sedimentary beds were nearly horizontal (Kalyani, 2013), in order to increase the contact area with the target formation horizontal drilling was performed. During the 1980s, many oil wells

were drilled horizontally by the operators in Austin chalk and it proved more effective than the vertical wells in producing hydrocarbon from this tight chalk formation (Bell, 1993).

The conjunction of techniques such as directional drilling, high volume fracturing and micro-seismic monitoring with the development of multi-well pads and multi stage fractures made production of hydrocarbon from shales and other unconventional reservoirs technically and economically feasible.

2.1.2 Rock Mechanics

Natural examples of fractures are veins and dikes. Due to the repeated natural fracturing due to relatively high pore fluid pressures results in the formation of mineral vein systems evident in crack seal (Laubach, Reed, Olson, Lander, & Bonnell, 2004) and Dikes are minor intrusions in the upper part of the crust and it propagates in the form of fluid filled cracks (Gill, 2010).

Due to the weight of the overlying rock strata and the cementation of the formation at great depth, the fractures in rocks are suppressed. So fracturing occurs when sufficient hydraulic pressure is provided by the fracturing fluids to overcome the tensile strength of the rock for the successful propagation of fracture into the formation (Economides and Nolte, 2000). In conventional terms, fractures are known to be oriented in a plane perpendicular to the minimum principal stress (Manthei, Eisenblätter, & Kamlot, 2003). In shale rocks, main fractures generate a network of micro fractures that are either opened or propagated by this main fracture. Application of lower viscosity fluids such as slickwater helps with generation of this network of micro-fractures.

Shales have very fine particles and grains. Conventional sandstones have permeability in the range of 0.5-20 md and gas shales have permeability in the range on 1-100 nd.

2.2 Hydraulic Fracturing Designs and Chemicals

Below are the various steps involved in implementing hydraulic fracturing in an unconventional well:

1) Commercial fracture design software is used to specify fracturing volume, rate, fracture length, height and complexity to design fractures that will stay in pay zone and achieve maximum production of hydrocarbon. The first few fractures are analyzed using micro seismic and fluid tracers to tune the results of the fracture model (Woodroof & Asadi, 2003) (King, 2012) (Fix & Frantz Jr, 1991).

2) Transport and storage of chemicals, fracturing water and equipment to the well construction site.

3) Preparation of fracturing fluid, followed by pumping it to the blender to mix with the proppants. This fracturing fluid with or without proppant, depending on the schedule designed for the fracturing stage, is injected into the formation through high pressure pumps.

4) Pumping of each fracture stage might last from 20 mins to 4 hours (King, 2012). High permeability flow paths are established in the formation due to networks of fractures. The fracturing process is also limited by loss of fluid into the formation as more rocks are contacted by the fracturing fluid.

5) For the first two-three weeks after the fracturing, flow back of the fracturing fluids will occur. Modelling of flow back behavior will help understand and optimize the well production operation (Gdanski, 2010).

6) The final stage is the production operation. This is generally automated with temperature and pressure sensors on the wellhead and downhole.

2.3 Fracturing Fluids

Fracturing fluids are essential component of fracturing process. Its main purpose is to create networks of fractures from the wellbore extending into the formation and to suspend and transport proppants to the fractures in the formation to sustain the conductivity of the fracture for production of hydrocarbon (Harris, 1988).

Selection of proper fracturing fluid has a direct impact on the production of hydrocarbon. It must have sufficient viscosity to carry proppant, create sufficient fracture width, limit fluid loss, should not damage the fracture conductivity during the flow back, should result in good clean up, and should be environmentally friendly and cost effective (Montgomery C. , 2013).

2.3.1 Water-Based Fracturing Fluids

Slickwater, linear fluids, cross linked fluids and viscoelastic surfactant fluids are popular water based fracturing fluids. Basic slickwater formulation (Fontaine, 2008) used for hydraulic fracturing may include:

- Water: Fresh water (TDS< 500 ppm) or treated produced water forms the base of the fracturing fluid. It is about 98-99% of the total volume of the fracturing fluid.
- Proppant: Used to keep the fracture open when hydraulic pressure is removed. Usually sand or ceramic particles are used as proppants. It's about 1-1.9% of the total volume of the fracturing fluid.
- Friction reducer: It is used to reduce the friction pressure of fluid flowing through the pipe at high pumping pressure, which in turn reduces the power output of the pump and fuel cost. Non-acid form of polyacrylamide is used as the friction reducer. It's about 0.025% of total volume.

- Disinfectant: Common biocides like glutaraldehyde are used to control the growth of microbes that would destroy the gelled fracture fluids or might generate sour gas like H_2S. It's about 0.005 % to 0.05 % of total volume (Enzien, 2011).
- Surfactants: Used to reduce surface tension and to prevent emulsion formation in the fracturing fluid
- Gelation Chemicals: Gaur gum and cellulose polymers are sometimes used to improve viscosity of the fluid to carry proppants (Hoeman, 2011).
- Scale inhibitors: They are phosphate esters or phosphonates used to prevent scale precipitates, ion concentration problems in scale and reduce blockage of tubing and equipment (Houston, 2009) (Blauch, 2009).
- Corrosion inhibitor: They are used to reduce corrosion which damages the pipes. Generally used if acids are used for fracturing process and it comprises of 0.2 to 0.5 % of the total acid volume. (King, 2012).

2.3.2 Oil-Based Fracturing Fluids

This type of fracturing fluid is compatible with almost any type of formation but the cost is higher compared to other fluids and this should be handled with greater concern towards personal safety as they are flammable. The most commonly used oil-based fracturing fluid is liquefied petroleum gas (LPG) (Taylor R & Lestz, 2006).

2.3.3 Acid Based Fracturing Fluids

Acids in fracturing fluid etch the channels in the formation rock which forms the walls of the fracture. Therefore, the rock must be partially soluble in acid so that the rock can be etched to form the fractures. But the formation must have a continuous carbonate or limestone phase, so that the fractures formed by etching will be continuous. Disadvantage of using this fracture fluid is that

there might be high leakoff due to rapid reaction of acid with the formation and disposal of significant calcium carbonates in the flow back fluids should be managed properly (Williams, 1979).

2.3.4 Alcohol Based Fracturing Fluids

In low permeability formations, high clay content, low bottom-hole pressure and minimal fluid recovery alcohol based fracturing fluids can be used. Methanol is generally used as the base fluid (Antoci, 2001). Compared to water-based fracturing fluids, it is 3-4 times more expensive and concerns about personal safety are the limiting factors of using alcohol based fracturing fluids.

2.3.5 Gaseous Fracturing Fluids

Liquid CO_2 and N_2 are popular gaseous fracturing fluids. Potential advantages of using them are less water usage, few chemical additives used, reduced formation damage and formation of more micro fractures. But as it has low viscosity, lack of proppant delivery is reported as their main disadvantage resulting in a decreased fracture conductivity ((Al-Adwani et al, 2008); (Wang et al, 2012); (Gupta et al, 2005)).

2.3.6 Foam Based Fracturing Fluids

Foams are the best fracturing fluid in places where water is scarce ((Neill et al, 1964) (Yost II et al, 1993) (Gupta et al, 2005)). CO_2 and N_2 based foams are widely used fracturing fluids. The main advantages of using energized foams as fracturing fluids are discussed below (Kohshour et al, 2016) (Products, 2013):

- Foam fracturing fluids minimize the amount of water used for hydraulic fracturing. In areas with water scarcity or strict local regulations on water usage, foam fracturing will be very

effective. Also it alleviates environmental concerns and treatment costs of produced water due to reduced usage of water to generate foam.

- As foams have better rheological properties than cryogenic and slickwater fracturing fluids, their proppant placement tend to be improved comparatively. They suspend and transport proppants more effectively compared to the gaseous fluids or slickwater.
- Fluid loss from fracturing fluid into the formation causes formation damage, results in capillary pressure shift and water blockage. The relative permeability to gas is significantly reduced due to water blockage (Parekh, 2004). Fluid loss is significantly reduced using foams as a fracturing fluid.
- Clean up efficiency of the energized fluids is significantly higher compared to water-based fracturing fluids, which will result in better productivity of hydrocarbons. Also fracturing fluids such as cross-linked fluids might damage fracture conductivity. This damage amount is significantly reduced with foams as fracturing fluids.

Challenges of using foam based fracturing fluids:

- Rheological characterization of foams is complex in a porous media and it is complicated to predict the flow behavior of foam fracturing fluids in porous media (Gandossi, 2013).
- Foam fracturing fluids might be corrosive or non-corrosive depending on the foam's gaseous and liquid phase, temperature, materials employed and presence of water. For example, at a temperature of 40^{o}C and pressure of 1160 psi, increase in water salinity from 1000 ppm to 10,000 ppm results in 87% increase in corrosion rate of X65 pipeline steel (Ansarizadeh et al, 2015). Therefore, when designing hydraulic fracturing process, engineers must design the characteristics of foam in such a way that corrosion is minimum.

- Cost of using foam fracturing fluids depends on transportation and storage of gas to the oilfield. For example, CO_2 must be compressed and transported to the field using pipeline or tankers. Transportation through already existing pipeline networks will reduce the cost significantly, otherwise the operation cost might increase (Benson at al, 2010).
- As the viscosity of foam increases with foam quality, higher surface pumping pressure is required for high quality foam (Gandossi, 2013).

2.4 CO_2 Foam as Fracturing Fluid

Choice of fracturing fluid has a direct impact on productivity of the well (Amstrong et al., 1996). CO_2 foam has been used and tested to give acceptable results as far back as the 1980s in South Texas (Friehauf at al., 2009). Recent studies indicate that fracturing using CO_2 foam can achieve economically significant hydrocarbon recovery and improve well performance by 1.6 to 2.1 times compared to non-foam based fracturing fluids like gelled or water-based fluids. (Burke and Nevison, 2011; Yost, 1994; Friehauf et al., 2009; Friehauf and Sharma, 2009; Linde, 2013).

2.4.1 Foams

Foam is a colloidal dispersion with liquid as the continuous phase and gas as the discontinuous phase (Schramm L. L., 1994). Foam lamellae separates the gas phase from the liquid phase and should be stable for a stable and durable foam. Foaming agents such as surfactants and finely divided solids are used to reduce the surface tension and protect the interface to prevent coalescence (Schramm L. L., 2000).

2.4.2 Foam Stability

Foams are not thermodynamically stable and their degree of kinetic stability is an important aspect of foam stability (Schramm L. L., 1994). Film thinning and film rupturing result in the instability of foams. In the process of film thinning, the total surface area is not reduced, but it results in

thinning of liquid film between the two gas bubbles. In film rupturing, the liquid film is ruptured, resulting in coalescence of two bubbles (Schramm L. L., 1994). Interfacial and bulk properties such as dispersion force, electrostatic force, repulsive force, stability of electrical double layer, and rheological properties affect the stability of the foam (Schramm L. L., 1994).

2.4.3 Mechanism of Foam Generation

The three main mechanism involved in foam generation are discussed below:

Snap off Mechanism

When the entry pressure of the gas is higher than the capillary pressure, gas enter the pore body through the pore throat, resulting in the formation of lamellae (Rossen W. R., 1996). Therefore, the lamellae is formed due to snap off when the local capillary pressure is lower than the entry pressure of the pore throat.

Division Mechanism

When a mobile lamella enters a pore throat it divides as it enters the branching point, provided the pore throat doesn't contain any liquid phase or another lamellae (Schramm L. L., 1994) . Thus breaking of mobile foam creates lamellae (Rossen W. R., 1996).

Leave Behind Mechanism

When the gas enters porous media already saturated with aqueous phase, the gas saturation increases and foam is generated at the pore throat during drainage (Rossen W. R., 1996).

2.5 Supercritical CO_2 Foam

In this research supercritical CO_2 ($scCO_2$) and aqueous phase are used to generate foam. When CO_2 is subjected to a pressure and temperature above critical point (end point of phase equilibrium curve) both liquid and vapor coexist (Sven, 2000). This is known as supercritical CO_2. The critical point for CO_2 is 31.1^oC and 1071 psia, and the critical density is 0.469 g/cm^3 (Reid et al, 1987). In

this research, all the tests performed using foam are at 1300 psi and 40°C, so the CO_2 used in this research is $scCO_2$. Aqueous phase used in this research are solutions of surfactant or surfactant-polyelectrolyte complex nanoparticles (PECNP) with brine. It is necessary to understand the surface chemistry, to understand the reason to add PECNP to the aqueous phase to stabilize the foam.

Repulsive electrostatic forces stabilize the foam by preventing the thinning of the film depending on the charge density and film thickness (Schramm L. L., 1994). Electrical double layer is formed based on the charge of the ions. The inner layer of the electrical double layer is made by the adsorbed ions and the diffuse layer includes ions governed by electrical and thermal motion (Schramm L. L., 2000).

Metastable common black films are formed when the foam is stabilized by repulsive forces. This happens when electrical double layer overlap between two charged interface. The total interaction energy (V_T) is the yield of both attractive (V_A) and repulsive force (V_R) between two charged surfaces. The DLVO (Derjaguin-Landau-Verwey-Overbeek) theory can estimate this energy change between two charged surfaces (Schramm L. L., 1994).

Equation 1,

$$V_T = V_R + V_A$$

Polyelectrolytes adhere to the interface and provides thick coating to the film and, prevents two interface from interacting. Thus stabilizing the interface through steric repulsion (Hunter, 1988) (Petkova, 2012). In this research, effect of PECNP with surfactant in the aqueous phase of the foam was studied and compared with foam generated by surfactant solutions only.

2.5.1 Surfactant

Surface active agents that lowers the surface or interfacial tension between two liquid phases or liquid and solid phase are called surfactants (Rosen, 2012). Surfactants are amphiphilic, it has hydrophilic head and hydrophobic tail (Lipid, 2012).

Surfactants reduce the interfacial tension, which in turn decrease of capillary pressure and surface energy, resulting in reduced drainage. In addition, they stabilize the interface by increasing the surface charge, thus increasing the repulsive force to stabilize the interface (Eftekhari, 2015).

Classification of Surfactants

Tail or hydrophobic part of surfactant generally consist of hydrocarbon chain and it is fairly similar among different surfactants. They have either one tail or two tails (double chained). Based on the charge of polar head group, surfactants are classified as anionic (negatively charged), cationic (positively charged), nonionic (no charge) and zwitterionic (contains both positive and negative charge). The surfactant used in this research (HDP 0761-12-2AM) to generate $scCO_2$ is an amphoteric (able to react both as an acid and base) surfactant.

2.5.2 Polyelectrolytes

Polymers with electrolytes in their repeating groups are known as polyelectrolytes. Polyelectrolyte solutions are electrically conductive like salts and viscous solutions like polymer (Gennes, 1979). Due to dissociation of groups in aqueous solution, they acquire charge. The entropy increases due to dissociation process, resulting in release of counter ions into the aqueous solutions, this in turn results in electrochemical interaction of polymer chain with the oppositely charged counter ions (Koetz J. S., 2001) (Koetz J. a., 2006) (Li, 2013). This process results in counter-ion condensation onto poly-ion chain (Manning, 1979).

Based on a polyelectrolytes' ability to dissociate, it can be classified as strong (completely dissociates in solution) and weak (partially dissociates in solution). Based on charge, polyelectrolytes can be classified as polyanion (negatively charged ionic group), polycation (positively charged ionic group) and polyampholytes (carry both positively and negatively charged ionic group) (Jenkins, Kratochvíl, Stepto, & Suter, 1996).

Polyelectrolyte used in this research are Polyethylenimine (PEI), which is a branched polycation and Dextran Sulfate, which is a polyanion.

2.5.3 Polyelectrolyte-Surfactant Interaction

Electrostatic and hydrophobic forces govern the stability of the surfactant-polyelectrolyte binding. Polyelectrolyte binding with surfactant molecule results in the release of counter ions, which in turn causes coulombic attraction between oppositely charged ions (Koetz J. a., 2006) (Li, 2013) (Lapitsky & Kaler, 2007) and this interaction depends on the charge density (Lapitsky & Kaler, 2007). Surfactant hydrophobicity and the ionic strength governs the hydrophobic interaction and the surfactant-polyelectrolyte binding below critical charge density is governed by hydrophobic interaction (Israelachvili, 1991) (Hayakawa, 1982).

Effect of Polyelectrolyte-Surfactant Interactions on Foam Stability

Dispersion forces (weak intermolecular force) and electrical double layer governs the stability of microscopic and mesoscopic thin liquid films in the foam (Kristen, 2010). Electrical double layer consists of Stern layer (inner layer with adsorbed counter ion) and diffuse layer where thermal motions and electrical forces influence the distribution of ions (Schramm L. L., 2000) (Schramm L. L., 1994). Zeta potential is the electro-kinetic potential between stationary Stern layer attached to the dispersed particle and dispersion medium (Schramm L. L., 2000). Higher zeta potential value increases the stability of the system.

Presence of polyelectrolyte affects the stratification (discontinuous thinning) of foam film. Concentration above the overlap concentration (C*) of the polyelectrolyte and below the critical aggregate concentration of the surfactant and polyelectrolyte causes oscillation of the disjoining pressure in the polyelectrolyte network in the film core, this causes stratification which is irreversible process (Kristen, 2010) (Koetz J. a., 2006). Increase in pressure causes layers of the network pressed out of the film and this steps of thickness follows power law scale, the relation between thickness and concentration for different type of polyelectrolytes are given below (Kristen, 2010) (Koetz J. a., 2006),

$\Delta h \propto c^{1/2}$ – Linear polyelectrolyte

$\Delta h \propto c^{1/3}$ – Branched polyelectrolyte like PEI

2.5.4 Polyelectrolyte Complex Nanoparticles Used in $scCO_2$ Foam Generation

Electrostatic and hydrophobic forces govern the formation of polyelectrolyte complex nanoparticle (PECNP) (Li, 2013). In this research, Dextran Sulfate (anionic polyelectrolyte) and PEI (cationic polyelectrolyte) are mixed in various ratios to form PECNP. Dextran Sulphate is water soluble and reduces the toxicity of PEI (Waree T & Middaugh, 2003).

This system was first studied and applied as delivery vehicle in pharmaceutical application by Tiyaboonchai (Tiyaboonchai, 2003). She adjusted the ratio of PEI to DS to control the particle size and found that colloidal protective nature of PEI prevents the aggregation of nanoparticles. This study on PECNP was used by Barati for the entrapment and controlled release of enzymes for fracture fluid cleanup (Barati, 2010). In his study, he found that PECNP system was stable under shear, thus flow through pipe lines and well bore will not affect the system (Barati, 2010). The same system was used by Bose et al. as a fluid loss additive and breaker encapsulating agent for hydraulic fracturing applications (Bose, 2014).

The above mentioned work provided a basis for this research to use PECNP to improve the surfactant generated $scCO_2$ foam as fracturing fluid for dynamic fluid loss control and efficient fracture clean up in hydraulic fracturing application.

2.6 Fluid Loss

Filtration of fluids on the surface of fracture or formation causes the invasion of filtrate into the formation from the fracturing fluid (Howard, 1957). The liquid invasion into the reservoir causes physical damage by processes such as clay swelling and hydraulic damage by shifting the capillary pressure and relative permeability curves (Ayoub, 2006). Fluid loss depends on permeability of the formation, pressure difference between injection and reservoir and initial water saturation. Damages due to fluid loss are significant in shale with smectite and montromorillonite due to increased clay content (Barati, 2009) and in case of ultra-tight formations, there might be significant fluid loss through naturally induced micro fractures (Barati and Liang, 2014).

2.6.1 Dynamic fluid loss

Effect of shear rate on the viscosity and filter cake formation are considered in the dynamic fluid loss. There are three stages in the dynamic fluid loss (Navarette & Cawiezel, 1996) (Vitthal, 1996) (McGowen, 1996) (Roodhart, 1985)

- Initiation of filter cake formation (spurt loss)
- Buildup of filter cake
- Equilibrium developed between pressure drop across the cake and shear stress due to fluid flow along the fracture.

The fluid loss during the equilibrium is shown using a dynamic fluid loss model, by Carter (Howard and Fast, 1957) demonstrated using

Equation 8.

2.7 Post Fracture Cleanup

Fracture conductivity has a direct impact on the well productivity. Viscous fracturing fluids such as cross linked gel might cause damage to fracture conductivity due to incomplete fracture cleanup (Barati and Liang, 2014; Barati et al., 2009). However, foams destabilize and breaks in the presence of crude oil (Schramm L. L., 1994), which will increase the post-fracture cleanup efficiency.

According to Schramm (Schramm L. L., 1994) crude oil destabilizes foam, based on the steps given below:

- Imbibition of oil into the foam lamellae, destabilizes the pseudo-emulsion film which might result in thinning (Talebian, 2013).
- Marangoni flow (mass transfer along an interface between two fluids due to surface tension gradient) due to penetration of oil causes contraction and expansion of lamellae.
- The spreading of oil across the interface might cause rupture of the lamellae.

Chapter 3. Methods and Materials

All the chemicals used during the course of this research are presented in this chapter. This chapter also describes the methodologies implemented to achieve a stable supercritical CO_2 foam using polyelectrolyte complex nanoparticles. Below are the high temperature, high pressure experimental setups used in this research:

- Zeta potential and particle size measurements through Omni instrument
- Rheometer setup to study the rheological properties of the supercritical CO_2 foam
- View cell setup to study the foam durability and stability both in the presence and absence of crude oil
- IFT setup to understand interfacial tension properties of both (air-surfactant/PECNP) and (CO_2- surfactant/PECNP) systems
- Dynamic fluid loss tests to study the fluid loss of CO_2 foam
- Sand pack tests to study the post-fracture cleanup efficiency of CO_2 foam

3.1 Chemicals

The chemicals used along with their physical properties, chemical properties and product specification are summarized below.

3.1.1 Surfactant

The surfactant used was an aqueous solution of a proprietary surfactant designated HDP 0761-12-2AM. We will refer to it as "2AM" in this research. It is an amphoteric surfactant which has a density of 1.0688 g/ml at 25^{o}C. It was provided by Harcos Chemicals Inc, Kansas City, Kansas, USA. (SDS# RD00364).

The main composition of 2AM is given in the Table 1 below, and based on this the surfactant is 30-40% active.

Table 1. Chemical composition of 2AM (obtained from MSDS sheet provided by Harcos Chemicals Inc)

Chemical name	CAS number	Percentage
Water	7732-18-5	60-<70
Sodium Chloride	7647-14-5	5-<10
3-Chloro-1,2-Propanediol	96-24-2	<0.2
Other components below reportable levels		30-<40

3.1.2 Polyethylenimine

The Polyethylenimine (PEI, Sigma Aldrich, St Louis, Missouri, USA. CAS# 9002-98-6) used in this work is a branched polycation composed of the amine group and two carbon aliphatic CH_2CH_2 spacer as the repeating groups and has an average molecular weight of 25,000 $g.mol^{-1}$ as reported by Sigma Aldrich. It contains primary, secondary and tertiary amino groups in the approximate ratio of 1:2:1 (Figure 1). The PEI is a liquid with a density of 1.03 g/ml at 25°C and viscosity is between $1.3*10^4$-$1.8*10^4$ cP at 50°C.

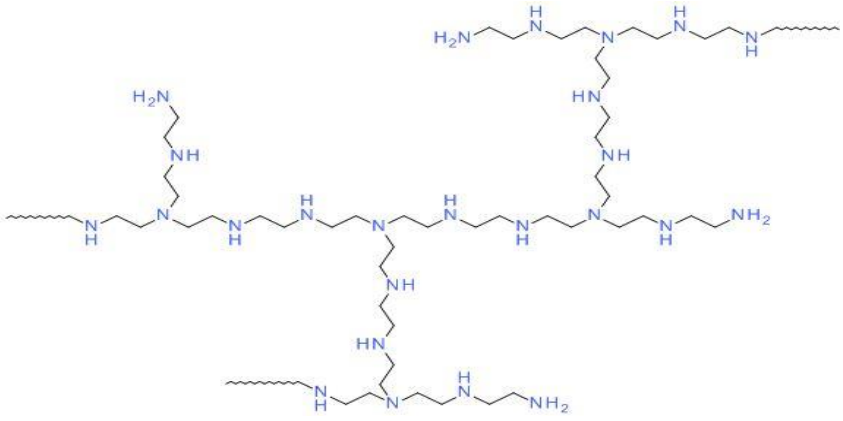

Figure 1. Chemical structure of branched PEI (Anandan, 2017) (Drawn by Stephen J. Johnson, used by permission)

3.1.3 Dextran Sulphate

Dextran Sulfate (DS) is a polyanion with an average molecular weight of 500,000 $g.mol^{-1}$. Figure 2 below shows the chemical structure of DS. It was purchased from Sigma Aldrich, St Louis, Missouri, USA. (CAS# 9011-18-1).

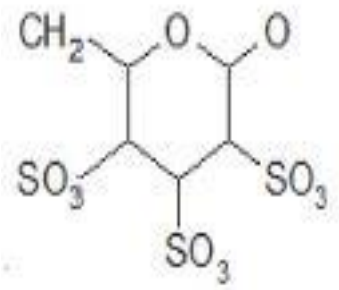

Figure 2. Chemical Structure of Dextran Sulphate Monomer (Barati, 2010) (Drawn by Stephen J. Johnson, used by permission)

3.1.4 Brine

2 wt% sodium chloride (NaCl) solution was prepared using deionized water. Sodium chloride was purchased from Fisher Chemical, New Jersey, USA (CAS# 7647-14-5, ACS certified).

3.1.5 Crude Oil

Mississippian limestone play (MLP) crude oil was used for both view cell and sand pack tests to study the fracture cleanup process. The density and viscosity of the crude oil at 40°C were 0.82 g/ml and 3.88 cP, respectively. The crude oil used was not filtered.

3.1.6 Hydrochloric acid

12N Hydrochloric acid was used to adjust the pH of PEI solution to prepare the polyelectrolyte complex nanoparticle. It was purchased from Fisher Chemical, New Jersey, USA (CAS # 7647-01-0, ACS certified).

3.1.7 Cores

Kentucky tight sandstone outcrop cores were used for the dynamic fluid loss experiment. These core plugs have the diameter and length of 0.88 in and 0.99 in, respectively. The porosity and permeability of the core were 12.91 % and 0.11 mD, respectively. Figure 3 shows the image of the dry Kentucky core used for the dynamic fluid loss experiment.

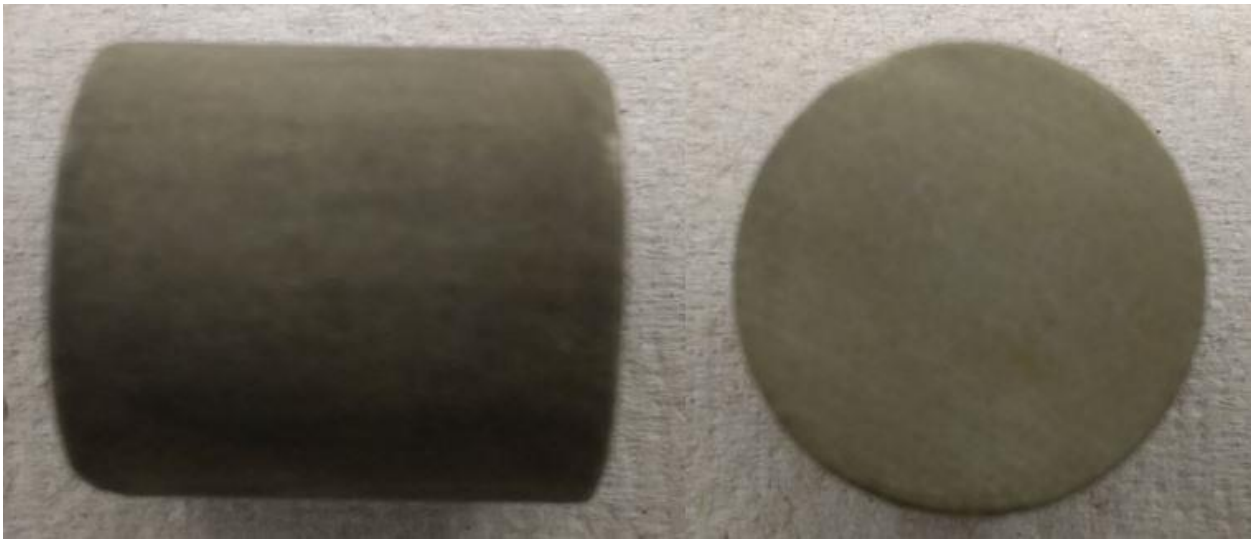

Figure 3. Image of dry Kentucky core

3.1.8 Proppants

Ceramic proppant of 20/40 mesh size was used for the sand pack test. The proppant was provided by CARBO Ceramics. Figure 4 shows the image of the proppant used.

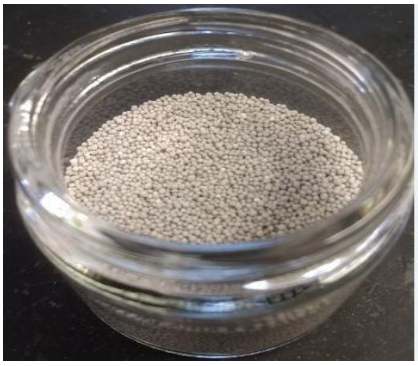

Figure 4. Proppant used for the sand pack test

3.2 Sample Preparation

3.2.1 Polyethylenimine Solution

A 1 wt% PEI solution was prepared using 2 wt% NaCl brine, stirred at 600 rpm for 60 minutes. The average initial pH of PEI solution was 11.2 which is basic in nature. PEI solution of pH 8, 8.5, 9, 9.5 were prepared by addition of 12N HCl solution. As pH of 8.5 gave the most optimized particles (presented in the Results and Discussion section), all the other tests were performed using PEI solution of pH 8.5. Titration curve of 322 g of 1 wt% PEI in 2 wt% NaCl with initial pH of 11.2 at 25°C using 12N HCl is shown in Figure 5 below,

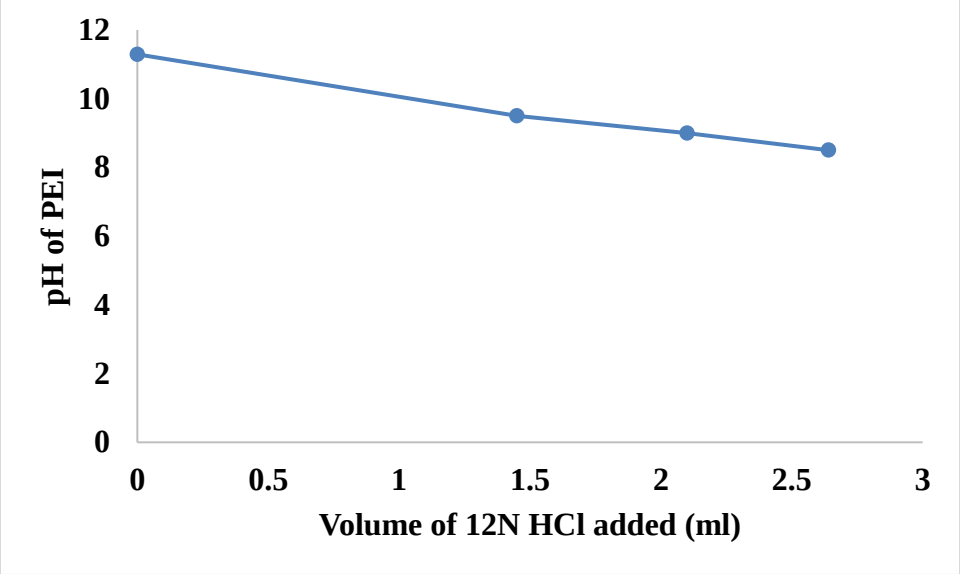

Figure 5. Titration curve of 322g of 1wt% PEI in 2wt% NaCl

3.2.2 Dextran Sulphate Solution

The DS solution was prepared in 2 wt% NaCl brine. The solution was stirred at 600 rpm for 60 minutes and the final concentration of the DS in the solution was 1 wt%. The pH of 1 wt% DS solution prepared using 2 wt% NaCl was measured to be 7.

3.2.3 Surfactant Solution

The surfactant (2AM) solution was prepared in 2 wt% NaCl brine. The solution was stirred at 600 rpm for 20 minutes and the final concentration of the 2AM in the solution was 1 wt%.

3.2.4 Polyelectrolyte Complex Nanoparticles (PECNP)

Initially four different mass ratios of 1:1:0.1, 2:1:0.1, 3:1:0.1 and 4:1:0.1 for solutions of PEI: DS: 2 wt% NaCl and four different pH values of 8, 8.5, 9 and 9.5 for 1wt% PEI were prepared. Based on the particle size and zeta potential tests (presented in the Results and Discussion section), 3:1:0.1 ratio of PEI: DS: 2wt% NaCl with pH of 8.5 for 1wt% PEI showed the most optimum properties. Therefore, for all the other tests PECNP was prepared in the ratio of 3:1:0.1 of PEI (1wt%, pH 8.5): DS (1wt %): 2% NaCl and was stirred at 600 rpm for 20 minutes.

3.2.5 Surfactant-PEI System

The surfactant-PEI solution was prepared using PEI (1 wt% PEI in 2wt% NaCl) of pH 8, 8.5 and 9 and in a ratio of 9:1. Surfactant solution of 1.11 wt% was prepared and mixed with PEI solution at 600 rpm for 20 minutes to prepare solutions of 2AM: PEI ratio of 9:1. The final concentration of surfactant in the 2AM: PEI solution was 1 wt%.

3.2.6 Surfactant-PECNP Solution

The surfactant solution was prepared in brine and was mixed with PECNP solution in 7 different ratios from 3:7 to 9:1 of 2AM: PECNP. Based on the particle size and zeta potential measurements (see Results and Discussion), 6:4, 7:3, 8:2, and 9:1 were determined to be the most optimized ratios for 2AM: PECNP. Surfactant solution of 1.67 wt%, 1.43 wt%, 1.25 wt% and 1.11 wt% were prepared and mixed with PECNP solution at 600 rpm for 20 minutes to prepare solutions of 2AM: PECNP ratio of 6:4, 7:3, 8:2, and 9:1 respectively. The final concentration of surfactant in the 2AM: PECNP solutions was kept constant at 1 wt%.

3.2.7 Foam Quality

Foam quality refers to volumetric gas content, i.e. gas volume by foam volume at a given temperature and pressure. The supercritical CO_2 foam quality of 70%, 80%, 90% and 95% were used to perform the rheology tests, view cell tests, dynamic fluid loss tests and sand pack tests. For all the four foam qualities the total foam flow rate was always maintained at 6 ml/min. For example, to generate 90% foam quality, the CO_2 pump was operated at a flow rate of 5.4 ml/min and the aqueous solution pump was operated at a flow rate to 0.6 ml/min, which resulted in a total flow rate of 6ml/min.

3.3 Experimental Procedure

3.3.1 Vial Tests

Vial tests were used as screening tests before zeta potential and particle size measurements were conducted. Surfactant-PEI and Surfactant-PECNP solutions were prepared and transferred to vials. The vials were hand shaken and left inside an oven maintained at 40°C. The decay of foam was analyzed by plotting foam height vs time. Figure 6 shows the vials with 2AM: PEI and 2AM: PECNP solutions.

Figure 6. Vials containing different solutions. Starting from left, 2AM-PEI and PEI: DS: 2% NaCl ratios of 1:1:0.1, 2:1:0.1, 3:1:0.1 and 4:1:0.1

3.3.2 Zeta Potential and DLS Particle Size Measurements

In order to select the optimized ratio of PEI: DS: 2 wt% NaCl, 2AM: PECNP as well as the most favorable pH of the final fluid system, zeta potential and mean particle size were measured for different samples using a Brookhaven Omni instrument (Brookhaven Instruments Corporation, New York, USA). Figure 7 below shows the Brookhaven ZetaPALS instrument.

Figure 7. Brookhaven Omni instrument

The electro kinetic motion of the particles away from the charged inner surface within the electrical double layer is measured by the zeta potential or electro kinetic potential. The significance of zeta potential is that its value can be related to the stability of colloidal dispersions; an increase in absolute zeta potential increases electrostatic repulsion and this confer stability and when the

potential is low, attraction exceeds repulsion and the dispersion will break and flocculate. The interaction energy between the charged particles is determined by the potential distribution, which in turn is responsible for the stability of particles towards coagulation and affects many aspects of the flow behavior of the colloidal suspension. (Hunter, 1988; Moayedi et al., 2011).

This instrument measures the particle size using dynamic light scattering at an angle of 90 degrees. Zeta potential of the sample was determined using mean particle size and electrophoretic mobility of each sample. The samples were diluted 10 times using 1mM KCl and three readings were taken to find the average zeta potential.

Based on the results of zeta potential test (shown in Results and Discussion section), PECNP formulation of 3:1:0.1 of PEI: DS: 2% NaCl with PEI ratio of 8.5 was found to be the most optimized ratio. This PECNP formulation was used in all surfactant-PECNP solutions that was used as aqueous phase to generate scCO_2 foam in all the rheometer, view cell, IFT, dynamic fluid loss and sand pack tests.

3.3.3 Experimental operating conditions

All the upcoming tests were performed at 1300 psi and 40°C. At this pressure and temperature CO_2 will be in supercritical state. In rheology, view cell, dynamic fluid loss and sand pack tests the total foam flow rate was always maintained at 6 ml/min for all the four foam qualities.

3.3.4 Rheology Test

Rheological properties of foam are essential components to suspend and transport proppant to the fracture. As CO_2 foams are pseudo plastic fluids their viscosity decreases with increase in shear rate. The viscosity of the surfactant generated CO_2 foam and surfactant-PECNP CO_2 foam were measured using an Anton Paar rheometer. Figure 8 shows the schematic flow diagram of the

rheometer setup. Three types of tests were performed to understand the rheological properties of the CO_2 foams. They were,

- Dynamic tests (foam generated and sheared continuously)
- Static tests (foam generation stopped, measuring cell was isolated and foam was sheared)
- Ramp tests (shear sweep was performed on the foam)

CO_2 foam generated using 1% 2AM, 9:1, 8:2, 7:3, 6:4 2AM: PECNP as aqueous phase at foam qualities of 70%, 80%, 90%, and 95% were all tested in rheology experiments. Results of foam performance with and without PECNP was compared to choose the most optimized system for dynamic fluid loss and clean up experiments.

Procedure

Figure 9 shows the image of the Anton Paar rheometer setup. Three ISCO pumps were required for this test. ISCO pump A was used for supercritical CO_2 injection, pump B for the aqueous phase and pump C to withdraw the CO_2 foam after coming out of the measuring cup to maintain the pressure constant in the setup. Pump A was refilled with CO_2 at 6°C and around 800 psi, and the temperature was increased to 40°C to increase the pressure of CO_2. All the pumps and lines were always maintained at 40°C using heaters. The system was pressurized to 1300 psi. Supercritical CO_2 and aqueous phase (surfactant or PECNP-surfactant) were pumped from two pumps A and B, respectively, through a 7-µm inline mixer to generate foam. Flow rates of ISCO pump A and B were set based on the desired foam quality at which the experiments were to be performed. CO_2 foam generated after the inline mixer was injected into the bottom of the annulus between two co-axial cylinders in the measuring cup, which was also maintained at 40 °C. The geometry is double gap and the cylinder that rotates was in the annulus between two stationary cylinders with the torque values of up to 300 mN.m, using a magnetic coupling (shown in Figure 10) providing drive

to rotate the cylinder. After exiting the top of the measuring cup, the foam passed through a glass view cell to check the quality of the foam at the beginning of the test. Next, foam reached the receiving ISCO pump, which was refilled at the same rate at which the foam was being injected, thereby maintaining the pressure in the system. The system was de-pressurized by slowly opening ISCO pump C exit valve after the test.

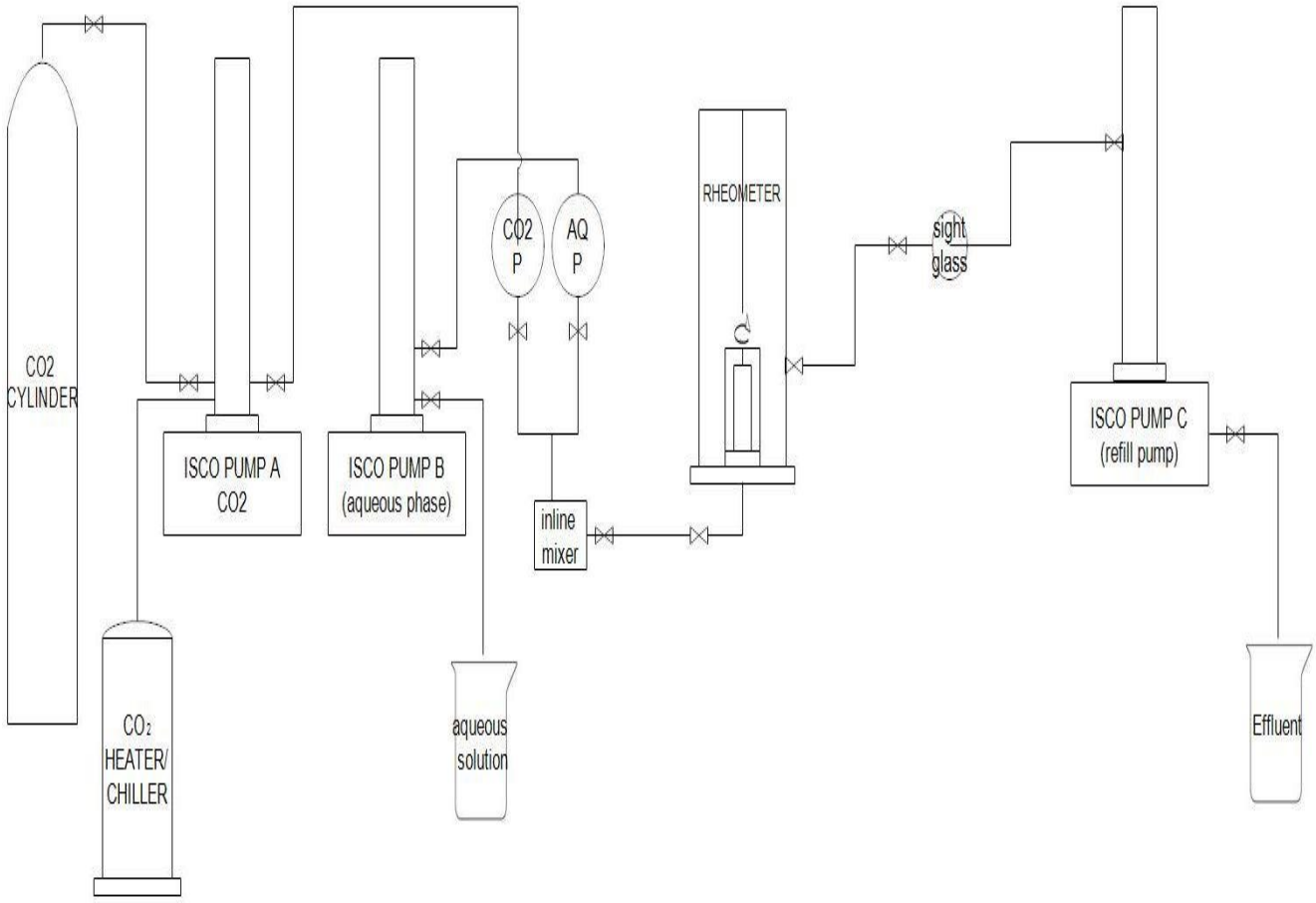

Figure 8. Schematic diagram of the Rheometer Setup (Anandan, 2017)

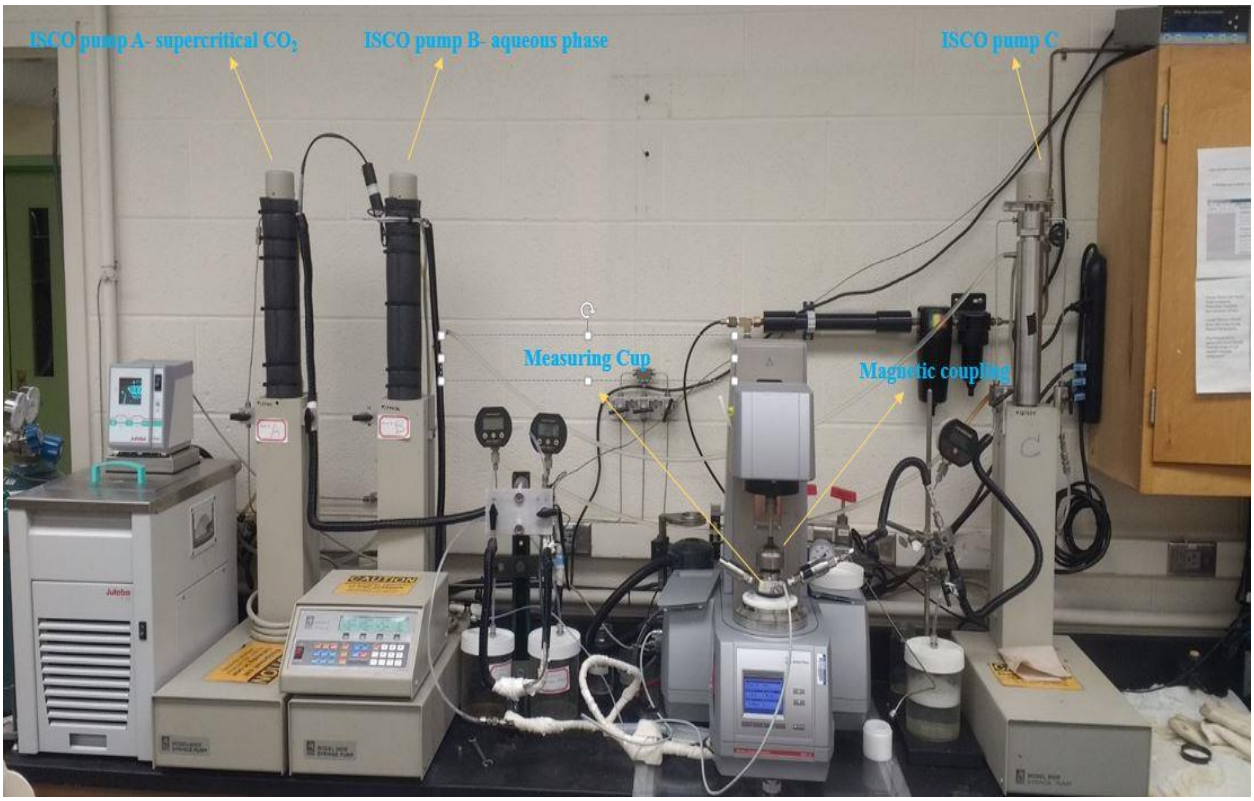

Figure 9. Anton Paar rheometer used for rheological measurements

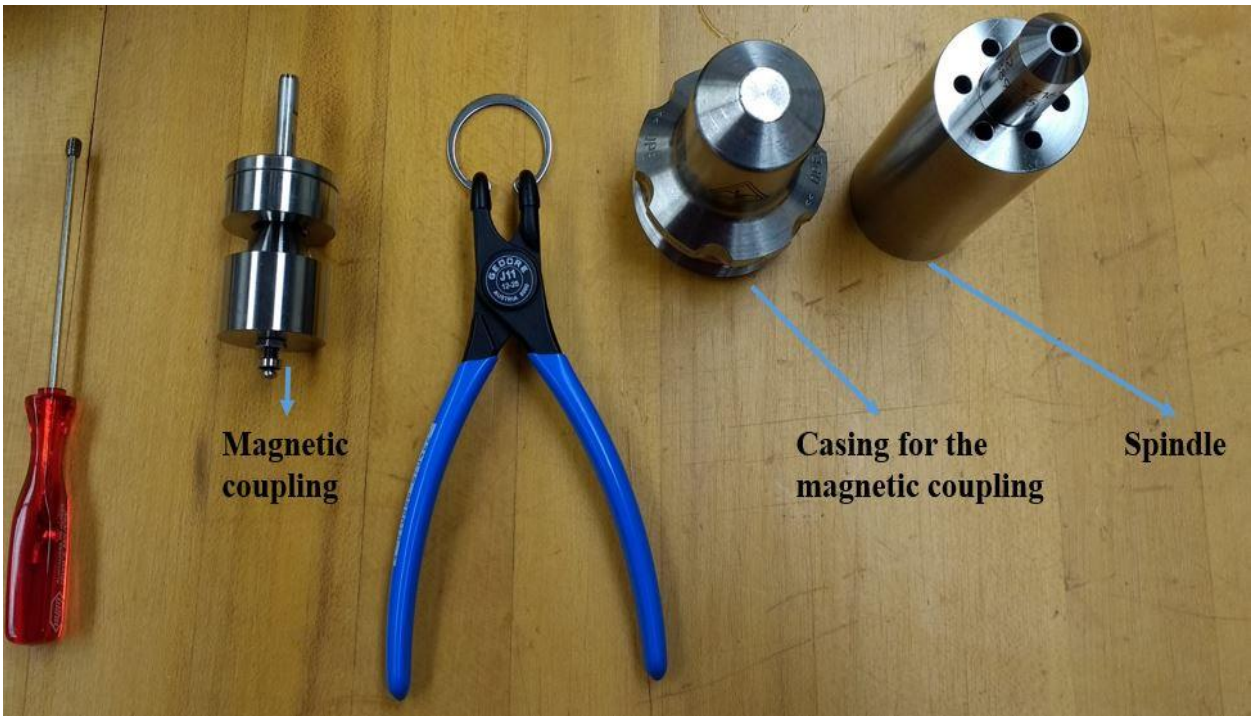

Figure 10. Various parts of the magnetic coupling and spindle setup

Dynamic test

In this test, the foam was generated continuously at the desired foam quality and sheared at 2000 s^{-1} for 45 minutes, with the viscosity being recorded at 30 s intervals (i.e. 90 measurements). The viscosity was measured against time. Figure 11 shows the screenshot of the rheoplus software used to run both dynamic and static tests.

Static Test

After the dynamic test, foam generation (i.e. all the three pumps) was stopped and valves on both sides of the rheometer were closed to isolate the measuring cup at constant pressure to perform static test. The foam in the measuring cup was sheared again at 2000 s^{-1} for 45 minutes with 90 measuring points and viscosity vs time was measured.

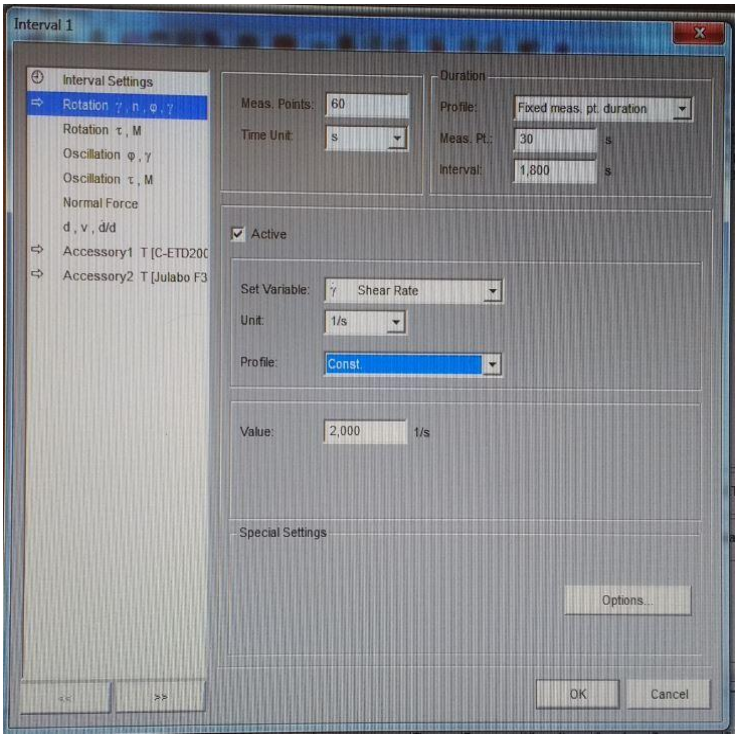

Figure 11. Screen shot of rheoplus software to run dynamic and static test

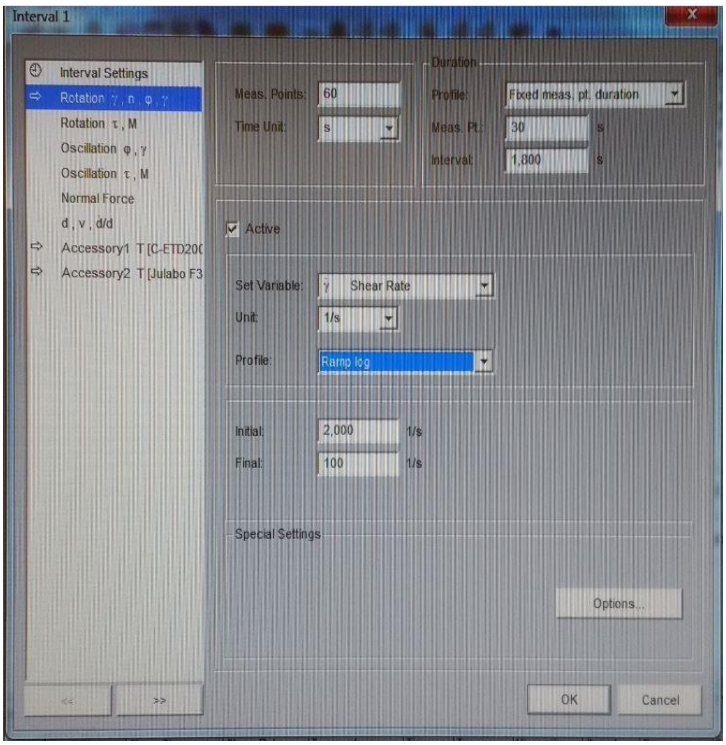

Figure 12. Screen shot of rheoplus software to run ramp test

Ramp Test

Ramp test was performed to understand the behavior of foam at different shear rate. Static foam was sheared from 2000 s^{-1} to 100 s^{-1} (ramp down) and then sheared from 100 s^{-1} to 2000 s^{-1} (ramp up) for a total time of 30 minutes with 60 measuring points for each test. Figure 12 shows the screenshot of the rheoplus software used to run ramp test. Oswald de Waele power law equation shown in Equation 2 was used find the flow consistency and flow behavior indices.

Equation 2,

$$\mu_{eff} = K \left(\frac{du}{dy}\right)^{n-1}$$

Where,

K: Flow consistency index

N: Flow behavior index

$\mu_{eff:}$ Effective viscosity

3.3.5 View Cell Test

In order to determine the stability and durability of the CO_2 foam, view cell experiments were performed. The experimental setup was designed to withstand high temperature and pressure, and was constructed inside a large oven. A sapphire view cell was used to observe the decay of foam, time-lapse images of the foam decay were acquired without opening the oven by using a GoPro camera and LED light source, were later analyzed to plot foam column height versus time. CO_2 foam generated using 1% 2AM, as well as solutions prepared with 9:1, 8:2, 7:3, and 6:4 ratios of 2AM: PECNP as aqueous phase were tested at foam qualities of 70%, 80%, 90%, and 95%. They were all tested in view cell experiment with and without crude oil. Results of foam performance with and without PECNP were compared to choose the most optimized system for dynamic fluid loss and cleanup experiments.

View Cell Test with No Oil

Figure 13 shows schematic diagram of the CO_2 foam setup. This setup was used to perform view cell tests (in the presence and the absence of crude oil), dynamic fluid loss tests and sand pack tests. Apart from these experiments, this setup can be used to perform core flood and shear loop, which was not part of this research. In Figure 13, the lines in the schematic are highlighted in green to show the path of refilling the left accumulator. In order to refill the LH accumulator, the gear pump used for pumping the surfactant solution was primed to remove air bubbles and was connected to valve 1. Next, valves 1 and 10 were opened, and the gear pump was turned on. Soltrol coming out after valve 10 was collected in a beaker. After refilling the left accumulator, the gear pump was stopped, disconnected and valve 1 was closed.

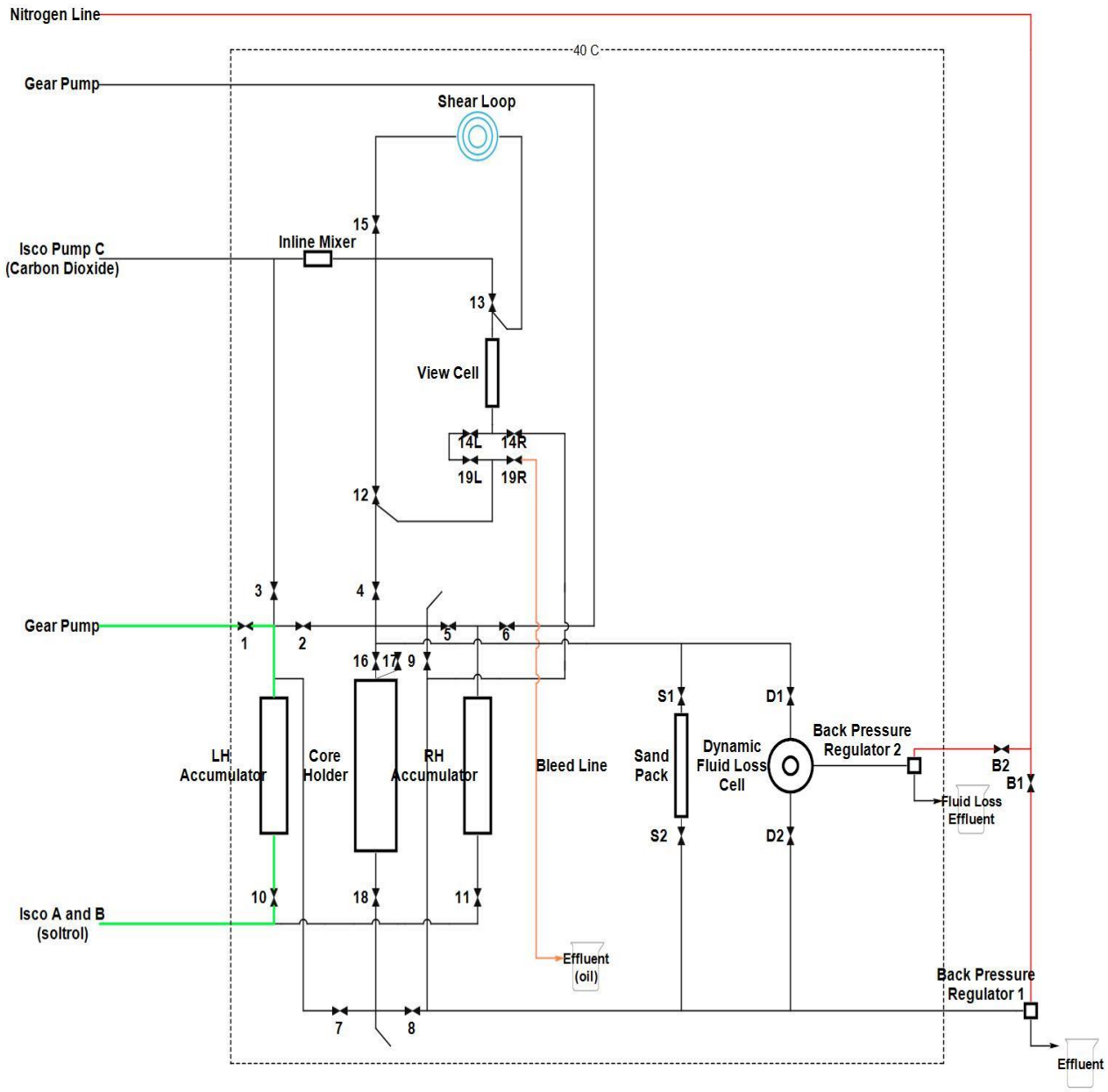

Figure 13. Schematic flow diagram to refill left accumulator

Pressurizing the system

Three ISCO pumps of capacity 103 ml were needed to run this test. Pump A&B act as one single pump and they pump the Soltrol into both left and right accumulator by opening valve 10 and 11, respectively. Pump C is used to pump supercritical CO_2. Pump C was refilled with CO_2 at 6°C and

the pressure at this temperature will be around 780 psi. The setup was pressurized by opening valve 10, 3, 13 and 14R and running the pump A&B at a lower flow rate of 5 ml/min. Then pressure was applied to back pressure regulator 1 using N_2 by opening valve B1. Pressure of BPR 1 was increased in steps of 25 psi, as the pump A&B are running this in turn will increase the system pressure. Once the system pressure reached 900 psi, pump A&B were stopped, valve 10 and 3 were closed, and pump C valve was opened to introduce CO_2 to the system. Then the temperature of pump C was set to 40°C. As the temperature of pump C increases from 6°C to 40°C, the pressure will increase. Therefore, the BPR#1 pressure was also increased in such a way that differential pressure (pressure difference between nitrogen and CO_2 side in the BPR) across diaphragm in the BPR were always less than 400 psi, because differential pressure above 400 psi may damage the diaphragm. Meanwhile oven was turned on and temperature was set at 40°C.

Running the Experiment

Once the system temperature and pressure reached 40°C and 1300 psi, respectively, valve 10 and 3 were opened and it was made sure that valve 13 and 14R are opened. Aqueous phase (surfactant or PECNP-surfactant) and supercritical CO_2 were injected through a 7-µm inline mixer to generate foam. Flow rates of ISCO pumps were set based on the desired foam quality at which the experiments were to be performed. After the view cell was filled with foam and pump C was almost empty, all the pumps were stopped and view cell was isolated by closing valve 13 and 14R. GoPro camera was switched on and set in time lapse mode to acquire image of foam decay every one minute. Green lines in Figure 14 below shows the flow path to run the view cell test.

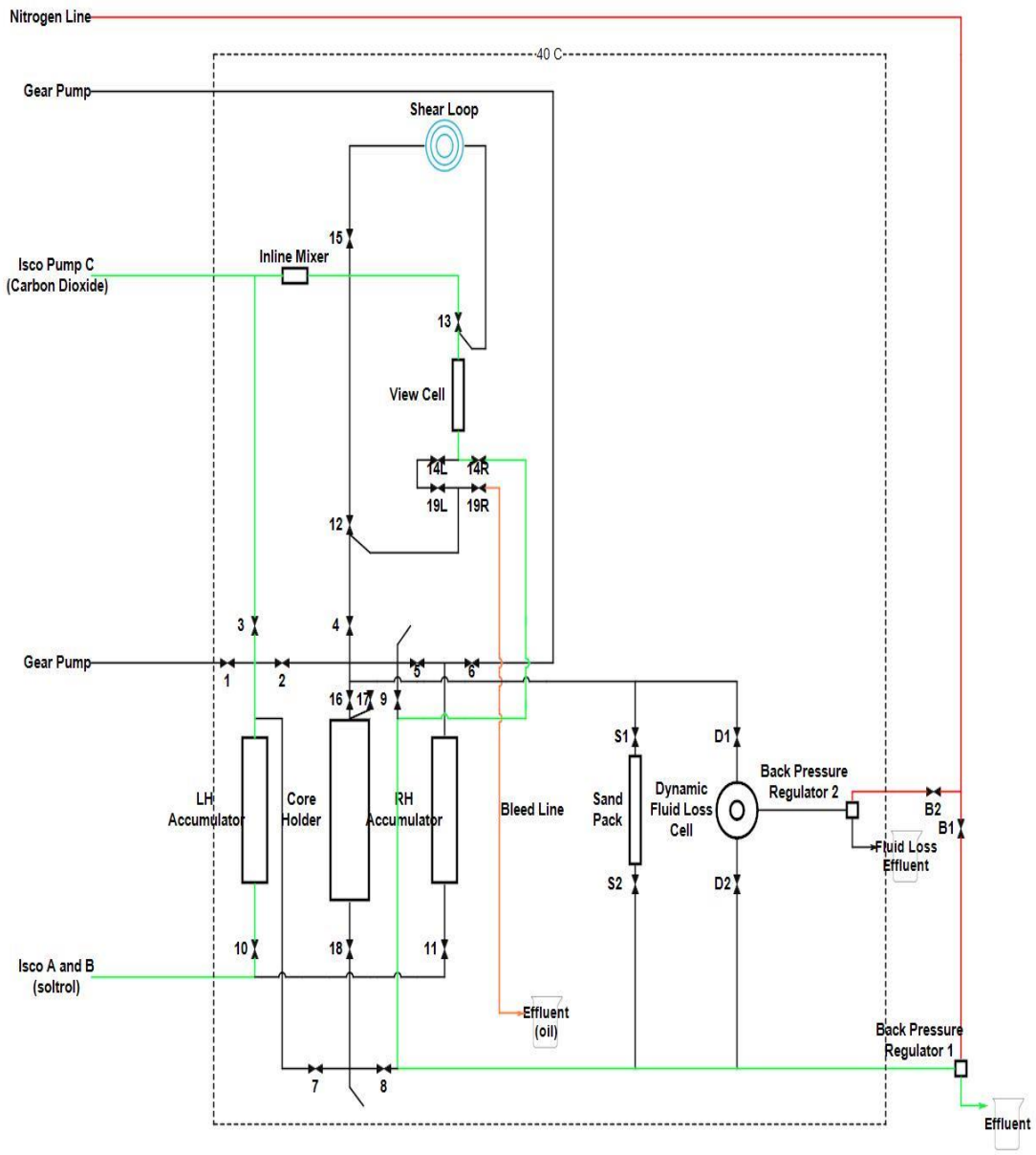

Figure 14. Schematic diagram to show the flow path of view cell test with no oil

Depressurizing and Cleaning the System

After the foam completely decayed, all the heaters and oven were turned off, valves 13 and 14R was opened, N_2 cylinder valve was closed and the system was depressurized by opening the BPR valve. Once the system pressure fell below 20 psig, the left accumulator was emptied by running pumps A&B. Then the left accumulator was refilled with RO water to clean the system. All the

lines and view cell were cleaned by opening valves 10, 3, 13 and 14R and running the pump A&B. Once the left accumulator was emptied, the pump was stopped and all the valves were closed.

View Cell Test In the Presence of Crude Oil

This test was performed to understand the stability and durability of CO_2 foam in the presence of crude oil.

Procedure

First, the left accumulator was refilled with aqueous phase (surfactant or surfactant-PECNP solution) following the same procedure as the view cell experiment with no oil.

Refilling the Right Accumulator

The right accumulator was refilled manually by disconnecting with lines and taking it out of the oven and pouring the crude oil manually into the accumulator by opening the top. After refilling the accumulator it was connected back to the system and the air was removed.

Pressurizing the Oil Line

Valve 11, 5, 4 and 19R were opened and pump A&B was ran to remove air from the line. Next, valves 14L and 19R where closed while 19L was kept open.. Then pump A&B was ran, as 14L was closed to increase the pressure of the right accumulator and the lines from the right accumulator till valve 14L passing through valves 5, 4, 12 and 19L. When the pressure reached 1300 psi, pump was stopped and valve 11 was closed. This was done to increase the pressure in the oil lines to keep the view cell at 1300 psi when oil is introduced inside the view cell later in the experiment.

Running the Experiment

Before running the experiment, the system was pressurized and foam was generated using the same procedure as the view cell testing with no oil. Once the view cell was filled with foam, valves 10

and 14R were closed. Valves 11, 5, 4, 19L and 14L were opened and pump A&B was ran at 2ml/min to pump oil inside the view cell through accumulator B. Once 1/3rd of the view cell was filled with oil, the pump was stopped and valves 13 and 14L were closed to isolate the view cell. GoPro camera was switched on and set in time lapse mode to acquire image of foam decay every one minute. Green lines in Figure 15 below show the flow path of CO_2 (highlighted in green) and yellow lines show the flow path of oil.

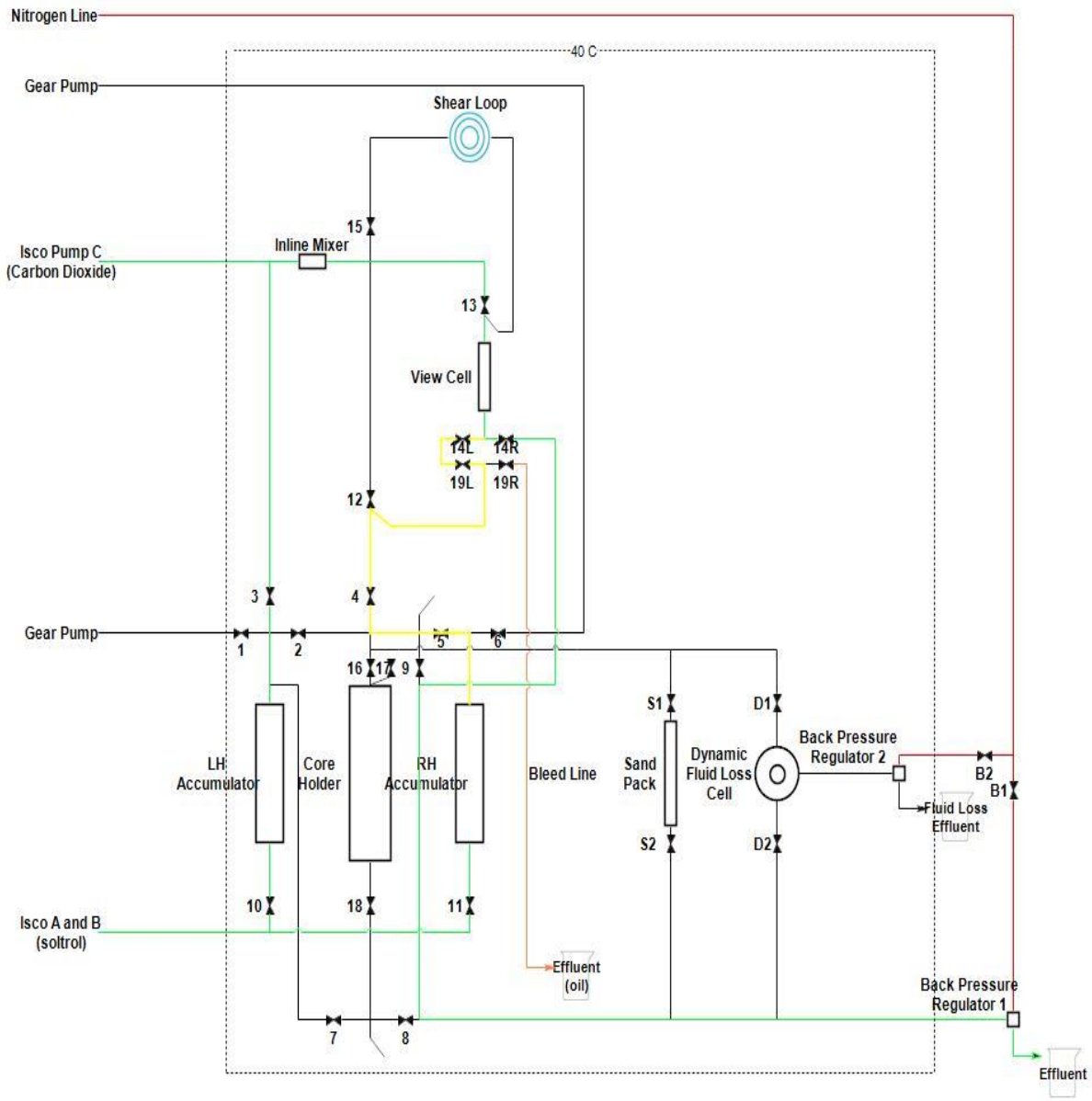

Figure 15. Schematic diagram with highlighted flow lines to run view cell test in presence of oil

Once the foam completely decayed, the system was depressurized and cleaned using the same procedure as the view cell testing with no oil.

3.3.6 Interfacial Tension Measurements

Pendant drop method was used to measure air-aqueous phase and supercritical CO_2-aqueous phase interfacial tension. The pendant drop method is well suited for many types of surface and interfacial tension measurements. Drop shape analysis was performed by photographing a drop in an optical bench arrangement and then the characteristic sizes of the drop can be measured on the photographic images. For pendant drops the maximum diameter and the ratio between this parameter and the diameter at the distance of the maximum diameter from the drop apex has been used to evaluate the size and shape parameters.

On the basis of the Young-Laplace equation describing the drop profile in pendant drop, it is possible to calculate the surface or interfacial tension from the image data. The DROPimage advanced program used in this study has the interface to calculate the IFT. The type of measurement, number and timing, calibration, data presentation and analysis are all controllable within the program.

For these experiments, IFT was measured between air-aqueous and supercritical CO_2-aqueous phase. Aqueous phases were RO water, 2% NaCl, 1% 2AM solution, as well as the 9:1, 8:2, 7:3, 6:4 ratios of 2AM over PECNP.

Pendant Drop Method

The pendant drop is a drop suspended from a needle in a bulk liquid or gaseous phase. The shape of the drop results from the relationship between the surface tension or interfacial tension and gravity. In the pendant drop method, the surface tension or interfacial tension was calculated from the shadow image of a pendant drop using drop shape analysis.

An increased pressure is produced inside the drop as a result of the interfacial tension between inner and outer phase. The correlation between the pressure difference Δp, the radii of curvature of the surface r_1 and r_2 and the interfacial tension is described by the Young- Laplace equation, shown in Equation 3 below:

Equation 3,

$$\Delta P = \sigma (1/r_1 + 1/r_2)$$

Where, r_1 and r_2 are radii of curvature of surface, ΔP is the pressure difference, σ is the interfacial tension.

Procedure

The ISCO pump was filled by the gaseous phase which is air for the first set of experiments and supercritical CO_2 for the second set of experiments. The left accumulator was filled with aqueous phase. All the lines were flushed by the aqueous phase solution. The measuring chamber was filled by the aqueous phase solution from the left accumulator using the hand pump and then the temperature of the heater around the setup was set at 40^{o}C. Figure 16 below shows the image of the IFT setup used to measure the interfacial tension.

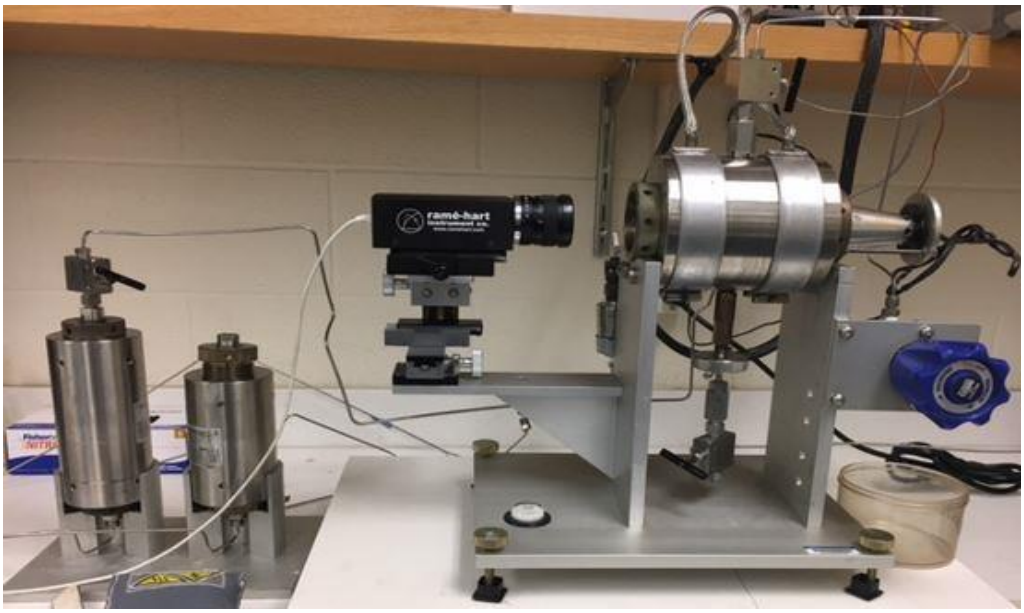

Figure 16. Image of the Interfacial tension setup

After the setup reached the desired temperature, camera had been set and the software was turned on the name and density of the aqueous phase used was entered. Then, the camera was calibrated in order to do accurate measurements. Horizontal Calibration was done, in which the metal rod is mounted vertically and was positioned as shown below in Figure 17 . There must be ample room at both sides of the rod, and no room at the top or bottom for calibration. In order to have a good calibration the metal rod was positioned in such a way that the needle was not visible in the camera and only the rod was focused in the camera.

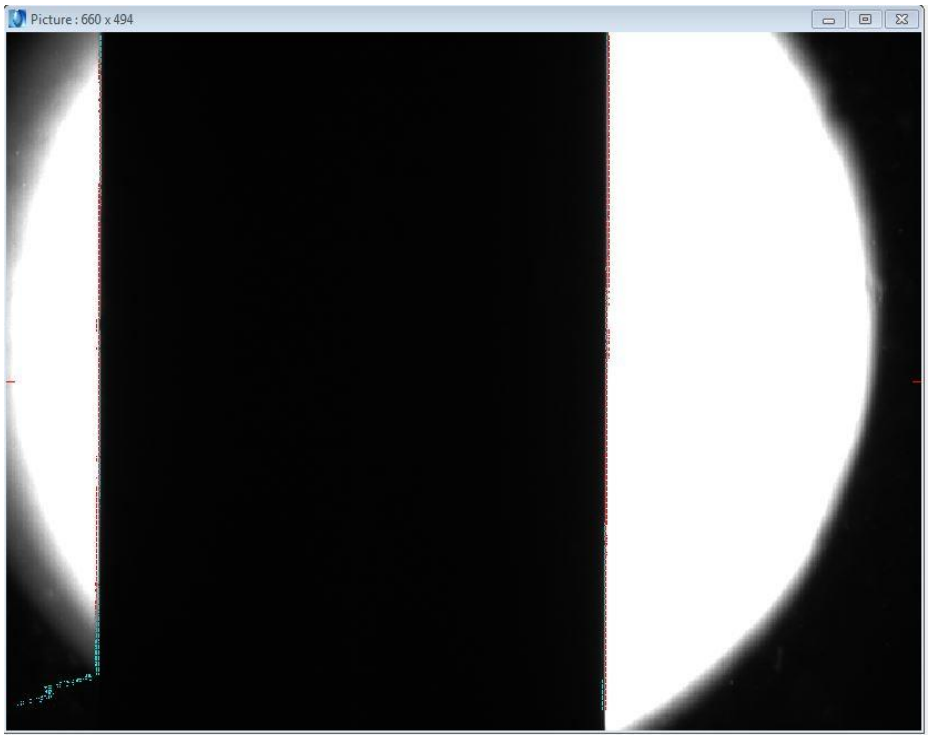

Figure 17. Position of the metal rod during calibration

If there is any air bubble in the chamber, it can be cleared by increasing the pressure of the chamber using injection of the aqueous phase into the chamber by closing the exit valve. Next, one bubble of air or CO_2 was sent to the chamber. Then the cross hair cursor was used, the purpose of this is to act as the reference for the edge detection (or filtering) routine. The vertical line always starts along the centerline of the image, while the horizontal line at the extreme top of the needle.

Figure 18 shows the image of cross hair cursor used for referencing.

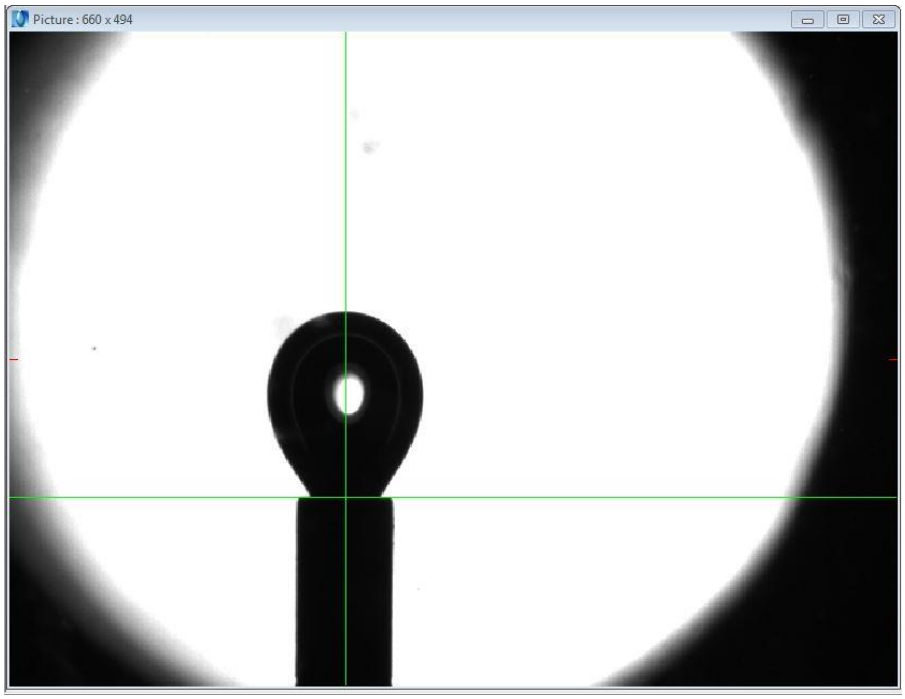

Figure 18. Image of cross hair cursor

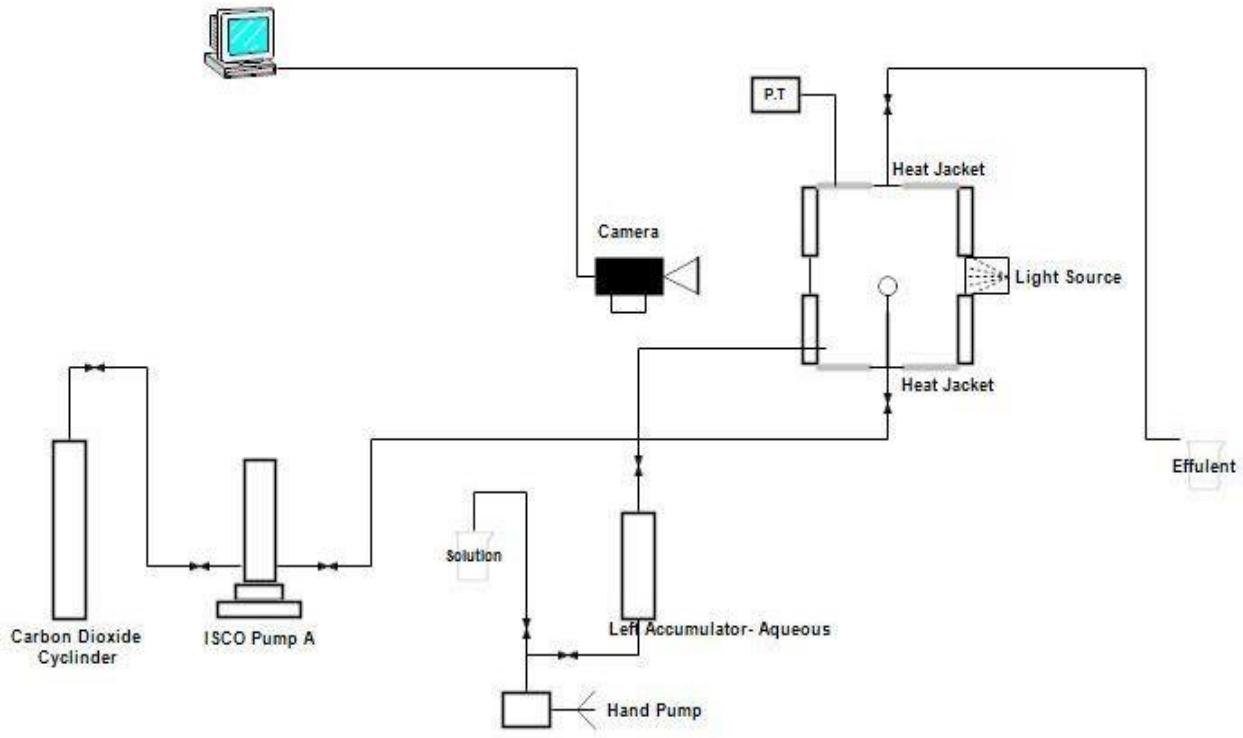

Figure 19. Schematic flow diagram of the IFT set up

The bubble's surface area was measured and interfacial tension was calculated using the DROPimage software. The pressure and temperature of the setup for this set of experiments kept on 1300 psi and 40^{o}C, respectively. Figure 19 shows the schematic flow diagram of the interfacial tension set up.

3.3.7 Core Saturation and Porosity Measurements

The cores were dried in an oven at 40°C for at least 24 hours. Then the dimensions of the core was measured using a Vernier caliper and it was weighed to get the dry weight. The core was then placed in a vacuum desiccator and evacuated to 3" inches of Hg vacuum pressure using a vacuum pump. The inlet valve to the desiccator was open to allow the 2% NaCl brine to fill the container with core. Core was completely immersed in the brine. The core was left immersed in the brine for 3-4 hours for saturation. Then the vacuum pump was turned off and exit valve was opened so that the desiccator reaches atmospheric pressure, core was taken out and gently wiped with dump Kimwipes and was weighed to get the saturated weight.

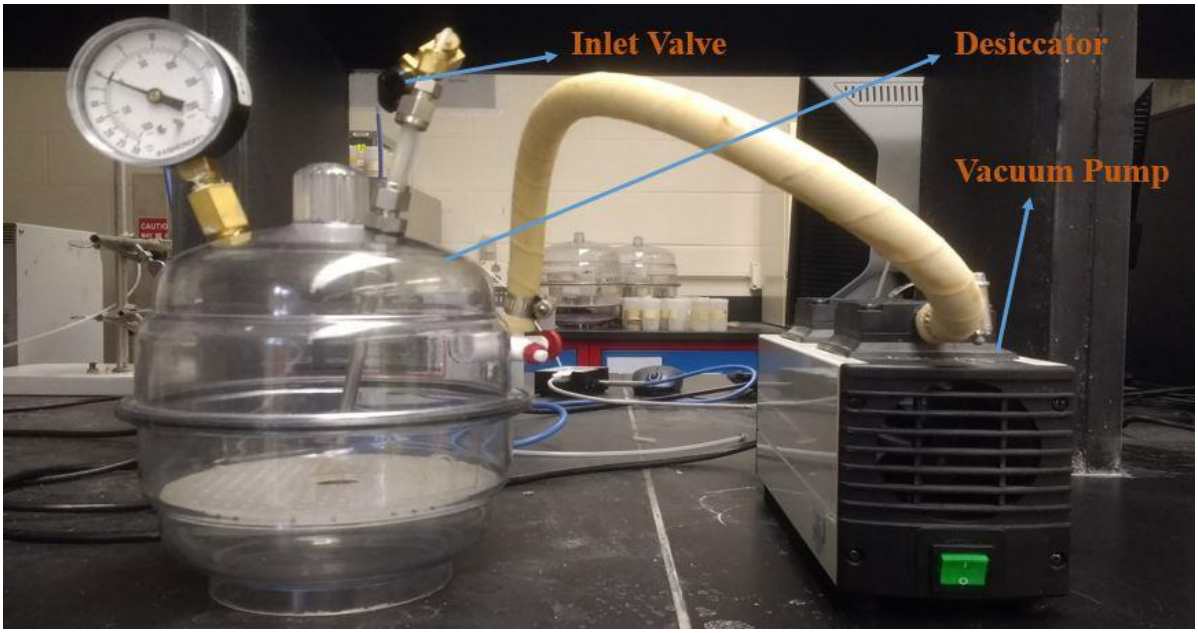

Figure 20. Image of the vacuum desiccator set up

Figure 20 above shows the vacuum desiccator setup. Porosity is calculated using Equation 4, Equation 5 and Equation 6.

Equation 4,

$$V_b\ (cm^3) = \pi * r^2 * h$$

Where,

V_b: Bulk Volume (cm^3)

r: radius of the core (cm)

h: height of the core (cm)

Equation 5,

$$V_p\ (cm^3) = (W_{sat} - W_{dry}) / \rho_{brine}$$

Where,

V_p: Pore Volume (cm^3)

W_{sat}: Saturated weight of the core (cm^3)

W_{dry}: Dry weight of the core (cm^3)

ρ_{brine}: Density of brine (g/cm^3)

Equation 6,

$$\Phi\ (\%) = (V_p/V_b) * 100$$

Where,

Φ: Porosity

3.3.8 Permeability Measurement for Fluid Loss Experiments

Brine flooding experiments were performed to measure the core permeability. Figure 21 shows the schematic flow diagram of the core flooding setup.

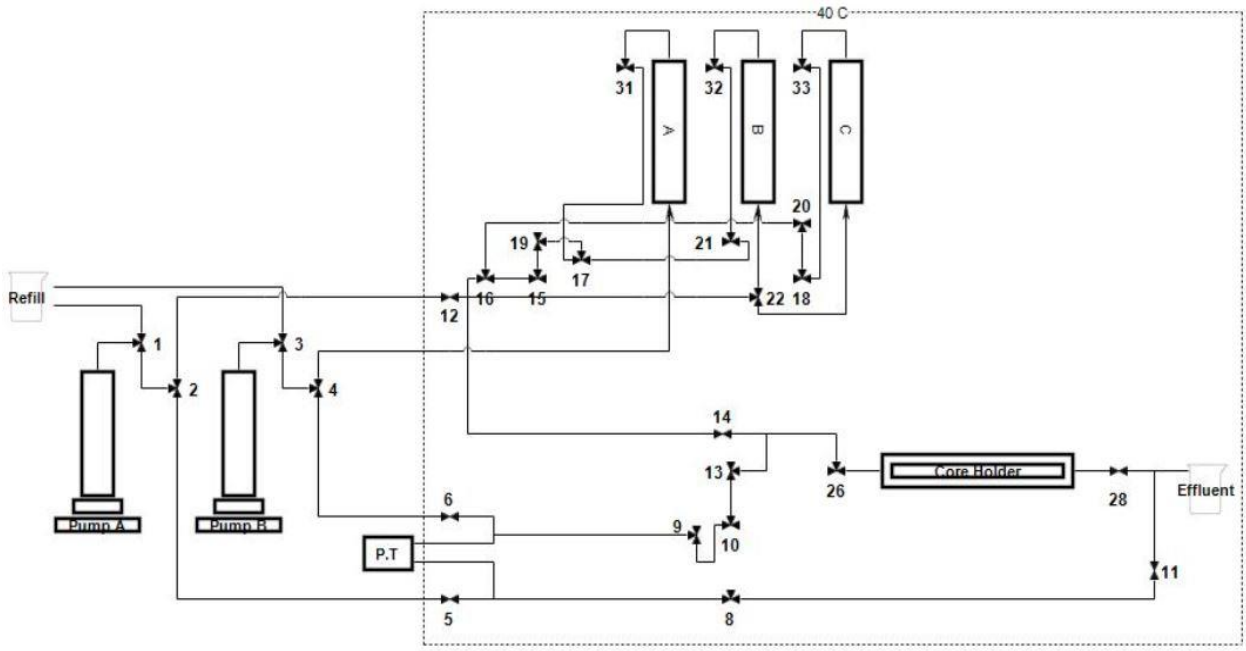

Figure 21. Schematic flow diagram of the core flood setup

Procedure

Filling the lines and pressure transducer with mineral oil

This procedure was performed to make sure the lines leading to pressure transducers were filled with mineral oil and to remove the air bubbles in the lines. From pump A, valve 1, 2 and 5 were opened towards pressure transducer and the mineral oil was bled off at a flow rate of 2ml/min. After this all valves were closed. From pump B, valve 3, 4 and 6 were opened towards pressure transducer and the mineral oil was bled off and the valves were closed. The lines leading to pump A were filled with mineral oil by opening valves 1, 2, 5, 8, and running the pump at a flow rate of 5 ml/min. The lines leading to pump B were filled with mineral oil by opening valves 3, 4, 6, 9, 10, and running the pump at a flow rate of 5 ml/min. Figure 22 below shows the image of the core flood setup.

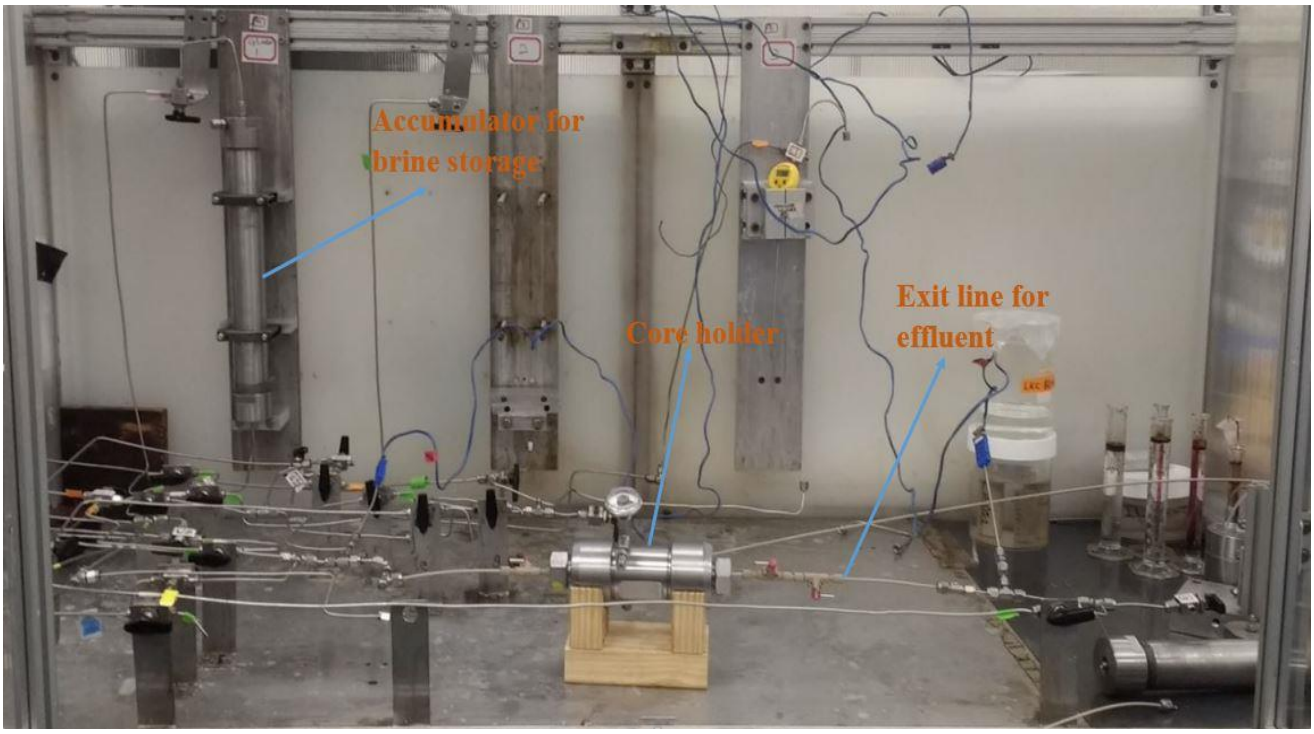

Figure 22. Image of the core flood setup

Running the experiment

The accumulator A was filled with brine manually by taking it out and pouring the brine into the cylinder. Accumulator B and C were not used for this experiment. The accumulator has a piston, above the piston is filled with brine and below the piston it's filled with mineral oil. Pump A was used to pump Soltrol which in turn will pump the brine out of the accumulator. All the flow lines leading to the core holder were filled with brine. Valves 33, 4, 31, 17, 19, 15, 16, 14 and 26 were opened towards the core holder and pump A was ran at the flow rate of 5 ml/min. This process will remove air bubbles leading to the core holder. Lines just before and after the core holder were filled with brine manually using syringe.

Then the core was placed in the core holder and confining pressure or overburden pressure was applied using hydraulic oil. Valves 8, 11, 9, 13 and 10 were opened to enable the pressure transducer to acquire pressure reading. Flow was initiated into the core holder with 3 different

flow rates and corresponding differential pressure was noted for different flow rates. This pressure vs. flow rate reading was used to calculate the permeability using the Darcy's law equation:

Equation 7,

$$Q= (k* A * (\Delta P))/ (\mu * L)$$

Where,

k - Permeability (mD)

A - Area (cm^2)

ΔP - differential pressure (psi)

μ - viscosity (cP)

L - Length of the core (cm)

Q - Flow rate (ml/min)

After acquiring the readings, pump was stopped, core holder was disconnected from the lines and accumulator A was filled with RO water. This procedure was repeated to clean the lines with RO water.

3.3.9 Dynamic Fluid Loss Experiments

A dynamic fluid loss cell has been used to measure the fluid loss caused by the fracturing fluid under the given pressure and temperature. Dynamic fluid loss experiments were followed by cleanup experiments as the last phase of my research. As 8:2 ratio of 2AM: PECNP was the most optimized system (discussed in results), CO_2 foam generated by it was used to perform fluid loss experiment at foam qualities of 70%, 80%, 90% and 95%. Its results were compared with CO_2 foam generated just by the surfactant solution (1% 2AM). Summation of the gaseous phase (CO_2) and aqueous phase fluid loss gave the total fluid loss. This value was used to calculate the fluid loss coefficient using the Carter leakoff equation,

Equation 8,

$$V_L = C_w * t^{(1/2)} + V_s$$

Where,

V_L - Total fluid loss (cm^3)

C_w - Fluid loss coefficient

t - Time (min)

V_s - Spurt fluid loss (cm^3)

Procedure

The dynamic fluid loss cell contains one inlet and two outlets. In addition to the inlet, there is an outlet for fluid loss connected to a back pressure regulator and the third one is the main outlet connected to a back pressure regulator. Nitrogen supply from a cylinder is used to apply pressure to the back pressure regulator. The inlets and outlets of the cell are made of quick connect fittings. Leakage is prevented by O-ring seals plus a rubber core holder in place which prevent any possible overpass of the core. Figure 23 below shows various parts of the fluid loss cell.

The following procedure was used to perform the dynamic fluid loss test.

First the left accumulator was refilled with the aqueous phase (just surfactant or surfactant- PECNP solution) using the same procedure discussed before in the view cell experiment, the flow path to refill the left accumulator is shown in Figure 13.

Figure 23. Various parts of the dynamic fluid loss cell

Three ISCO pumps were needed to run this test. Pump A&B acts as one single pump and it pumps the liquid in both left and right accumulator by opening valve 10 and 11 respectively. Pump C is used to pump supercritical CO_2.Pump C was refilled with CO_2 at 6°C and the pressure at this temperature will be around 780 psi. The setup was pressurized by opening valve 10, 3, 12, 4, D1, D2 and running the pump A&B at a lower flow rate of 5 ml/min. Then pressure was applied to back pressure regulator 1 and 2 using N_2 by opening valve B1 and B2. Pressure of BPR 1 was increased in steps of 25 psi, as the pump A&B are running this in turn will increase the system pressure. Once the system pressure reached 900 psi, pump A&B was stopped, valve 10 and 3 were closed, and pump C valve was opened to introduce CO_2 to the system. Then the temperature of pump C was set to 40°C. As the temperature of pump C increases from 6°C to 40°C the pressure

will increase, so the BPR 1 and 2 pressure was also increased in such a way that differential pressure of BPR was always less than 400 psi. Meanwhile oven was turned on and temperature was set at 40°C. When the BPR 2 pressure reached 1250 psi, valve B2 was closed and the BPR 1 pressure was increased to 1300 psi and stopped. The fluid loss line was kept 50 psi lesser than the main effluent line of the fluid loss cell.

Then valves 10, 3, 12, 4, D1 and D2 were opened. Flow rates of pump A&B and pump C were set based on the foam quality needed to run the experiment and pump was turned on. Foam was generated using an inline mixer. Flow path of the dynamic fluid loss line is highlighted using green color in Figure 24. After foam was passed through the fluid loss line, there was effluent both in fluid loss side as well as main line of the fluid loss cell. The gaseous phase of the fluid from the fluid loss line was analyzed for CO_2 using an Alicat gas analyzer and aqueous phase from the fluid loss line is collected in a burette and volume collected vs time was noted.

After the experiment, all the heaters and the oven were turned off, nitrogen cylinder valve was closed and the system was depressurized by opening the main BPR valve. Once the system pressure reaches below 20 psi, left accumulator was emptied by running pump A&B. The left accumulator was then refilled with RO water for cleaning the system. All the lines and view cell were cleaned by opening valves 10, 3, 12, 4, D1, D2 and running the pump A&B. Once the left accumulator was emptied, the pump was stopped and all the valves were closed.

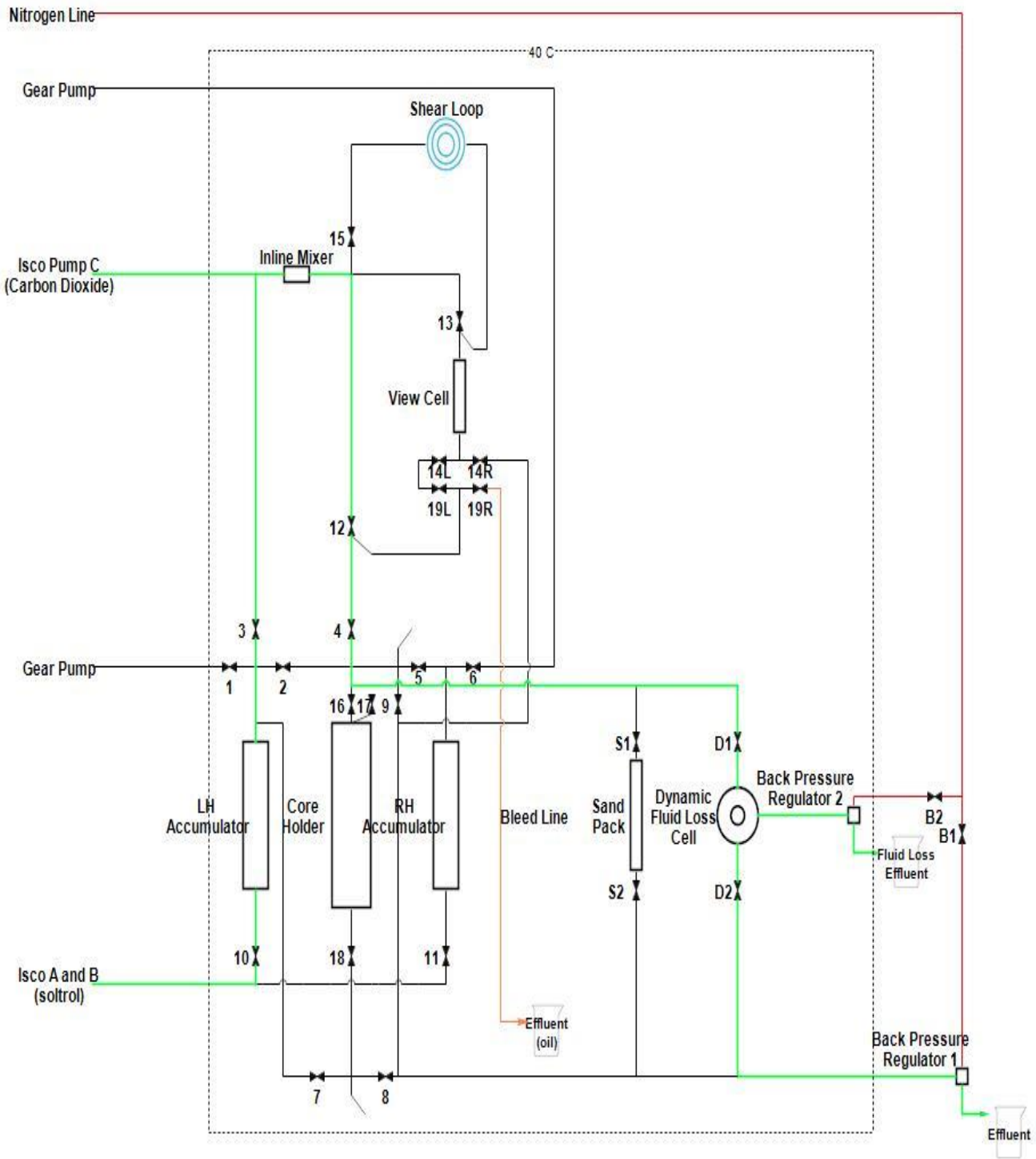

Figure 24. Schematic flow diagram of the dynamic fluid loss experiment

3.3.10 Tracer Test

Tracer test was performed using UV absorbance on the sand pack to determine the pore volume by analysis of concentration profile. Before the UV analysis sand was loaded in the sand pack and it was saturated with brine.

Procedure to load sand

Put bottom end cap to the sand pack and place it on a holder. Place a funnel on the top of the sand pack and slowly add proppants to the sand pack by shaking the sand pack with a vibrator. Figure 25 shows the image of sand pack while loading it with proppant.

Figure 25. Image of sand pack while loading it with proppant

After loading the sand pack with proppants close the top with an end cap.

Procedure to saturate the sand pack

Sand pack was connected to the desiccator and the valve on the other end of sand pack was closed. Then the system was vacuumed till it reached a pressure of -30 inches of Hg by turning on the vacuum pump, after that the inlet line to sand pack was immersed in a container containing brine and the valve was opened to allow brine to saturate the sand pack. This process was continued till there was no air bubble visible in the line. After saturation the pump was turned off and the sand pack was disconnected from the desiccator and both ends of the sand pack were caped. Figure 26 shows the image of the setup used to saturate the sand pack.

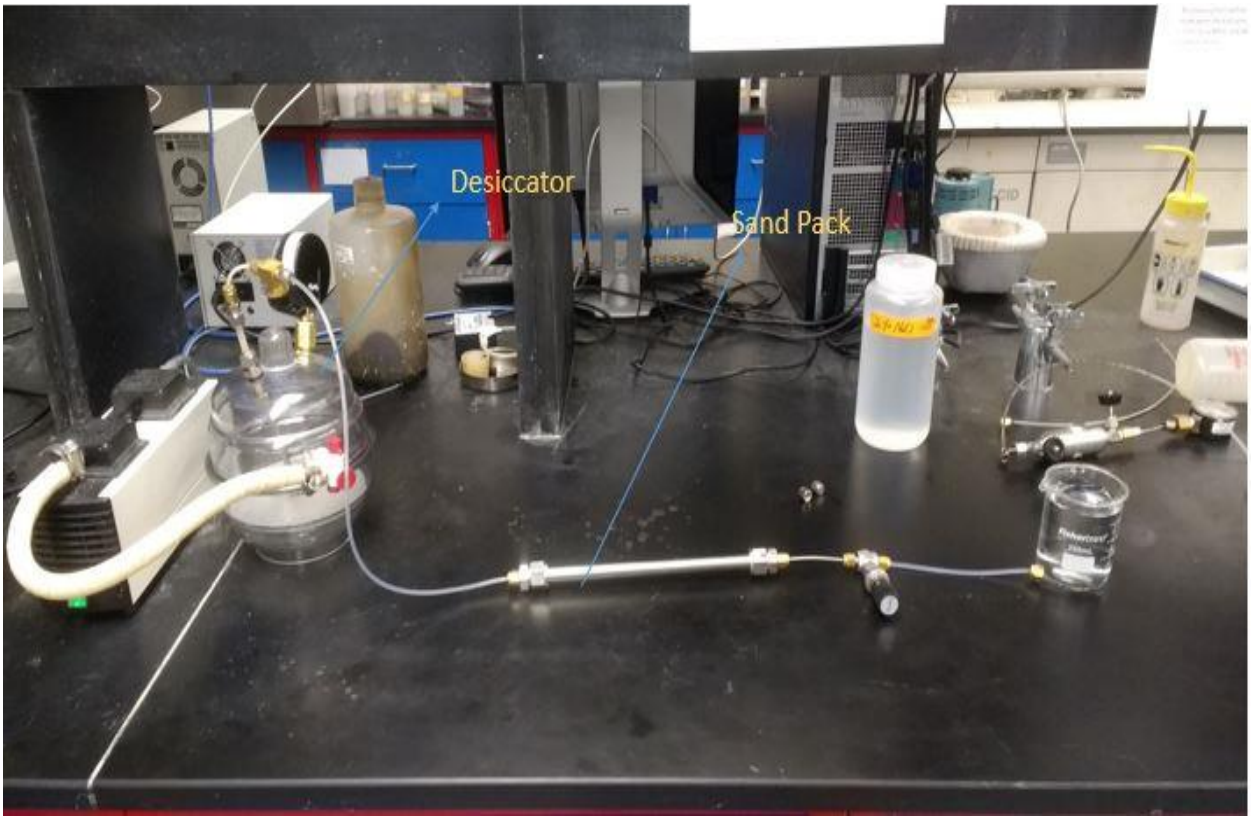

Figure 26. Image of setup used to saturate the sand pack

UV tracer test

A 10,000 ppm potassium nitrate tracer was used to displace RO water and vice versa in sandpack to determine the pore volume. . The absorbance of the fluid was recorded in real-time by UV light travelling from the light source through an optic cable to the flow cell then the spectrophotometer. The light passing through the effluent fluid detected nitrate ions at a wavelength set at 302.08 nanometers, per instructions on the Deuterium-Halogen Model DAH 2000. Light source absorbance was measured and logged in real-time through spectrophotometry methods by the utilization of a USB4000 OceanOptics Spectrophotometer. The absorbance data was converted to normalized concentration profiles. Analysis of the normalized concentration profiles led to the determination of the pore volume of the sand pack.

Before beginning the dispersion process, the RO water was pumped through the sandpack at 20.00 mL/min displayed flow rate to attempt to flush out any air bubbles in the sand pack. Air bubbles in the system would cause discrepancies in the absorbance data being plotted in SpectraSuite software. The Eldex pump was calibrated using the instruction below.

The two Eldex pumps were tested at 8 and 12 mL/min. Calibration of the pump was completed twice for each flow rate since there were two different fluids being injected into the sandpack from different pumps. It is necessary to calibrate the pumps because depending on the viscosity of the fluid being injected, the flow rate displayed on Eldex pump could be different than the actual flow rate of the pump. Therefore, for each run of the experiment, the effluent fluid was collected in a tared beaker. At the end of the run, the stopwatch, pump, and SpectraSuite software were stopped simultaneously and the weight of the beaker and effluent was measured and recorded. The mass of the effluent was determined by subtracting the initial mass of the beaker from the combined mass of the beaker and effluent. The total volume of the effluent in the beaker was determined by

dividing the mass of the effluent by the density of the fluid, which was assumed to be 1.0 g/cm^3 for the RO water and the potassium nitrate tracer. The volume of effluent was finally divided by the elapsed time recorded on the stopwatch, resulting in the actual flow rate of the Eldex pump. Equation 9 below shows the formula used to calculate actual flow rate.

Equation 9

$$Q_{real} = \frac{Mass\ Effleuent\ (g)}{Density\ Effluent\ (\frac{g}{cm^3})} \times \frac{1\ mL}{1\ cm^3} \times \frac{Elapsed\ Time}{\frac{60\ sec}{1\ min}}$$

The light source utilized in the dispersion of a linear porous medium experiment was the Deuterium-Halogen Model DAH 2000 which emits light in the UV-visible range of light (Figure 27). The light source was turned on upon arrival to the laboratory allowing the light source enough time to warm-up before being calibrated. For calibration, RO water was utilized as the reference fluid. The purpose of this piece of equipment was to emit light through a blue optical cable to the flow cell and then to the USB4000 Ocean Optics Spectrophotometer (Figure 28). The absorbance of the injected fluid was measured by the spectrophotometer as fluid passed through the flow cell. The measured absorbance values were recorded in the SpectraSuite software for each of the different flow rates run during the experiment.

In the flow cell, the nitrate was detectable by UV absorbance at a wavelength of ~302 nm. As displayed on the light source, the wave length of the spectrophotometer was set to 302.08 nm for the duration of the experiment. Strip charts were created for each of the different tested flow rates under the appropriate settings and the software was enabled to auto save.

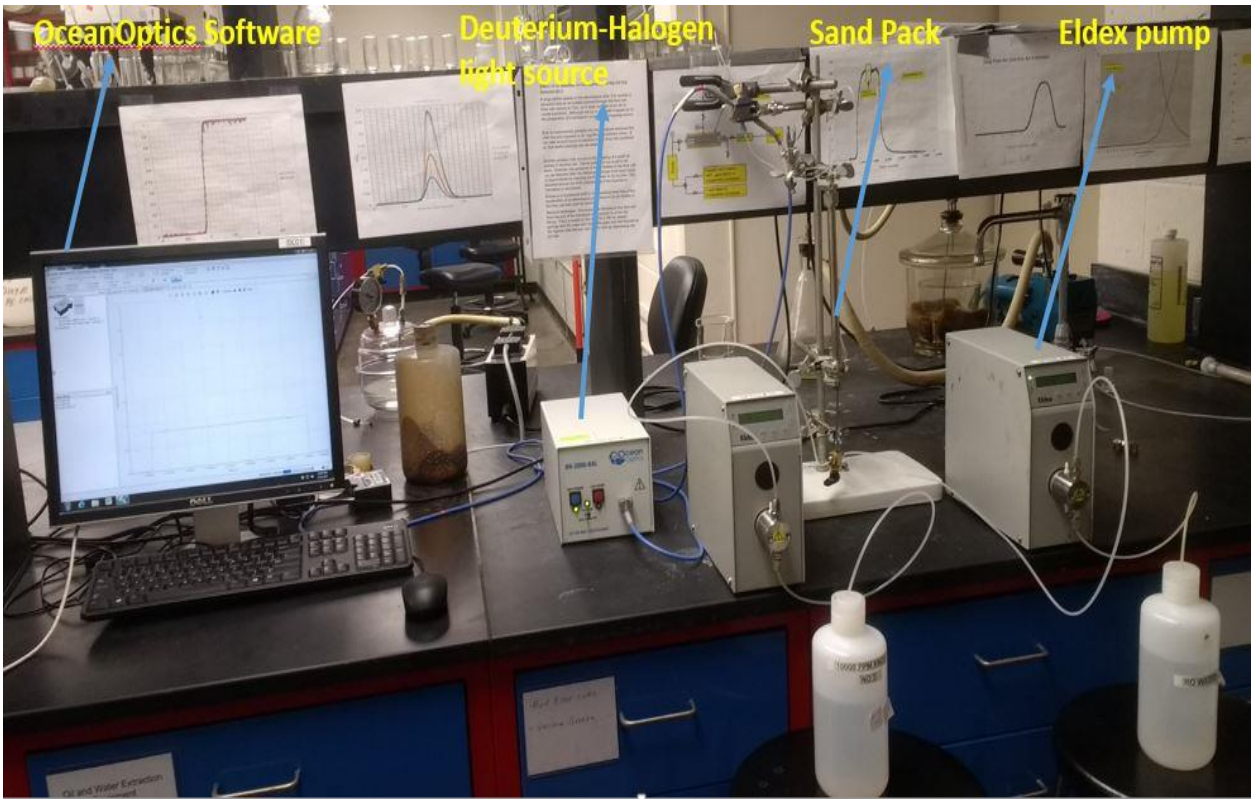

Figure 27. Image of UV Analysis setup

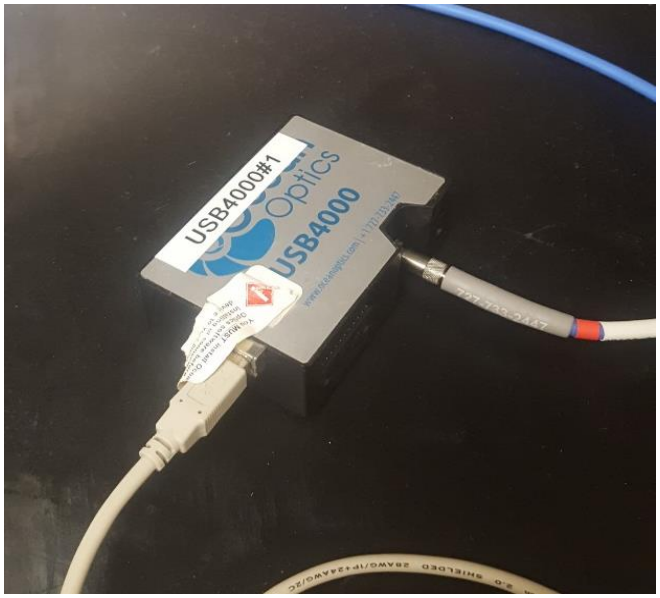

Figure 28. USB4000 OceanOptics Spectrophotometer

Figure 29 is a schematic of the experimental set up for the dispersion in a linear porous medium experiment. One of the Eldex pumps injects potassium nitrate tracer and the other one injects RO water into the sand pack. Whichever fluid is being pumped at the time enters the sand pack through a 3-way connection valve then exits the sand pack and flows through an outlet capillary tube to the flow cell. The fluid was subjected to UV light while inside the flow cell. The data for the fluid's absorbance was sent to the computer attached by a USB port. Once the data was in the computer, it is recorded in a Strip Chart in the SpectraSuite software. Finally, after passing through the flow cell, the effluent was collected in a tared beaker to be weighed.

Prior to testing, the computer was powered on and the SpectraSuite software was opened to calibrate the light source. While running the fluids through the system and collecting absorbance data, the Eldex pumps were calibrated. Data was recorded at 8 and 12 mL/min. Both the potassium nitrate tracer pump and the RO water pump were set to run at these desired flowrates. The density of both fluids used was 1.0 g/cm^3.

The sand pack was injected with RO water prior to the first run of tracer fluid to ensure the porous medium was filled with RO water and no other substance. Next, the sandpack was injected with the potassium nitrate tracer at a flow rate of 20.00 mL/min. The effluent was collected in a tared beaker after it passed through the sand pack and the flow cell all while the absorbance of the fluid was measured in real-time. Once the strip chart on the computer displayed a constant absorbance value, the pump, timer, and strip chart recording were stopped simultaneously.

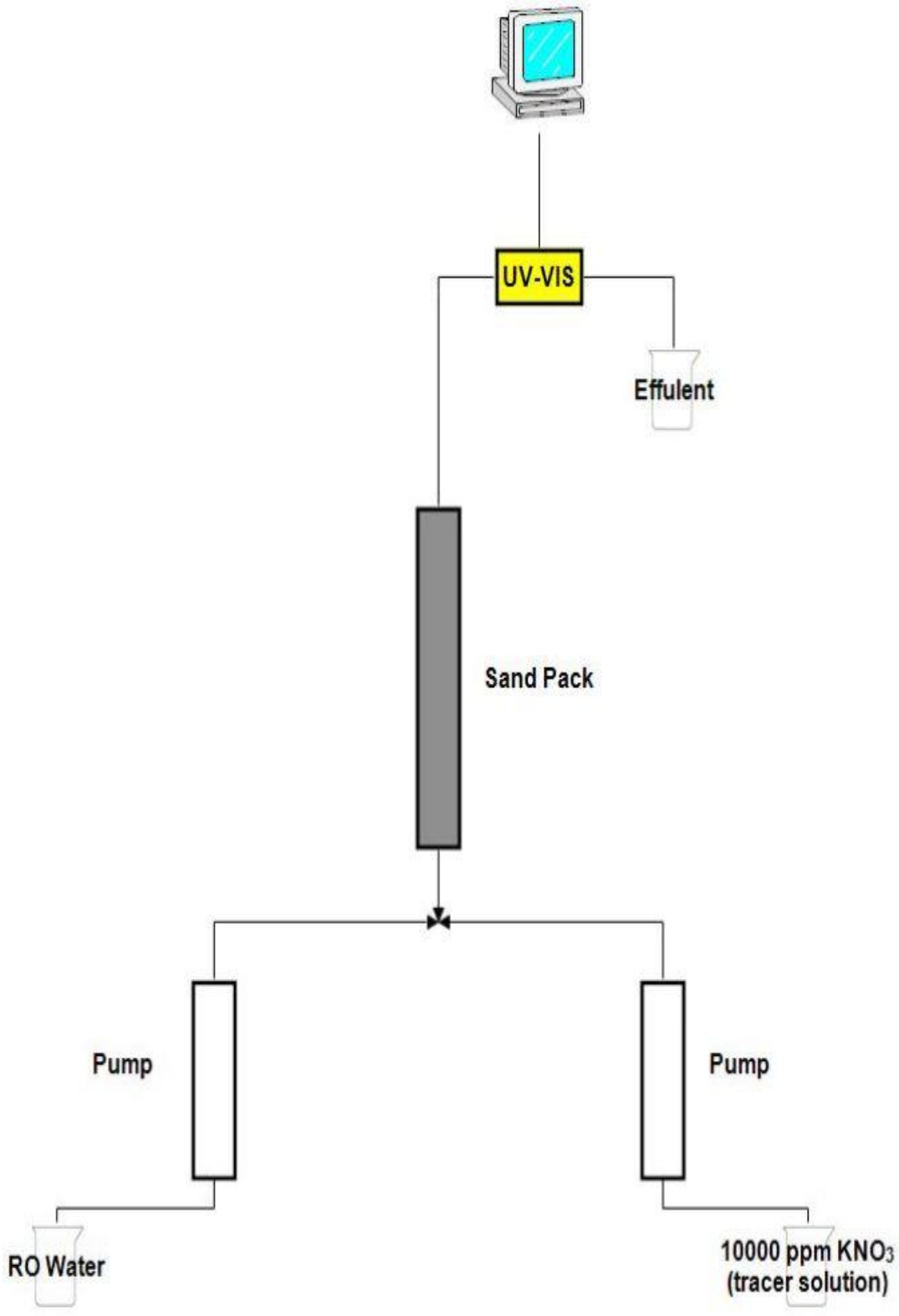

Figure 29. Schematic flow diagram of the UV analysis experimental setup

The weight of the effluent and the beaker were measured and recorded, and the process was repeated with RO water displacing potassium nitrate tracer from the sand pack. However, when RO water was injected to displace tracer, one was looking for the absorbance trend to reach zero. As stated before, each run was timed with a stopwatch and times were recorded for each RO and tracer run. The Beer-Lambert law can be utilized in the analysis of a mixture by spectrophotometry methods.

Equation 10,

$$Absrobance = 0.8254 * Concentration - 0.0055$$

After calculating concentration from equations above, it was normalized using Equation 11 shown below:

Equation 11,

$$C_D = \frac{C - C_o}{C_i - C_o}$$

The volume injected was calculated using Equation 12 shown below:

Equation 12,

$$V_i = \frac{Q_{real}}{\frac{60\ sec}{1\ min}} \times t_c$$

Once the volume of injected fluid is calculated, normalized concentration were found RO water and the potassium nitrate tracer. The curves allow the pore volume of the sand pack to be calculated utilizing a material balance. The pore volume of the fluid occurs at the point where the area above and area below the curve are equivalent. The areas were determined using the Trapezoidal rule. Equation 13 and Equation 14 below show the area above and below the curve respectively.

Equation 13,

$$\int_{V_T}^{0}(1-C_D)dV_w = \sum_{j=n}^{j=1}\frac{\left(1-C_{D_j}\right)+\left(1-C_{D_{j-1}}\right)}{2}\times\left(V_{w_j}-V_{w_{j-1}}\right)$$

Equation 14,

$$\int_{0}^{V_T} C_D dV_w = \sum_{j=1}^{j=n}\frac{\left(C_{D_j}+C_{D_{j+1}}\right)}{2}\times\left(V_{w_{j+1}}-V_{w_j}\right)$$

3.3.11 Fracture Cleanup

Post-fracture cleanup efficiency of fracturing fluid is an important parameter which affects production. Fracture clean up experiment was performed using a sand pack. Figure 30 shows the steps needed to perform cleanup studies. As the fluid system with 8:2 ratio of 2AM: PECNP was the most optimized system (discussed in the Results and Discussion section), CO_2 foam generated by it was used to perform sand pack experiments at foam qualities of 70%, 80%, 90% and 95%. Its results were compared with CO_2 foam generated just by the surfactant solution (1% 2AM).

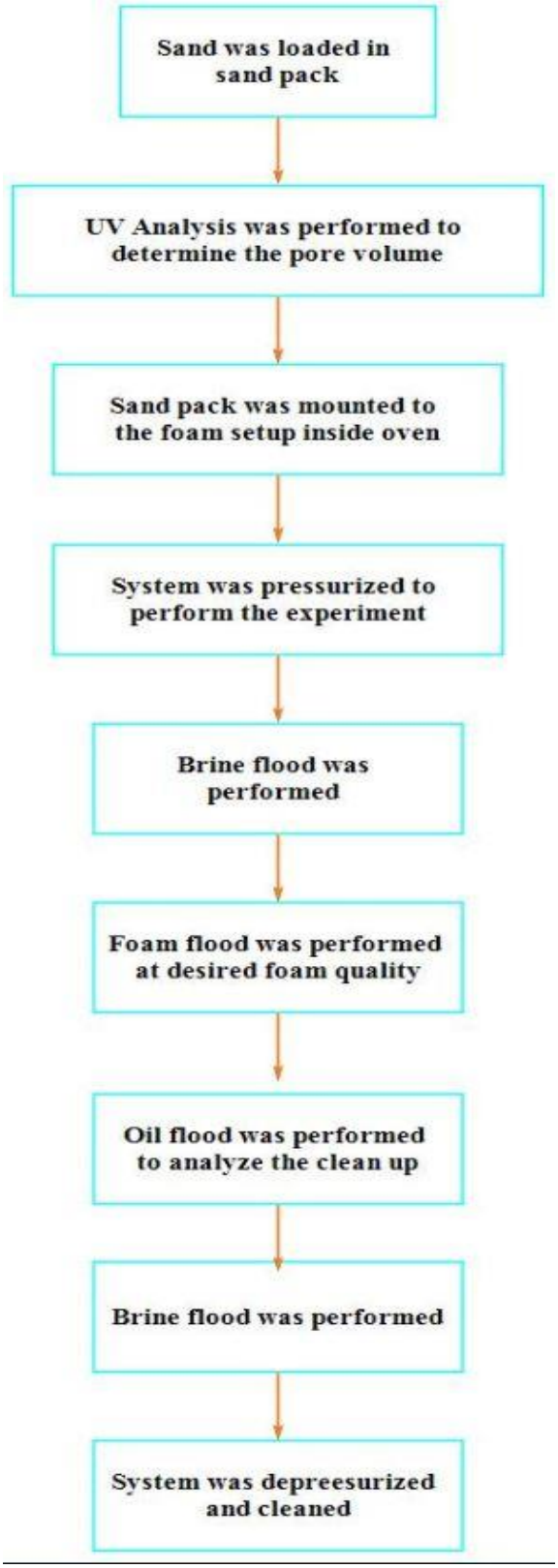

Figure 30. Flow chart with steps required to perform the fracture cleanup procedure.

Procedure to perform sand pack experiment

Three ISCO pumps were needed to run this test. Pump A&B acts as one single pump and it injects the liquid in both left and right accumulator by opening valve 10 and 11, respectively. Pump C is used to pump supercritical CO_2.

Brine flood:

Left accumulator was refilled with brine using the same procedure used in view cell experiment. The schematic of the setup is shown in Figure 13 and the flow lines used to refill the left accumulator re highlighted using green color. Valve 10, 3, 12, 4, S1 and S2 are opened and pump A&B was run at a flow rate of 5 ml/min, simultaneously pressure was applied to back pressure regulator 1 in steps of 25 psi using nitrogen till the pressure reached 1,300 psi and all the heaters and oven were turned on and the temperature was set to 40^{o}C. Once temperature reached 40^{o}C, pump was run at a flow rate of 6, 10 and 12 ml/min and corresponding differential pressure across the sand pack was recorded using lab view software. After the brine flood, system was depressurized and the left accumulator was emptied.

Foam Flood:

After brine flood, left accumulator was refilled with aqueous phase (just 1% 2AM or 8:2 2AM: PECNP) needed to generate foam. Pump C was refilled with CO_2 at 6^{o}C and temperature of pump C was increased to 40^{o}C to increase the pressure from 780 psi to 1300 psi. Then valves 10, 3, 12, 13, 14R, 4, S1 and S2 were opened. Pump A&B were run at a flow rate of 5 ml/min, simultaneously pressure was applied to back pressure a regulator 1 in steps of 25 psi using nitrogen till the pressure reached 1300 psi and all the heaters and oven was turned on and the temperature was set to 40^{o}C. Valve 13 and 14R were closed because we don’t want the foam to enter the view cell.

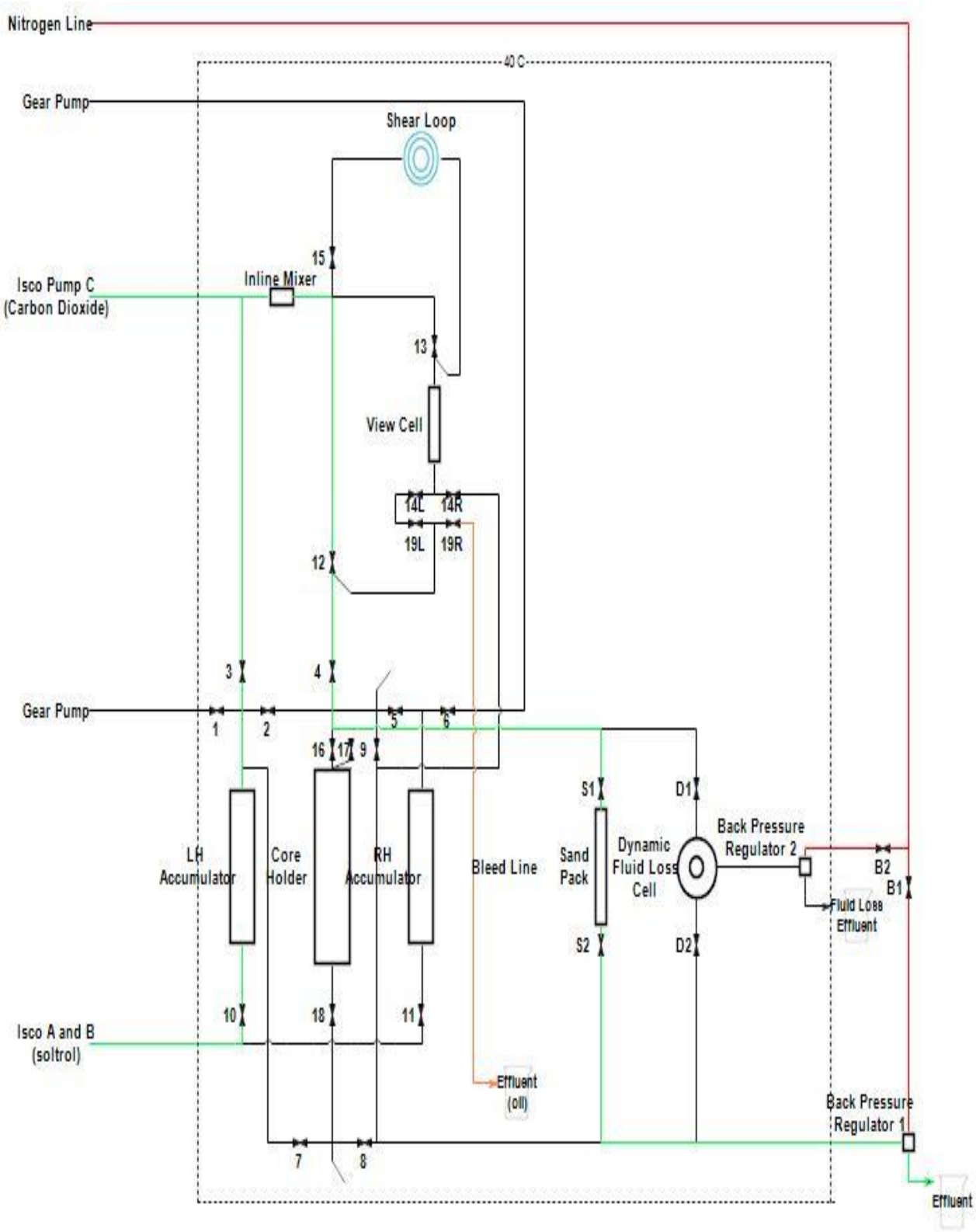

Figure 31. Schematic flow diagram showing the flow path for foam flood

The pump C valve to the system was opened to introduce CO_2 to the system. The foam of desired quality was generated by running pump A&B and C, and was injected into the sand pack. After the foam flood, pump A&B and C were stopped, and valve 10, 3. 12 and 4 were closed. Now the entire sand pack is filled with CO_2 foam. In Figure 31, flow path of the foam flood is highlighted in green color.

Oil Flood:

Oil flood is the most important part of this experiment because, this actually represents post-fracture clean up during production of hydrocarbon.

Before starting the experiment, the right accumulator was refilled manually by disconnecting with lines and taking it out of the oven and pouring the crude oil manually into the accumulator by opening the top. After refilling the accumulator it was connected back to the system.

Valve 10 was closed and valve 11 was opened. Keeping the valve 5 closed, pump A&B was run to increase the pressure in right accumulator to 1300 psi. After reaching the pressure, pump was stopped. Valve 5, S1 and S2 were opened. Then, pump A&B was run at a flow rate of 6 ml/min, the total flow rate during foam flood, so the oil flood was performed at the same flow rate. The effluent was collected in the burette and the volume of the aqueous phase (1% 2AM or 8:2 2AM: PECNP solution) was noted.

The differential pressure across sand pack was recorded using lab view software. Reaching the plateau in pressure vs time means we have reached the end of the cleanup process. So the pump was stopped. Valves S1 and S2 were closed to isolate the sand pack from rest of the system. Figure 32 shows the flow path for oil flood highlighted in green color.

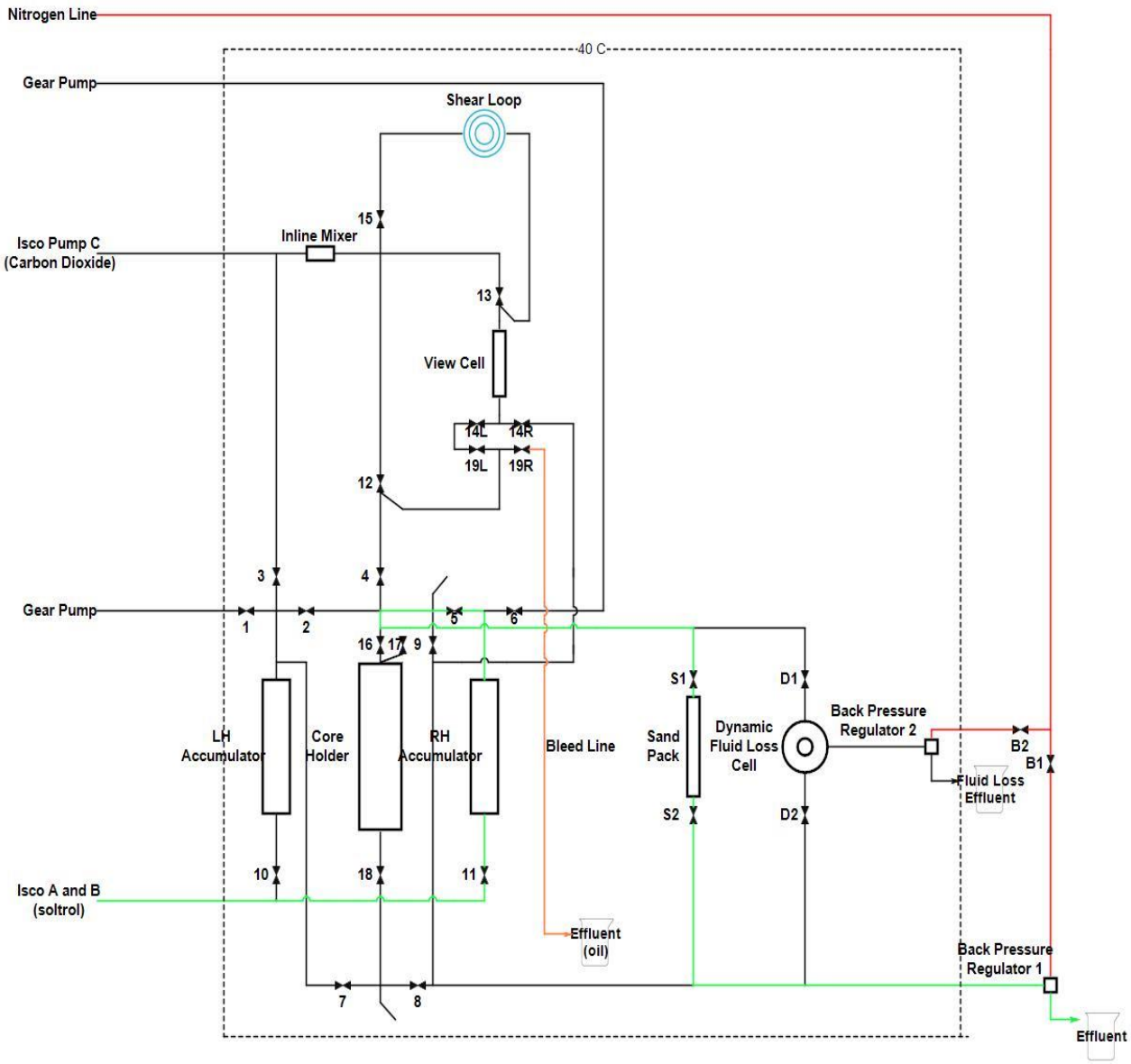

Figure 32. Schematic diagram showing the flow path for oil flood

Depressurizing and cleaning after oil flood:

As the lines contain oil after oil flood, it must be cleaned before performing brine flood. First the system was depressurized by opening valve 10, 11, 3, 12, 4, 13 and 14R, and opening the BPR 1 valve slowly. This path was choose because, sand pack is at a pressure of 1300 psi with crude oil inside, so we had to isolate and maintain the same condition throughout the cleaning process.

Using the aqueous phase solution in the left accumulator the lines were cleaned by opening valve 10, 3, 121, 4 and D1, and running the pump A&B, and the effluent was collected in a beaker. The pump was stopped once the left accumulator was emptied. Figure 33 shows the flow path for cleaning, the flow lines are highlighted using green color.

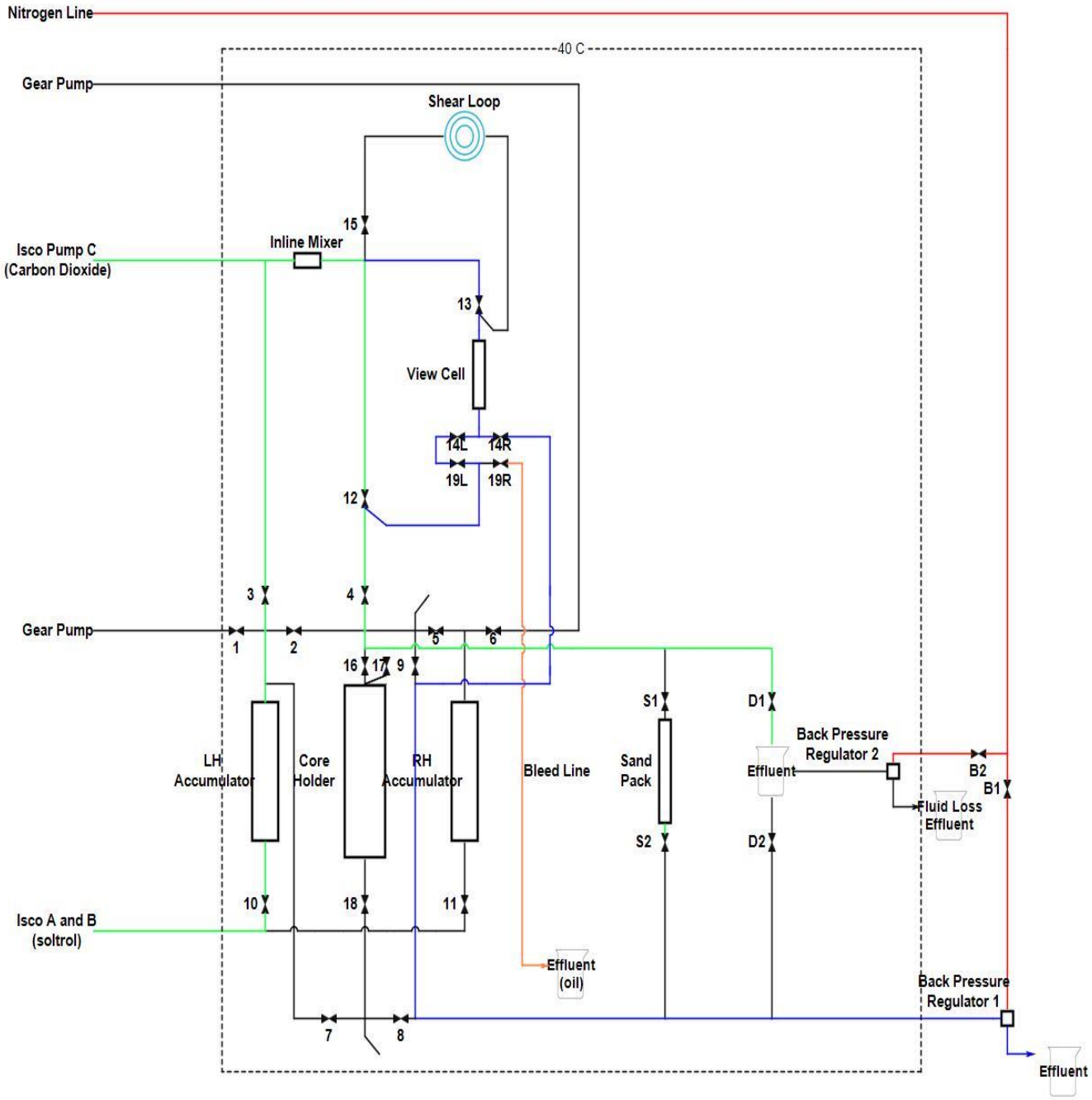

Figure 33. Schematic diagram showing the flow path for cleaning after oil flood highlighted using green color

Brine flood after oil flood:

The left accumulator was filled with brine. Valve 10, 3, 12, 13, 14R and 4 were opened and D1 was closed. Pump A&B was run at a flow rate 5 ml/min, simultaneously pressure was applied to BPR1 in steps of 25 psi through nitrogen. Once the pressure reached 1300 psi, pump was stopped and valve 13 and 14R were closed, while valve S1 and S2 were opened. Pump A&B was run at a flow rate of 6ml/min to perform the brine flood. The flow path for brine flood is shown in Figure 31 and the flow lines are highlighted using green color. The effluent was collected in a burette and the volume of oil collected was noted. The differential pressure across sand pack was recorded using lab view software. Once the pressure plateaued, the pump was stopped.

De pressurizing and cleaning the system after the oil flood:

First all the heaters and the oven was turned off. Then the system was depressurized by opening valve 10, 3, 12, 4, 13, 14R, S1 and S2, and opening the BPR 1 valve slowly. Once the pressure of the system reached less than 20 psi, the left accumulator was emptied. The left accumulator was refilled with RO water. As we used view cell for pressurizing and depressurizing the system, two pathways were used to clean the system. Path way 1 was cleaned by opening valve 10, 3, 12, 4, S1 and S2, and pump A&B was run at a flow rate of 10 ml/min. This is shown using green lines in Figure 33. Path way 2 was cleaned by opening valve 10, 3, 13, 14R, 12, 19L and 14L, and pump A&B was run at a flow rate of 10 ml/min. This is shown using blue lines in Figure 33.

Once the left accumulator was empty, pumps were stopped and all the valves were closed.

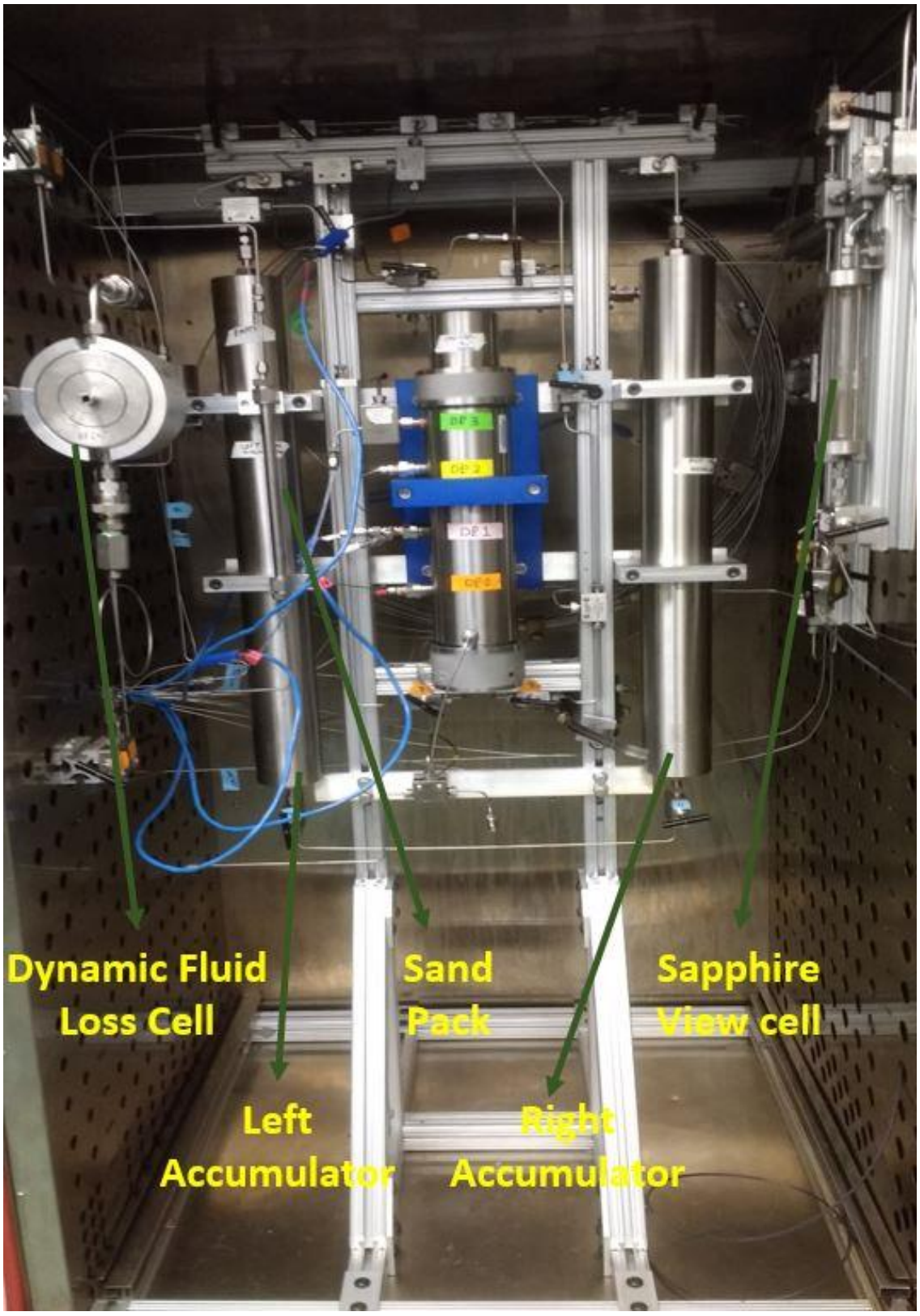

Figure 34. CO_2 foam setup inside the oven

3.3.12 Density and Viscosity Measurement

Density Measurement:

The density of the aqueous phase and oil was measured using Anton Paar Model DMA 4100M density meter. The change of the natural frequency of a hollow oscillator when filled with different fluids helps to find the density. The mass, and thus the density of the liquid or gas changes this natural frequency due to a gross change of the oscillation caused by the introduction of the liquid or gas. The density of the fluid contained in this hollow oscillator is calculated by the measured time period of this oscillation.

Procedure

The instrument was turned on. Before injecting the sample through the port, it was cleaned using RO water and air was pumped after cleaning with RO water. In case of crude oil, it was cleaned using toluene and acetone before pumping air. After cleaning the temperature was set to 40^{o}C and air/water checks were performed. Then the sample was injected and the instrument was run to measure the density. After density measurement, appropriate solvents were used to clean and dry the cell. Port to inject sample is shown in the Figure 35 below.

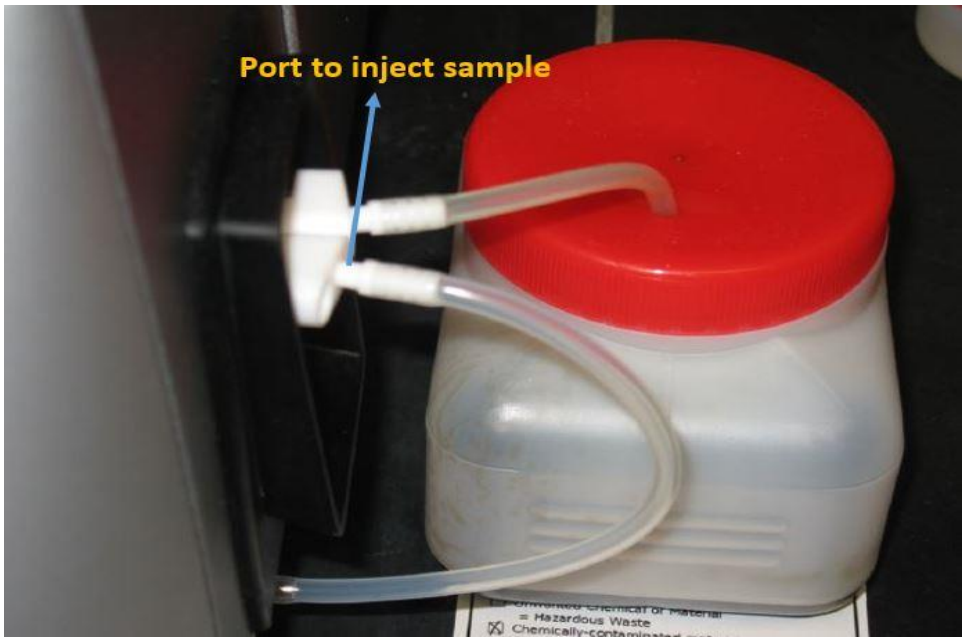

Figure 35. Image of density meter with the port to inject sample

Figure 36. Image of the interface used in the Anton Paar Model DMA 4100M Density meter

Viscosity Measurement:

Brookfield DV-II+Pro viscometer was used to measure the viscosity of crude oil and surfactant solution samples. It's a wells cone and plate viscometer equipped with CP-40 cone. The principle of operation of the viscometer was to drive the spindle immersed in the sample. Spring deflection measures the viscous drag experienced by the spindle. The rotary transducer measures the spring deflection and presents in terms of percentage torque. Based on this measurements all the rheological properties are calculated. Figure 37 shows the image of the viscometer.

Figure 37. Image of the Brookfield DV-II+Pro viscometer

Procedure:

Preparation for viscometer startup:

The viscometer was turned on and auto zero button was pressed. The spindle (CP-40) was installed using a wrench. The gap between the cone and the plate was properly set to allow room for the sample.

Calibration of the viscometer:

The viscometer was calibrated using a standard oil named S20. S20 has a viscosity of 29.25 cP at 25^{o}C.

Measurement:

Temperature was set at 40^{o}C using a temperature control bath. Sample cup was removed and 0.5 ml of sample was poured into it using a syringe. Sample cup was placed back and reference marker was positioned at signed mark. Motor was turned on and desired speed was set. The viscosity was measured between 10-100 percent of torque.

Cleaning:

After measurement the sample cup and cone was cleaned using toluene and acetone if crude oil was the sample, otherwise in case of aqueous sample RO water was used. After cleaning the parts were dried before measuring the viscosity of next sample.

Chapter 4. Results and Discussion

4.1 Vial Tests

Vial tests were used as the first screening criteria to determine optimized polyelectrolyte complex ratios. Next, the optimized systems were measured for their zeta potential and effective diameter. PEI: DS: 2% NaCl ratios of 4:1:0.1, 3:1:0.1, 2:1:0.1 and 1:1:0.1, with PEI pH of 8, 8.5 and 9 were used to prepare surfactant-PECNP solutions. This gave 12 different systems, in addition to this, 3 more systems of PEI-surfactant was prepared with PEI pH of 8, 8.5 and 9. In all the above solutions final concentration of surfactant was 1 wt%. This 15 different systems were tested to choose the optimized PECNP ratios for further screening through zeta potential measurements.

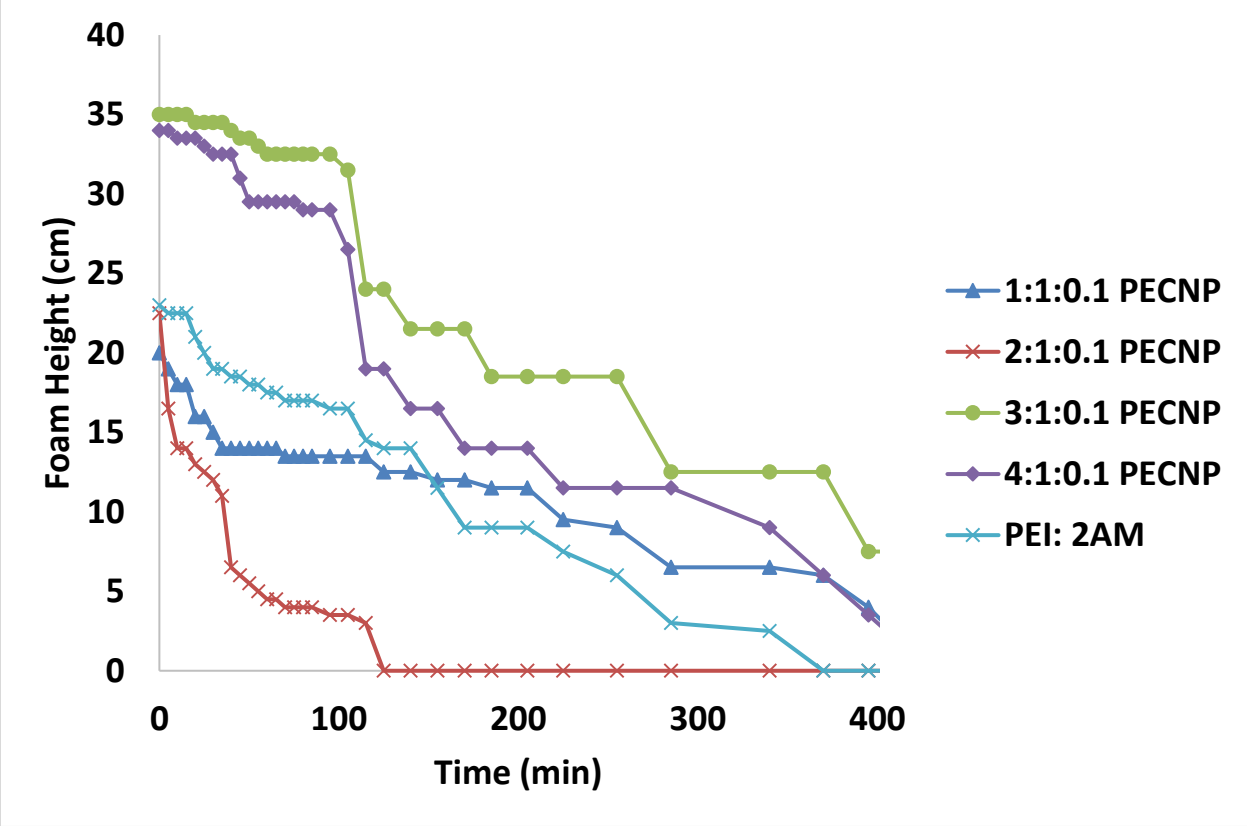

Figure 38. Foam height vs time for different PEI: DS: 2% NaCl systems with PEI pH of 8

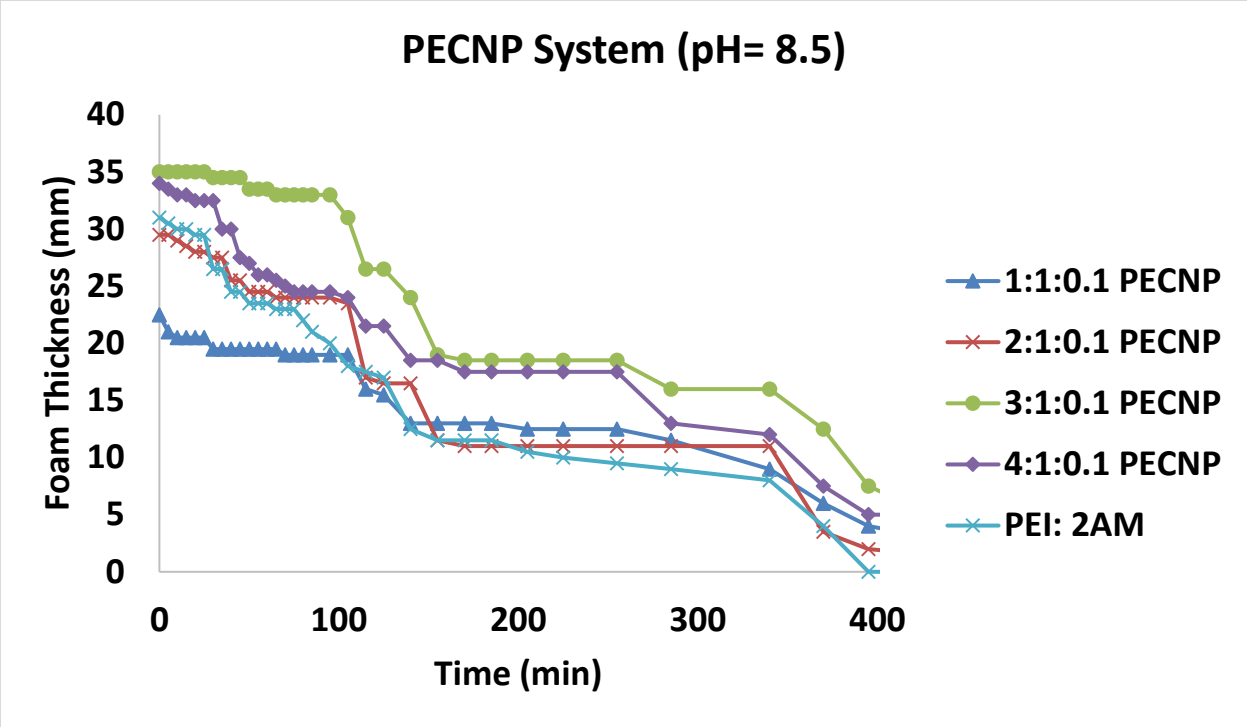

Figure 39. Foam height vs time for different PEI: DS: 2% NaCl systems with PEI pH of 8.5

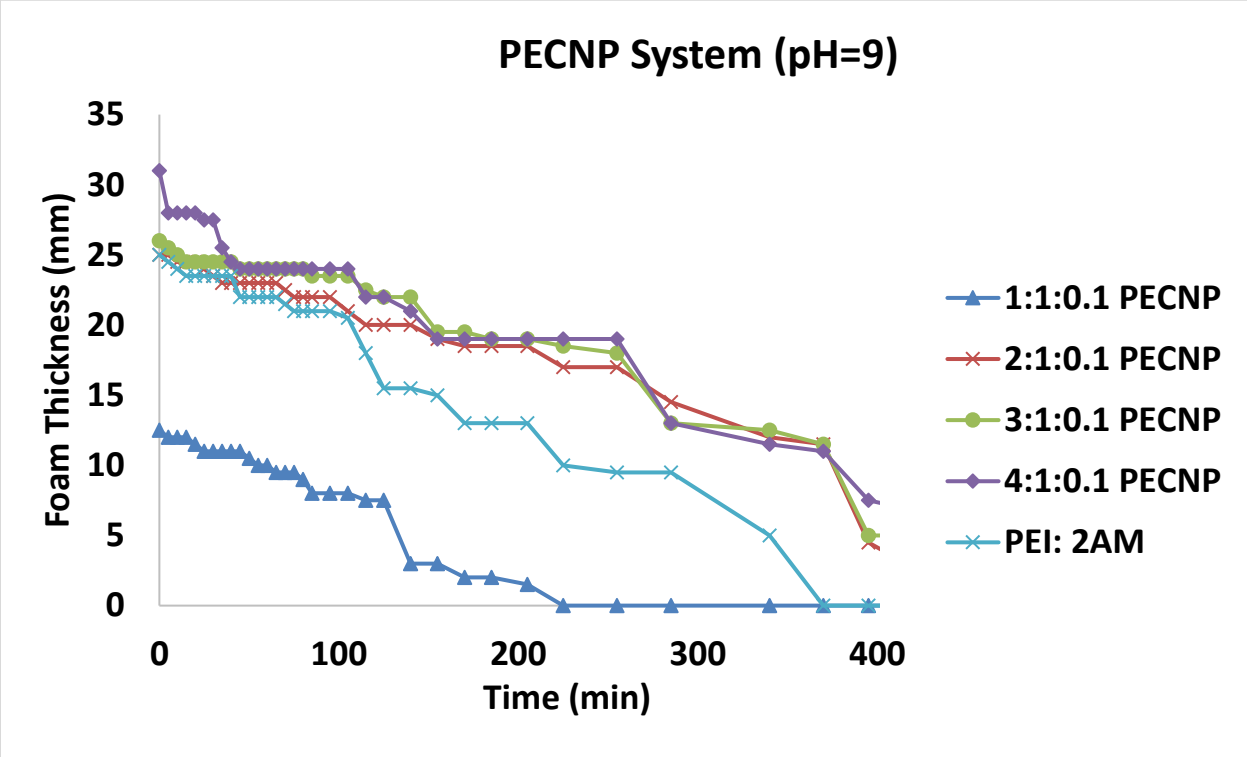

Figure 40. Foam height vs time for different PEI: DS: 2% NaCl systems with PEI pH of 9

It is clear from Figure 38, Figure 39 and Figure 40 that PEI: DS: 2% NaCl ratios of 4:1:0.1 and 3:1:0.1 gave the most optimized results in all three different pH of PEI. Therefore, these two ratios of PEI were tested for zeta potential and effective diameter.

4.2 Zeta Potential and Particle Size Measurements

Zeta potential test was used as the second screening test to determine the most optimum system of pH of 1wt% PEI, PECNP and surfactant: PECNP. Later, these optimized systems were used to perform the IFT, rheology and view cell tests. PECNP systems tested were of 3:1:0.1 and 4:1:0.1 ratios of PEI: DS: 2% NaCl with 1 wt% PEI pH of 8, 8.5, 9 and 9.5. The most optimized PECNP system based on this test was used to prepare surfactant-PECNP solutions. Surfactant-PECNP systems tested were from 9:1 to 3:7 of 2AM: PECNP ratios.

Surfactants increase electrostatic repulsive forces in foams to provide stability (Schramm L. L., 2000), but drainage of the surfactant from the interface destabilizes the foam (Koetz J. a., 2006). Zeta potential measures the electro kinetic motion of the particles away from the charged inner surface. Degree of colloidal stability is directly impacted by the magnitude of zeta potential.

Many aspects of the flow behavior colloidal suspension and stability of particles towards coagulation is determined by the interaction between charged particles and potential distribution. Electrostatic repulsion is increased by increase in zeta potential, this results in a more stable foam. (Moayedi, 2011) (Hunter, Zeta Potential in Colloid Science: Principles and Application, 1988). A measure of degree of non-uniformity of distribution of the particle sizes or heterogeneity in the colloidal dispersion is polydispersity.

Table 2. Effective diameter, polydispersity and zeta potential of different PECNP ratios and pH of 1wt% PEI prepared using 2 wt% NaCl

PECNP	pH	Effective Diameter (nm)	Polydispersity	Zeta Potential (mV)
3:1:0.1	8	223.99 ± 2.21	0.178 ± 0.078	22.63 ± 1.32
3:1:0.1	**8.5**	**177.38 ± 1.09**	**0.268 ± 0.014**	**24.37 ± 1.22**
3:1:0.1	9	157.28 ± 2.31	0.232 ± 0.005	13.84 ± 1.86
3:1:0.1	9.5	180.63 ± 1.06	0.142 ± 0.012	11.29 ± 2.34
4:1:0.1	8	164.59 ± 0.29	0.243 ± 0.006	11.39 ± 0.65
4:1:0.1	8.5	162.38 ± 0.75	0.263 ± 0.011	16.24 ± 2.48
4:1:0.1	9	164.84 ± 1.55	0.542 ± 0.110	14.09 ± 2.99
4:1:0.1	9.5	177.2 ±1.02	0.180 ± 0.003	10.97 ± 1.15

From Table 2, it is clear that PECNP ratio of 3:1:0.1 of PEI: DS: 2% NaCl at 1 wt% PEI (pH of 8.5) showed the highest zeta potential. Therefore, this system of PECNP was used to prepare different ratios of surfactant-PECNP solutions for the next zeta potential test. In Table 2 and Table 3 the most optimum systems are highlighted.

Table 3. Effective diameter, polydispersity and zeta potential of different surfactant-PECNP systems prepared using PECNP ratio of 3:1:0.1 with PEI pH of 8.5

2AM Solution: PECNP	Effective Diameter (nm)	Polydispersity	Zeta Potential (mV)
9:1	**214.15 ± 3.78**	**0.207 ± 0.010**	**24.42 ± 2.32**
8:2	**173.56 ± 1.01**	**0.246 ± 0.015**	**19.45 ± 1.54**
7:3	**185.82 ± 1.72**	**0.198 ± 0.003**	**19.90 ± 1.13**
6:4	**186.58 ± 0.66**	**0.203 ± 0.010**	**19.81 ± 1.28**
5:5	180.76 ± 0.22	0.205 ± 0.005	14.44 ± 4.04
4:6	189.63 ± 1.81	0.212 ± 0.008	14.17 ± 0.18
3:7	188.18 ± 1.72	0.220 ± 0.012	14.28 ± 1.74

Based on the results shown in Table 3, among seven different systems of surfactant-PECNP, ratios of 9:1. 8:2, 7:3 and 6:4 showed the highest zeta potential.

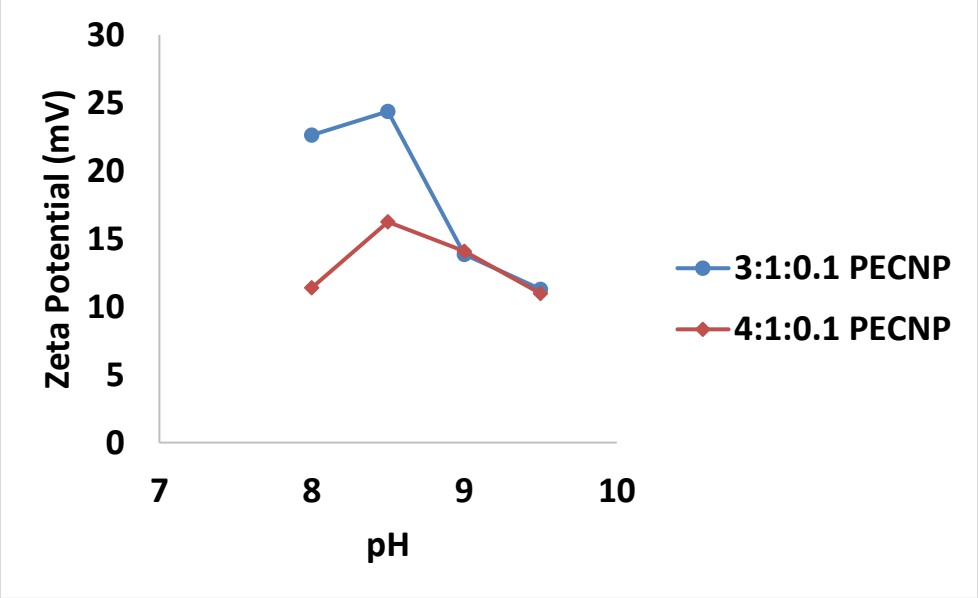

Figure 41. Zeta potential vs pH for different PECNP ratios

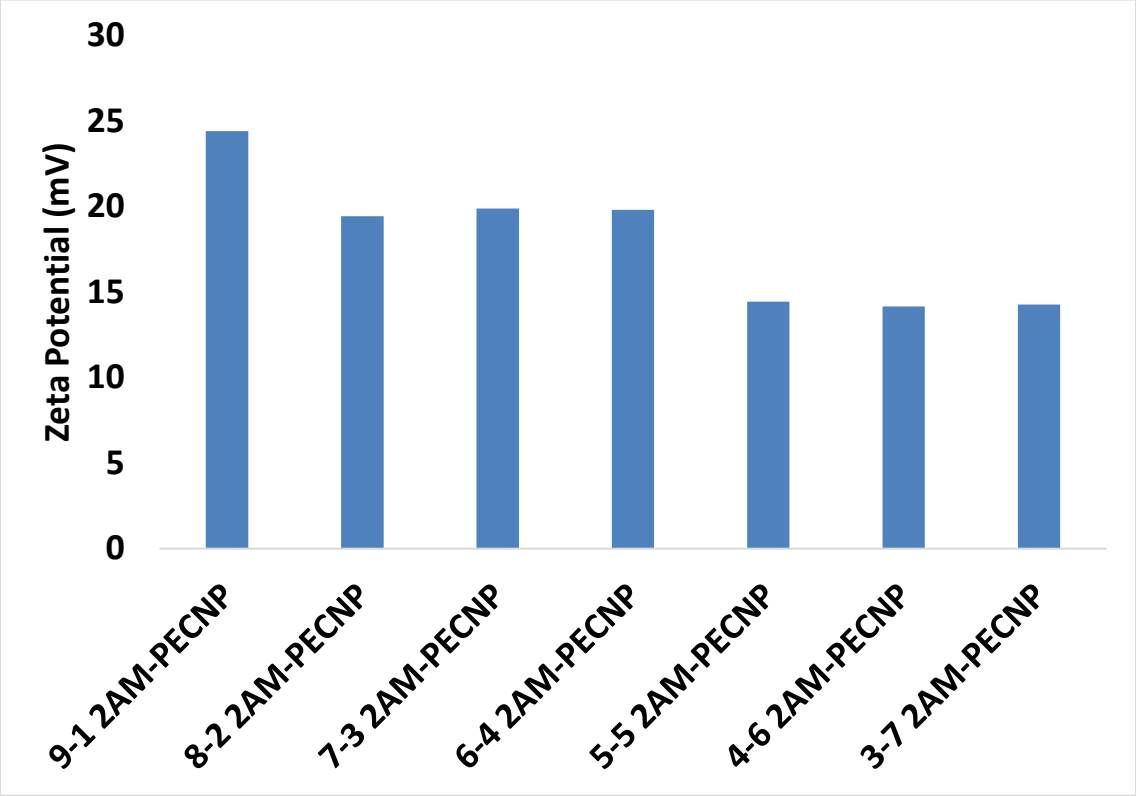

Figure 42. Zeta potential of different surfactant-PECNP system

Figure 41 and Figure 42 are the graphical representations of Table 2 and Table 3. It can be observed that surfactant-PECNP ratios of 9:1, 8:2, 7:3 and 6:4 prepared using PECNP ratio of 3:1:0.1 of PEI: DS: 2% NaCl with PEI pH of 8.5 was the most optimum system. Therefore, these systems were used to prepare CO_2 foams of different quality to perform rheology and view cell tests.

4.3 Interfacial Tension Measurements

Interfacial tension exists when two phases are present. Interfacial tension is the force that holds the surface of a particular phase together. The main forces involved in interfacial tension are adhesive forces (tension) between the liquid phase of one substance and either a solid, liquid or gas phase of another substance. IFT is the Gibbs free energy per unit area of interface at a fixed temperature and pressure. IFT occurs because a molecule near an interface has different molecular interaction than an equivalent molecule within the bulk fluid. Surfactant molecules preferentially position themselves at the interface and thereby lower the interfacial tension (Schramm L. L., 2000). The common units for surface tension are dynes/cm or mN/m.

The critical micelle concentration (CMC) of 2AM is 300 ppm (obtained from MSDS sheet). As the application of this research is hydraulic fracturing, in all the 2AM-PECNP solutions, the final concentration of 2AM was 1 wt% which is above CMC.

Tests were performed for both Air-aqueous phase and $scCO_2$-aqueous phase. Aqueous phase solutions were 2AM-PECNP ratios of 9:1, 8:2, 7:3 and 6:4 and just surfactant solution with no PECNP (1 wt% 2AM). The PECNP ratio was 3:1:0.1 with PEI pH of 8.5.As the measured IFT was dynamic in nature, plot of IFT vs time was plotted.

4.3.1 Air-Aqueous Phase Results

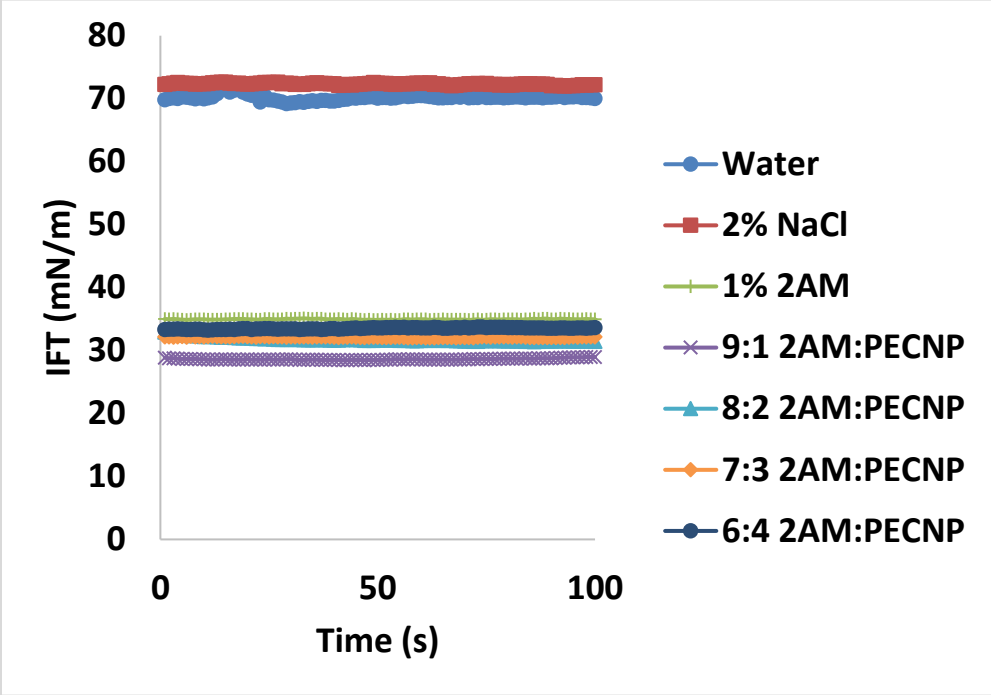

Figure 43. IFT vs time for different surfactant-PECNP system as the aqueous phase and air as the gaseous phase

Aqueous phase	Mean IFT (mN/m)
RO Water	70.17
Brine (2% NaCl)	72.34
1% 2AM (Surfactant)	34.95
9:1 2AM:PECNP	**28.63**
8:2 2AM:PECNP	**31.76**
7:3 2AM:PECNP	32.13
6:4 2AM:PECNP	33.52

Table 4. Mean IFT for different surfactant-PECNP system as the aqueous phase and air as the gaseous phase

From Table 4 and Figure 43 it can be observed that salinity increases IFT, as brine has higher IFT than RO water. Due to preferential positioning of surfactant molecules in the interface, adding surfactant to the brine drastically reduced the IFT. However, adding PECNP further reduced the IFT even further, with surfactant-PECNP ratios of 9:1 and 8:2 having the lowest value of IFT.

4.3.2 scCO$_2$- Aqueous Phase Results

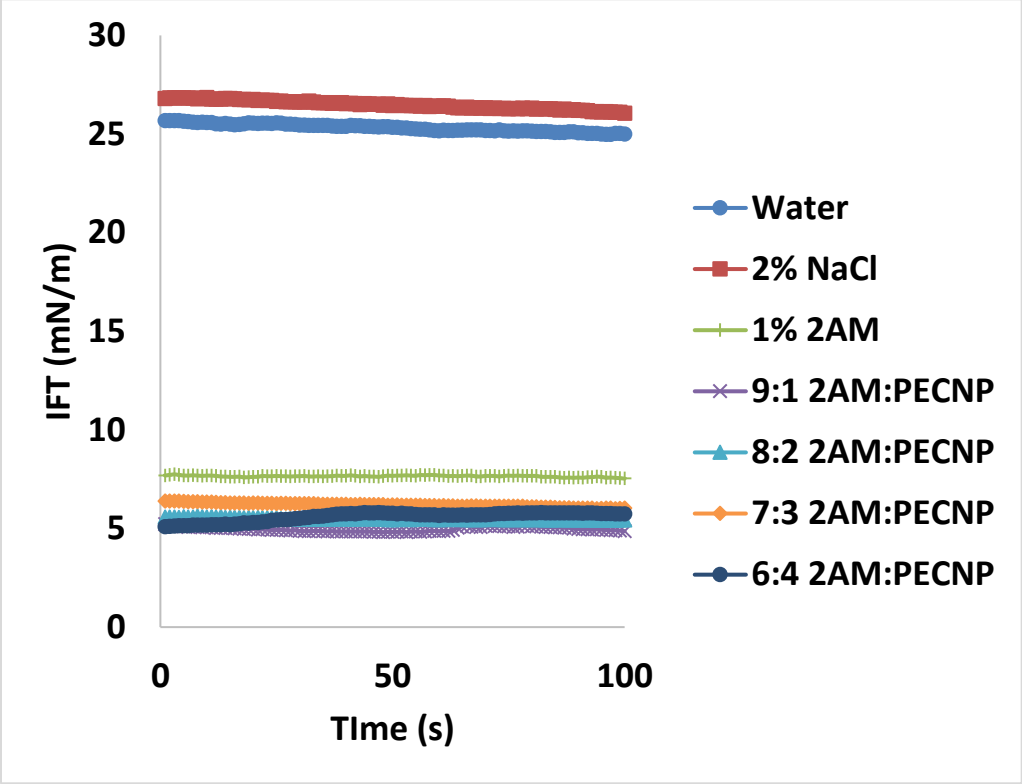

Figure 44. IFT vs time for different surfactant-PECNP systems as the aqueous phase and supercritical CO$_2$

Aqueous phase	Mean IFT (mN/m)
RO Water	25.32
Brine (2% NaCl)	31.04
1% 2AM (Surfactant)	7.65
9:1 2AM:PECNP	**4.97**
8:2 2AM:PECNP	**5.48**
7:3 2AM:PECNP	6.18
6:4 2AM:PECNP	5.59

Table 5. Mean IFT for different surfactant-PECNP systems as the aqueous phase and supercritical CO_2.

IFT study of CO_2- aqueous phase followed the same trend as air-aqueous phase. From Figure 44 and Table 5, it can be observed that salinity increases IFT, as brine has higher IFT than RO water with $scCO_2$. Due to preferential positioning of surfactant molecules in the interface, adding surfactant to the brine drastically reduced the IFT. However, adding PECNP further reduced the IFT, with surfactant-PECNP ratios of 9:1 and 8:2 having the lowest value of IFT.

Overall all the systems of $scCO_2$- aqueous phase had lower IFT than air-aqueous phase. Adding surfactant reduced the IFT and surfactant-PECNP ratio of 9:1 and 8:2 showed the lowest IFT in both the CO_2- aqueous phase and air-aqueous phase IFT measurements.

4.3 Rheology Measurements

Viscosity of the fracturing fluid is a very important parameter to suspend, transport and deliver the proppant to the fracture. Three main reasons to perform the rheological measurements of $scCO_2$ foams are:

1) Effect of addition of PECNP on viscosity of supercritical CO_2 foam at 70%, 80%, 90% and 95% foam qualities.

2) To find the most optimum surfactant-PECNP ratio

3) To investigate the effect of foam quality on viscosity

The viscosity of the foam provides resistance to prevent the foam from rupturing. The bulk viscosity and surface viscosity directly influence the thinning of the common black film and newton black film, respectively, and film stability controls the stability of the foam (Schramm L. L., 2000). As the CO_2 used to generate the foam is in supercritical state it's very difficult to measure the interfacial viscosity. Thus, only the bulk viscosity is measured in the rheological experiment.

For the hydraulic fracturing application, it's important to understand the rheological properties of the fracturing fluid. Low viscous fracturing fluids such as slickwater might fail to effectively carry proppants and highly viscous fracturing fluids such as crosslinked gel might damage the fracture conductivity and have a negative impact on the productivity of well (Barati, 2010) (Barati., 2014). Therefore, the study of rheological properties of CO_2 foam is important for its application as fracturing fluid.

4.3.1 Dynamic Test

In the dynamic test, foam was generated continuously and its viscosity was measured against time. The flow rate of foam for all the dynamic tests was 6 ml/min. Depending on the foam quality,

$scCO_2$ and aqueous phase flow rates were adjusted. For example, to generate 80% foam quality, CO_2 was pumped at a flow rate of 4.8 ml/min and aqueous phase was pumped at a flow rate to 1.2 ml/min, which resulted in a total flow rate of 6 ml/min.

As the foam is generated continuously and injected into the measuring cup, a perpendicular force is provided to the foam at the given flow rate in addition to the torque applied by the spindle to shear the foam. Foam was sheared at 2000 s^{-1}.

Effect of PECNP on viscosity of CO_2 foam for a given foam quality:

Supercritical CO_2 foam systems of quality 70%, 80%, 90% and 95% generated by different surfactant-PECNP systems that are compared in Figure 45 to Figure 48. It can be observed from these graphs that:

1) Addition of PECNP resulted in a significant increase in the viscosity of the foam.

2) Surfactant-PECNP ratio of 8:2 is the most optimal system for all the four foam qualities.

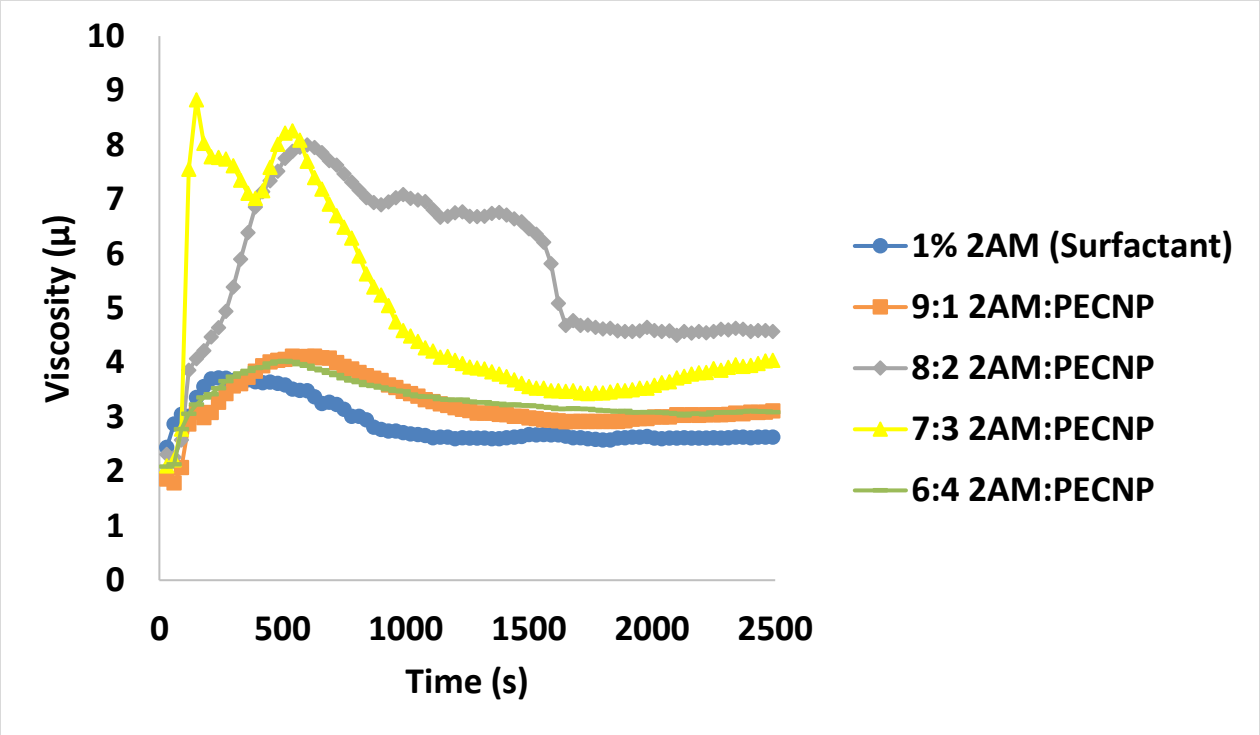

Figure 45. Viscosity vs time for different surfactant-PECNP systems at 70% foam quality under constant shear for dynamic test with foam generated continuously at 6 ml/min

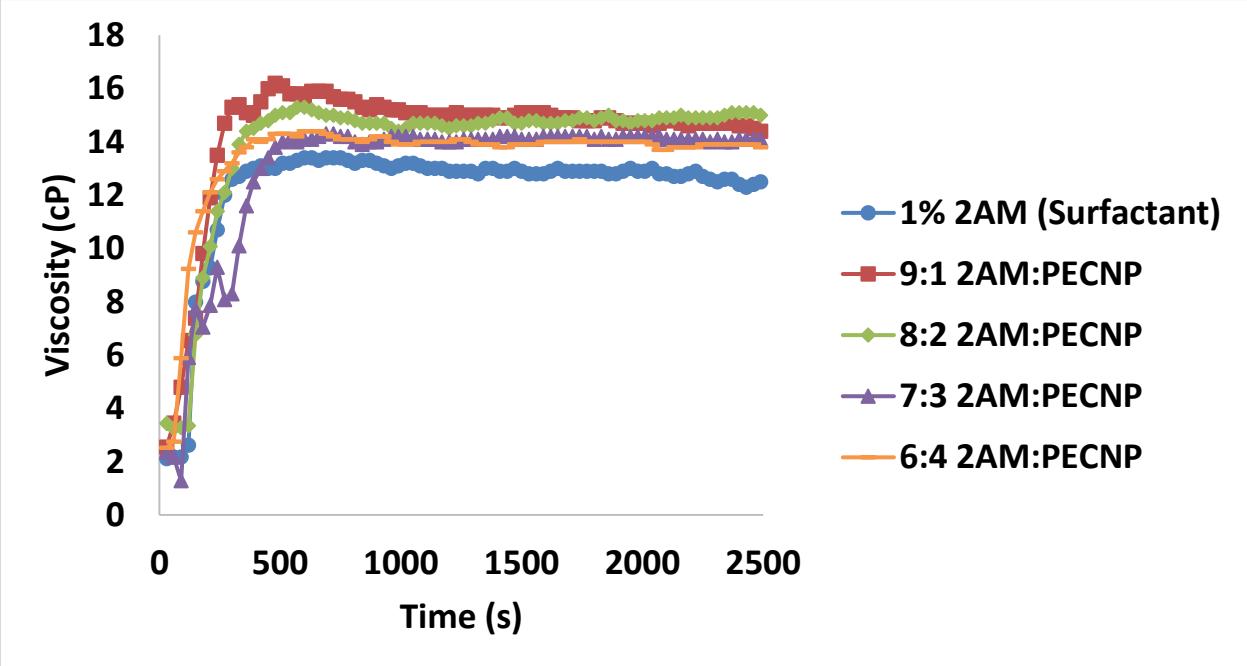

Figure 46. Viscosity vs time for different surfactant-PECNP systems at 80% foam quality under constant shear for dynamic test with foam generated continuously at 6 ml/min

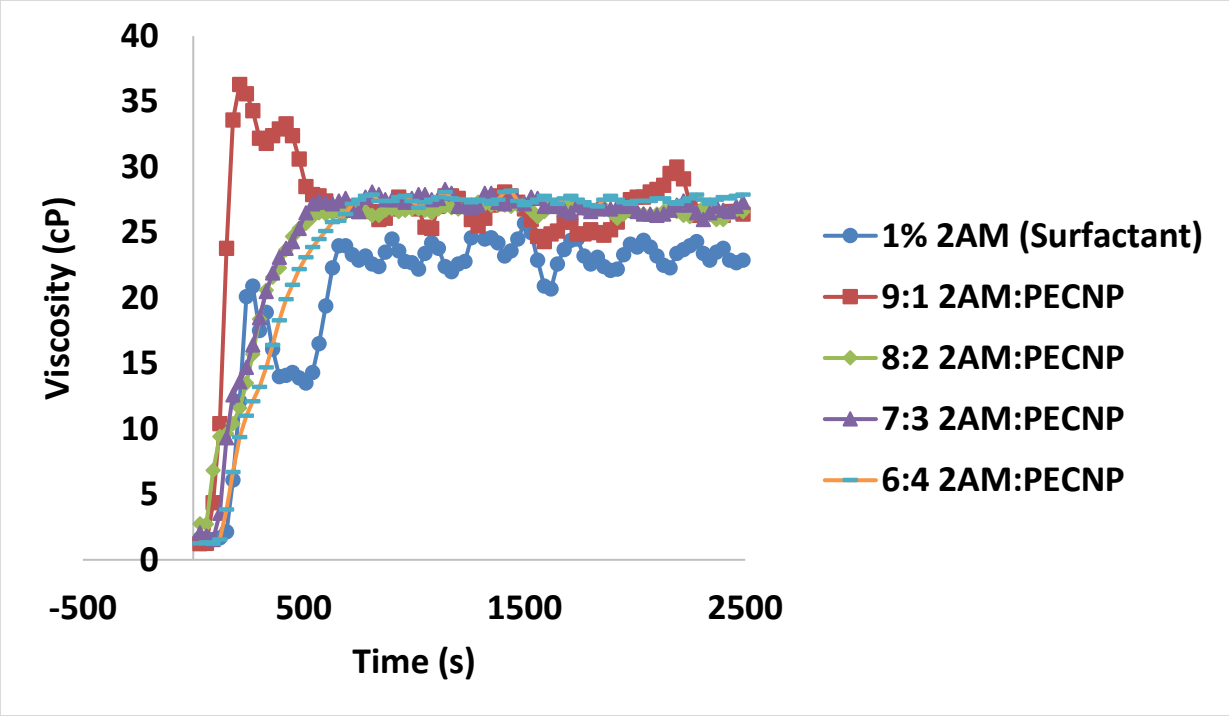

Figure 47. Viscosity vs time for different surfactant-PECNP systems at 90% foam quality under constant shear for dynamic test with foam generated continuously at 6 ml/min

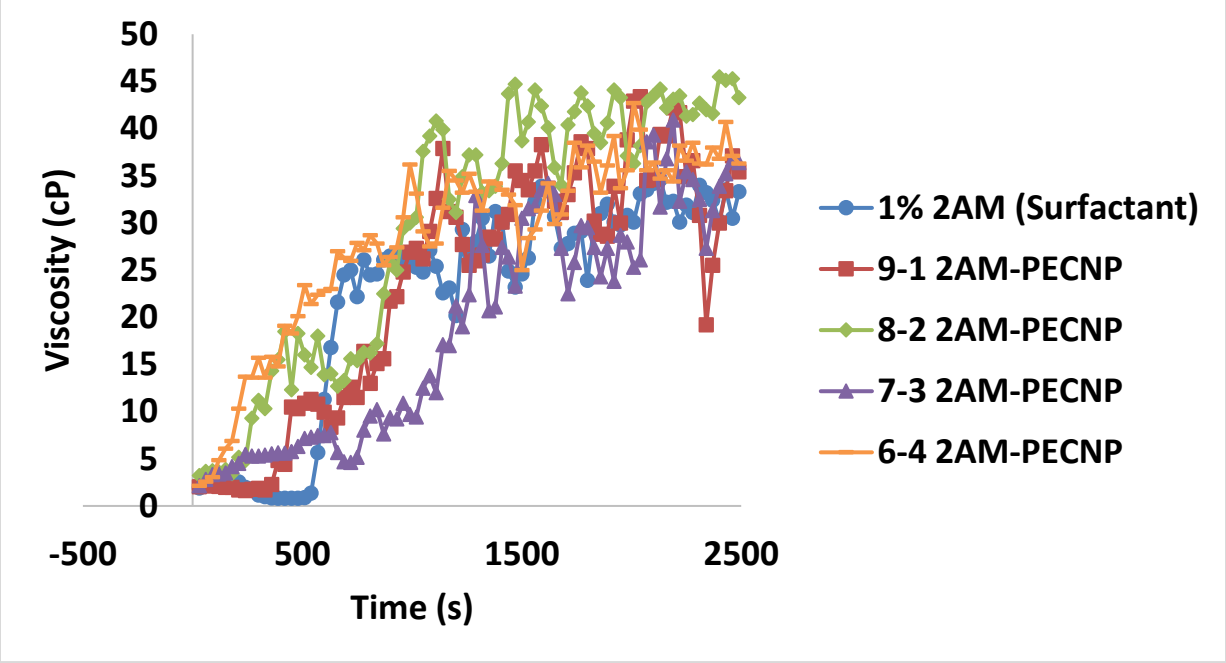

Figure 48. Viscosity vs time for different surfactant-PECNP systems at 95% foam quality under constant shear for dynamic test with foam generated continuously at 6 ml/min

Effect of foam quality on viscosity of CO_2 foam:

Influence of foam quality on viscosity of CO_2 foam generated by 8:2 2AM: PECNP as the aqueous phase is shown Figure 49 below.

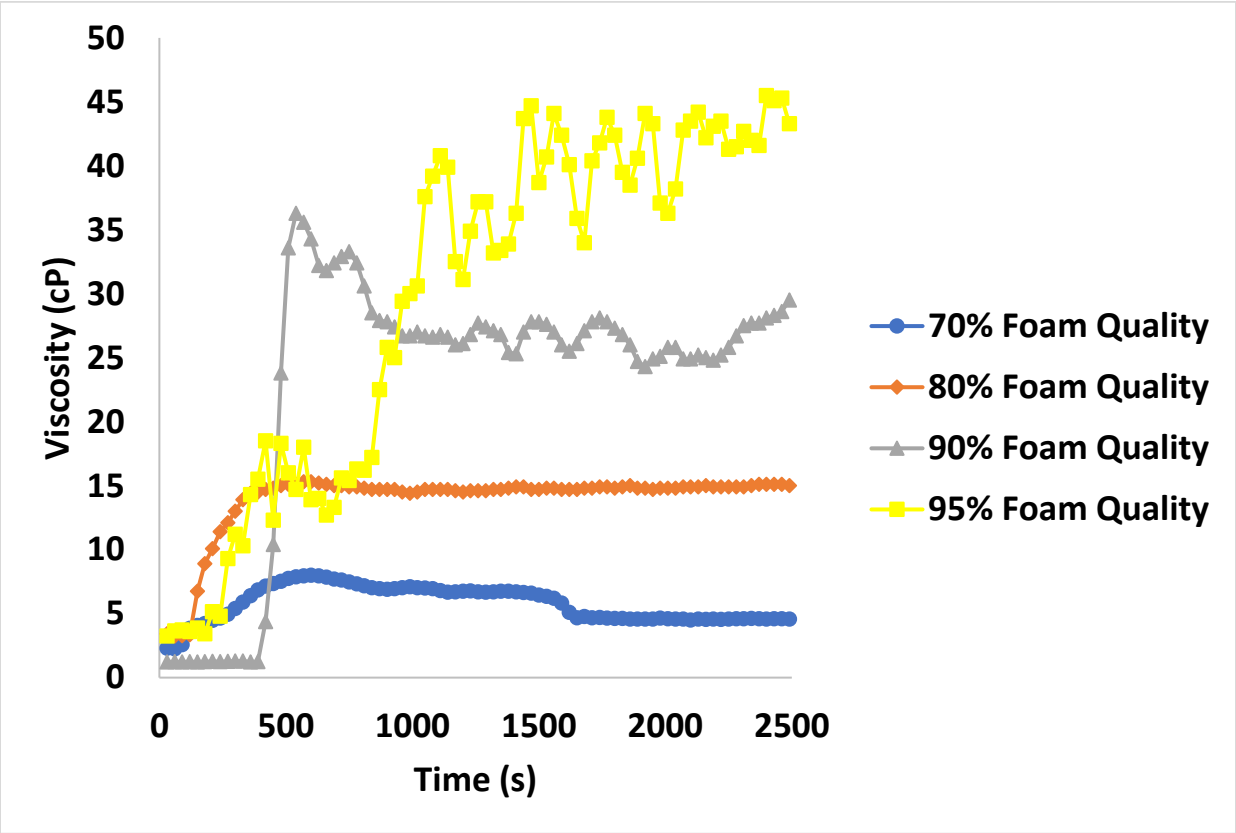

Figure 49. Viscosity vs time for optimal surfactant-PECNP systems in each of the four different foam quality under constant shear for dynamic test with foam generated continuously at 6 ml/min

It can be observed from Figure 49 that increasing the foam quality increased the viscosity of the CO_2 foam.

4.3.2 Static Test

After the dynamic test, foam generation was stopped and, valves before and after the measuring cups were closed to isolate the measuring cup with CO_2 present in the annulus. This foam was sheared under constant shear rate of 2000 s^{-1} to measure the viscosity with time. Effect of PECNP and the foam quality on viscosity was studied.

Effect of PECNP on viscosity of CO_2 foam for a given foam quality:

From Figure 50 to Figure 53, it can be observed that static test results were similar to dynamic test results, i.e. addition of PECNP significantly increased the viscosity of the $scCO_2$ foam.

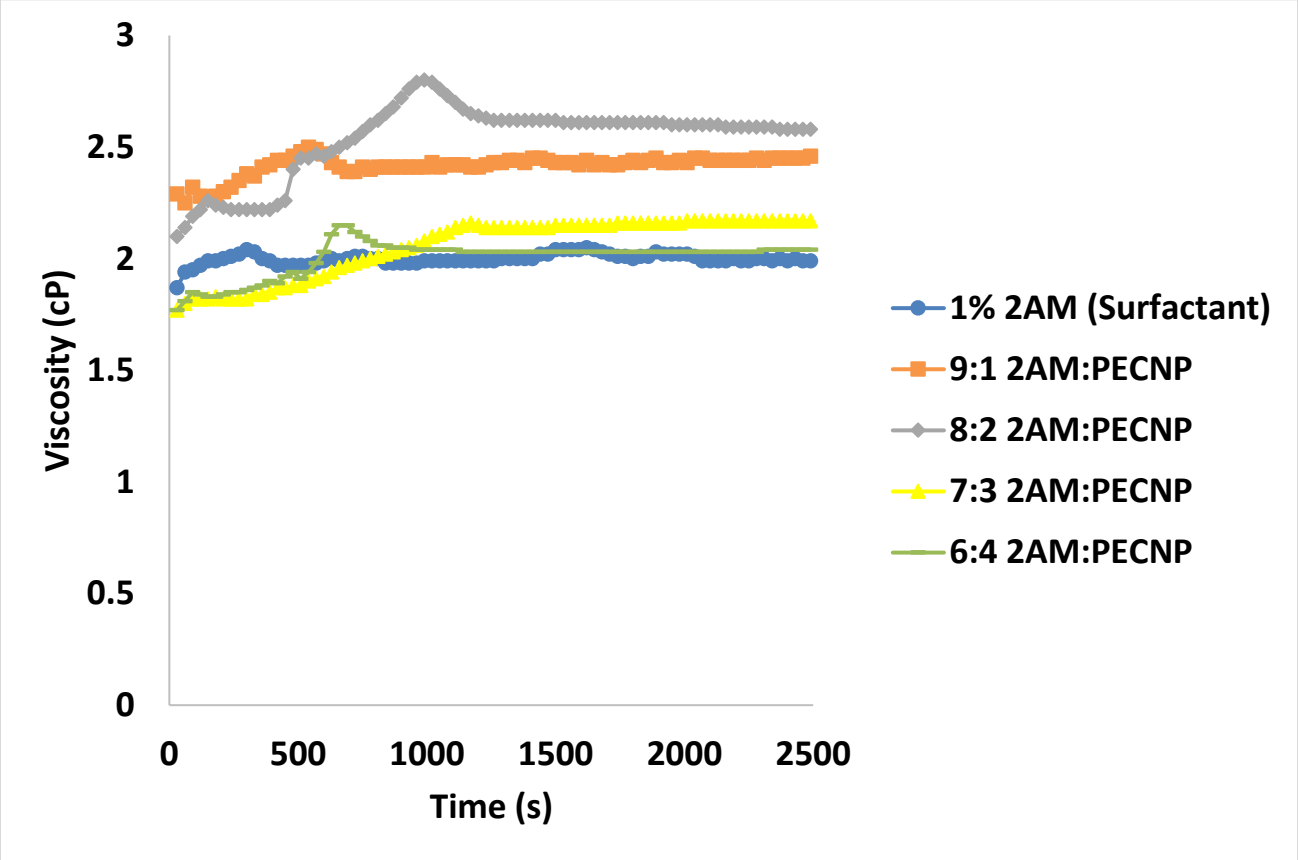

Figure 50. Viscosity vs time for different surfactant-PECNP systems at 70% foam quality under constant shear for static test

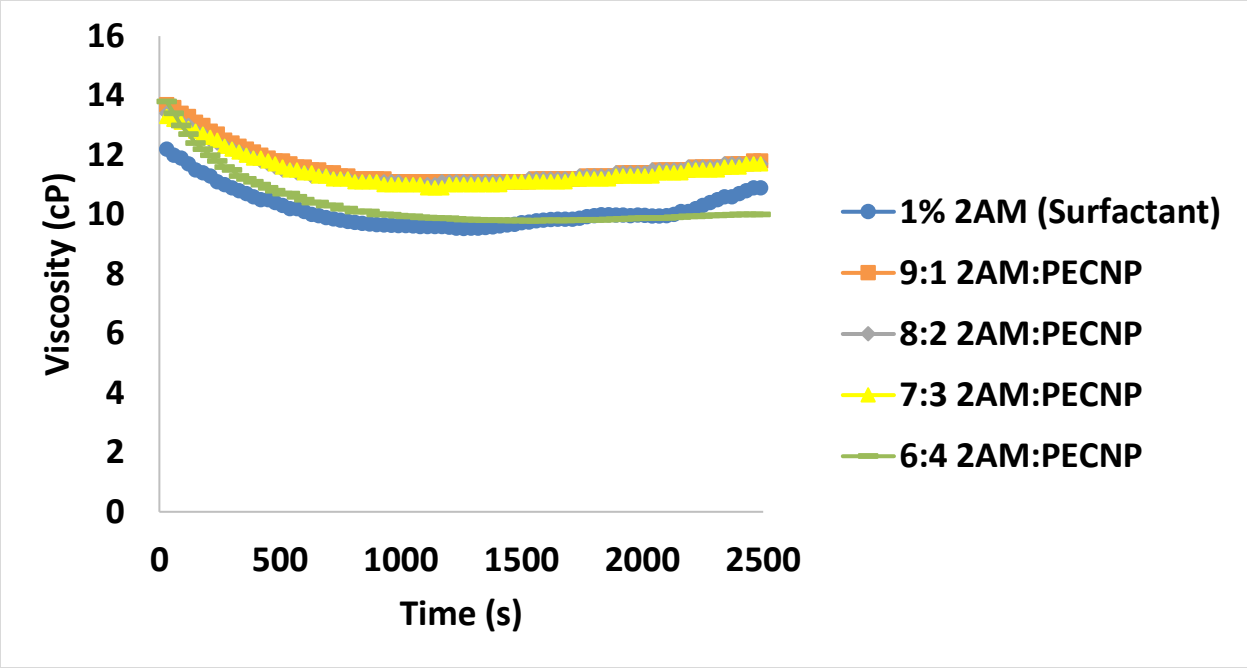

Figure 51. Viscosity vs time for different surfactant-PECNP systems at 80% foam quality under constant shear for static test

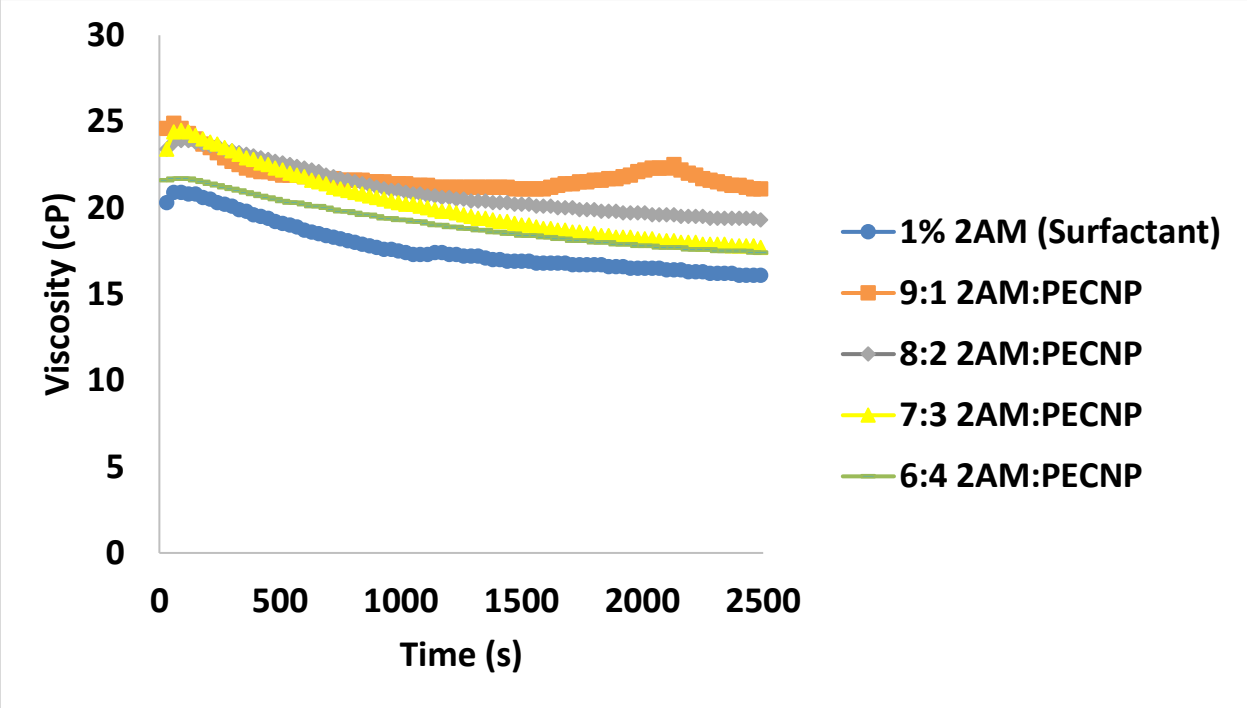

Figure 52. Viscosity vs time for different surfactant-PECNP systems at 90% foam quality under constant shear for static test

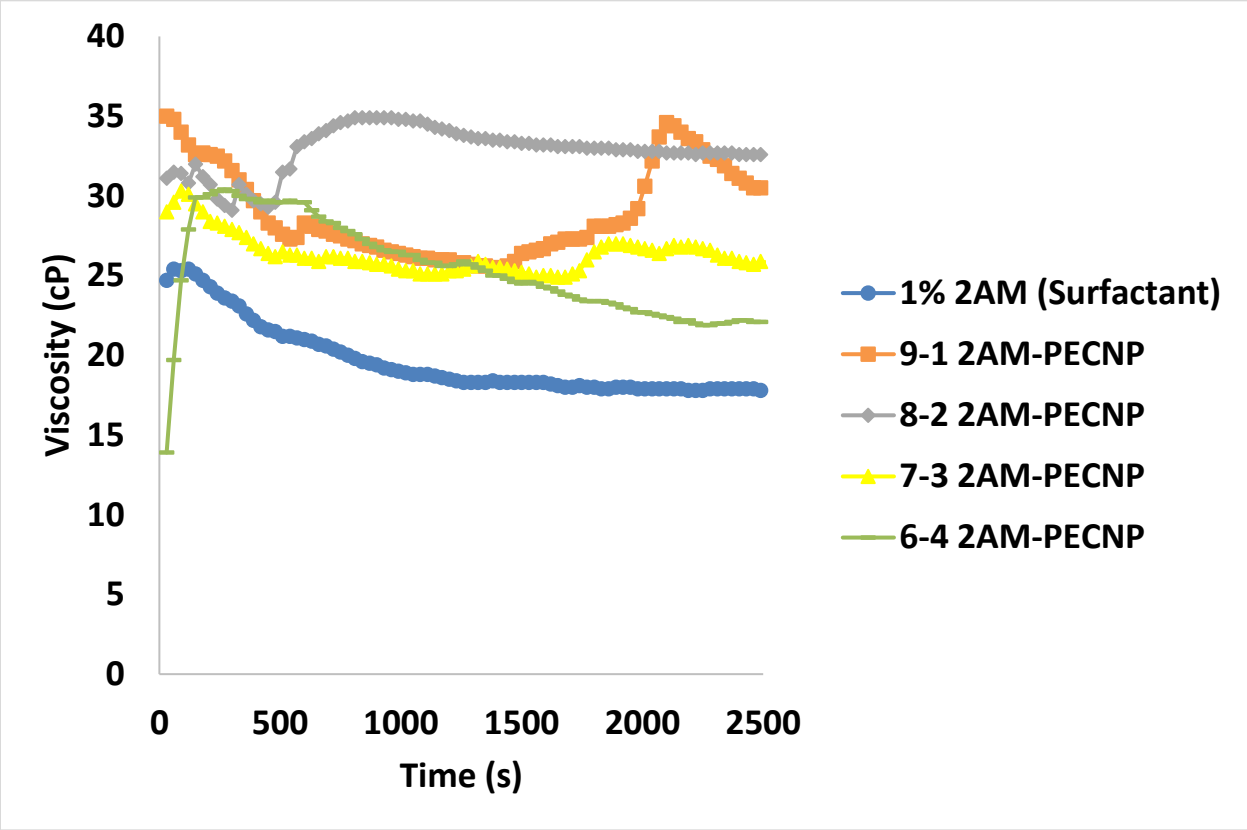

Figure 53. Viscosity vs time for different surfactant-PECNP systems at 95% foam quality under constant shear for static test

Effect of foam quality on viscosity of scCO$_2$ foam:

Influence of foam quality on viscosity of CO_2 foam generated by 8:2 2AM: PECNP as the aqueous phase is shown Figure 54.

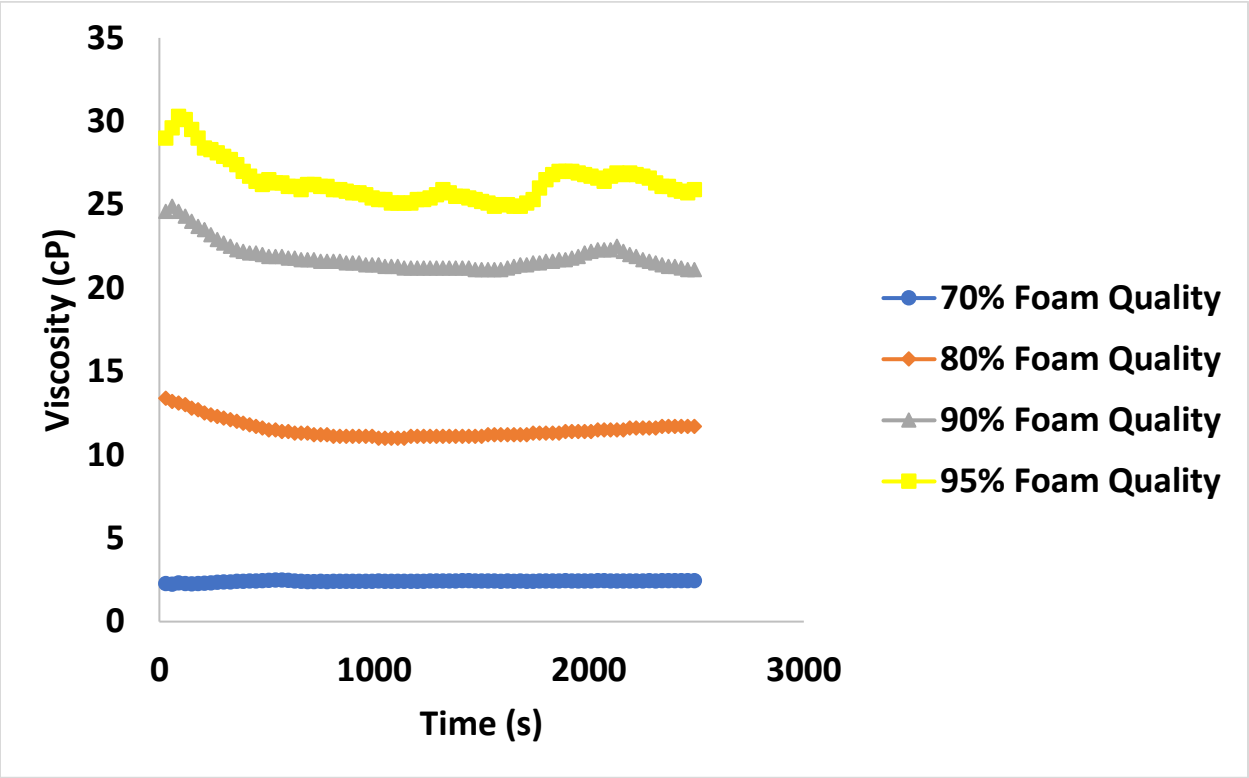

Figure 54. Viscosity vs time for optimal surfactant-PECNP systems in each of the four different foam quality under constant shear rate for static test

It can be observed from Figure 54 that increase in foam quality increased the viscosity of the CO_2 foam.

4.3.3 Ramp Test

After the static test, ramp test was performed on the $scCO_2$ foam. In this test, shear sweep from 2000 s^{-1} to 100 s^{-1} and again back from 100 s^{-1} to 2000 s^{-1} was performed on different foam systems. Based on this, flow consistency index (K) and flow behavior index (n) was found using Ostwald-de Waele equation (power-law model).

$$\mu_{eff} = K\,\gamma^{\,n-1}$$

Table 6. Summary of flow behavior index and flow consistency index for different surfactant-PECNP systems of 70% foam quality obtained from the ramp test

Foam System	n	K	R^2
1% 2AM-Reference	0.544	22.715	0.979
9:1 2AM:PECNP	0.549	43.084	0.965
8:2 2AM:PECNP	**0.468**	**49.399**	**0.978**
7:3 2AM:PECNP	0.518	44.881	0.955
6:4 2AM:PECNP	0.609	19.339	0.992

Table 7. Summary of flow behavior index and flow consistency index for different surfactant-PECNP systems of 80% foam quality obtained from the ramp test

Foam System	n	K	R^2
1% 2AM-Reference	0.568	296.68	0.993
9:1 2AM:PECNP	0.516	364.29	0.981
8:2 2AM:PECNP	**0.487**	**453.77**	**0.993**
7:3 2AM:PECNP	0.536	352.34	0.997
6:4 2AM:PECNP	0.533	353.21	0.994

Table 8. Summary of flow behavior index and flow consistency index for different surfactant-PECNP systems of 90% foam quality obtained from the ramp test

Foam System	n	K	R^2
1% 2AM-Reference	0.569	389.59	0.998
9:1 2AM:PECNP	**0.569**	**463.26**	**0.998**
8:2 2AM:PECNP	0.575	397.58	0.997
7:3 2AM:PECNP	0.568	431.13	0.995
6:4 2AM:PECNP	0.563	415.32	0.994

Table 9. . Summary of flow behavior index and flow consistency index for different surfactant-PECNP systems of 95% foam quality obtained from the ramp test

Foam System	n	K	R^2
1% 2AM-Reference	0.691	321.68	0.998
9:1 2AM:PECNP	0.568	429.42	0.978
8:2 2AM:PECNP	**0.549**	**584.17**	**0.998**
7:3 2AM:PECNP	0.468	487.37	0.998
6:4 2AM:PECNP	0.543	525.16	0.995

From Table 6 and Table 9, it can be observed that:

1) As the flow behavior index for all the systems in less than one, CO_2 is a shear thinning or pseudo plastic fluid.

2) Addition of PECNP significantly increased the flow consistency index.

3) Increase in the foam quality increased the foam consistency index.

4.4 View Cell Test

View cell test was performed on foam generated by different surfactant-PECNP systems both with and without crude oil. Foam height with time was monitored in an isolated view cell. The main purpose of performing the view cell test are to understand the following.

1) The effect of addition of PECNP on stability of supercritical $scCO_2$ foam for 70%, 80%, 90% and 95% foam qualities.

2) To find the most optimum surfactant-PECNP ratio.

3) Effect of foam quality on stability of CO_2 foam

4) The behavior of foam in the presence of crude oil

4.4.1 View Cell Test with No Oil

Supercritical CO_2 foam systems of quality 70%, 80%, 90% and 95% generated by different surfactant-PECNP systems are compared in the Figure 55 to Figure 58. It can be observed from these graphs that:

1) Addition of PECNP resulted in a significant increase in the stability of the foam in all the four different foam qualities.

2) Surfactant-PECNP ratio of 8:2 is the most optimal system.

Effect of PECNP on stability of CO_2 foam for a given foam quality in the view cell test

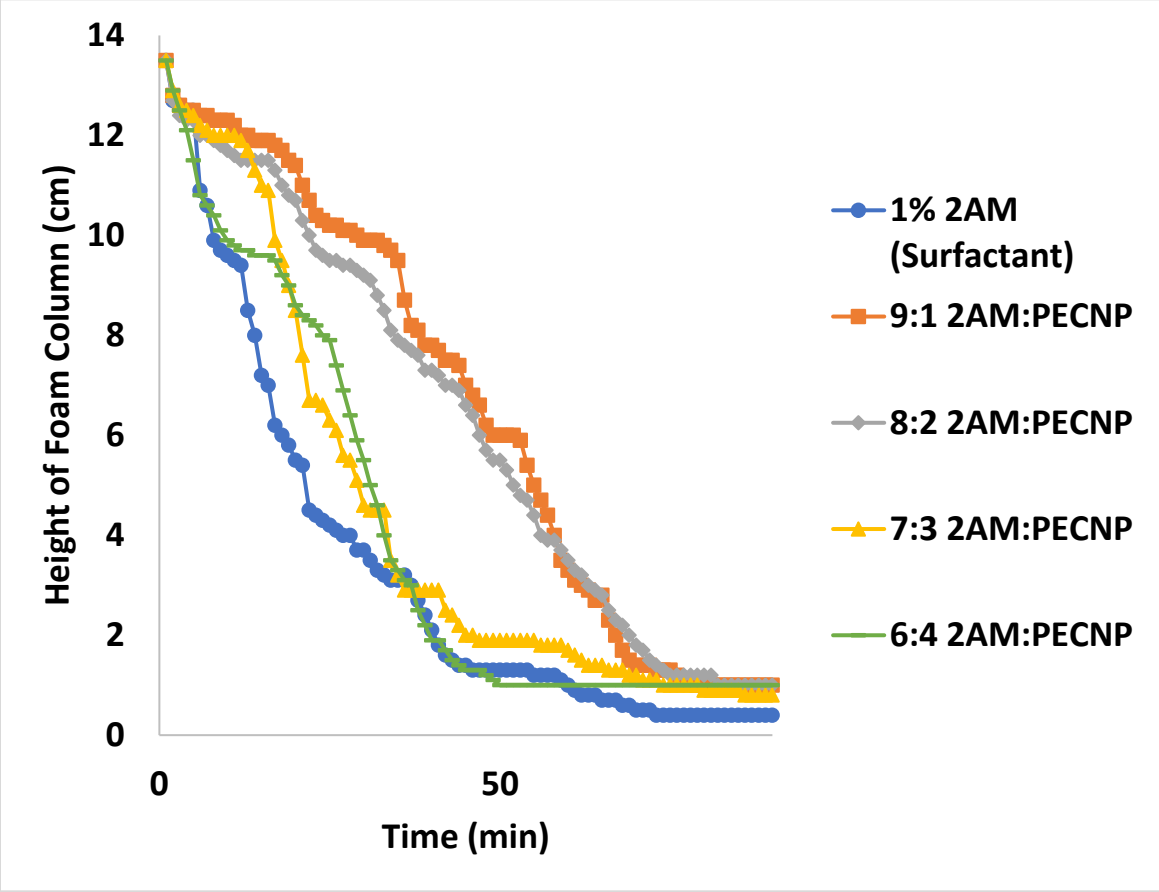

Figure 55. Height of foam column vs time for different surfactant-PECNP systems at 70% foam quality

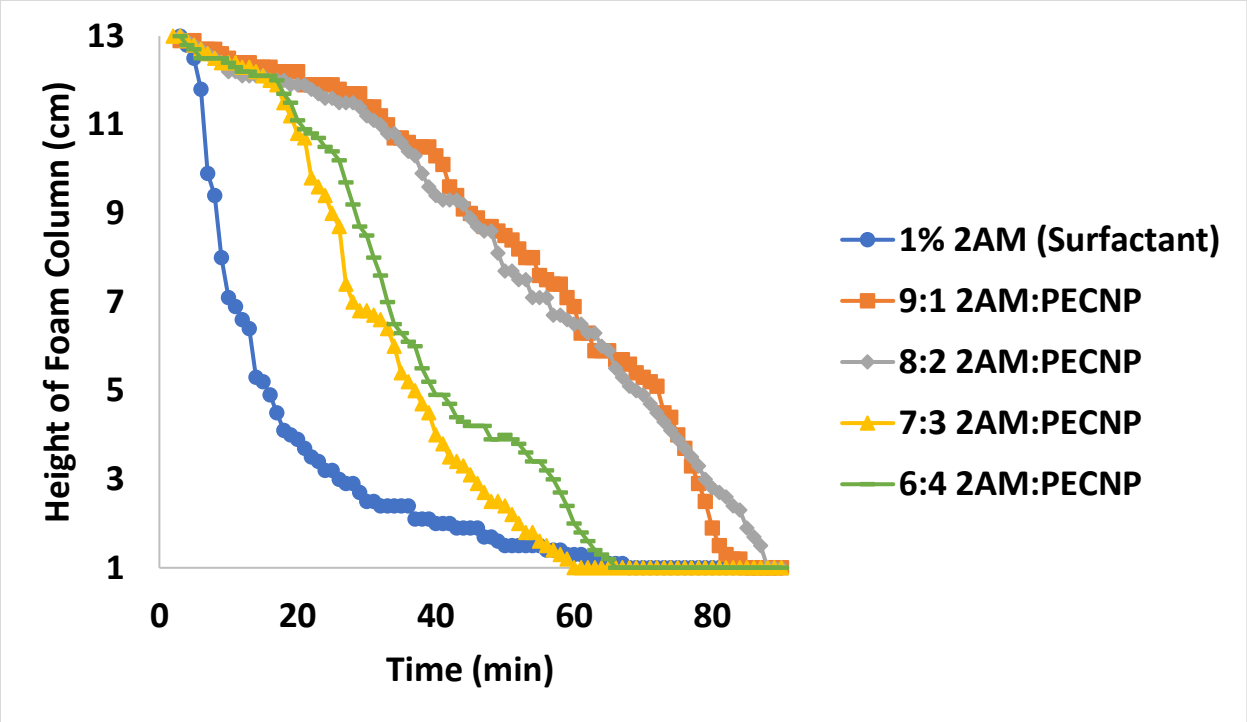

Figure 56. Height of foam column vs time for different surfactant-PECNP systems at 80% foam quality

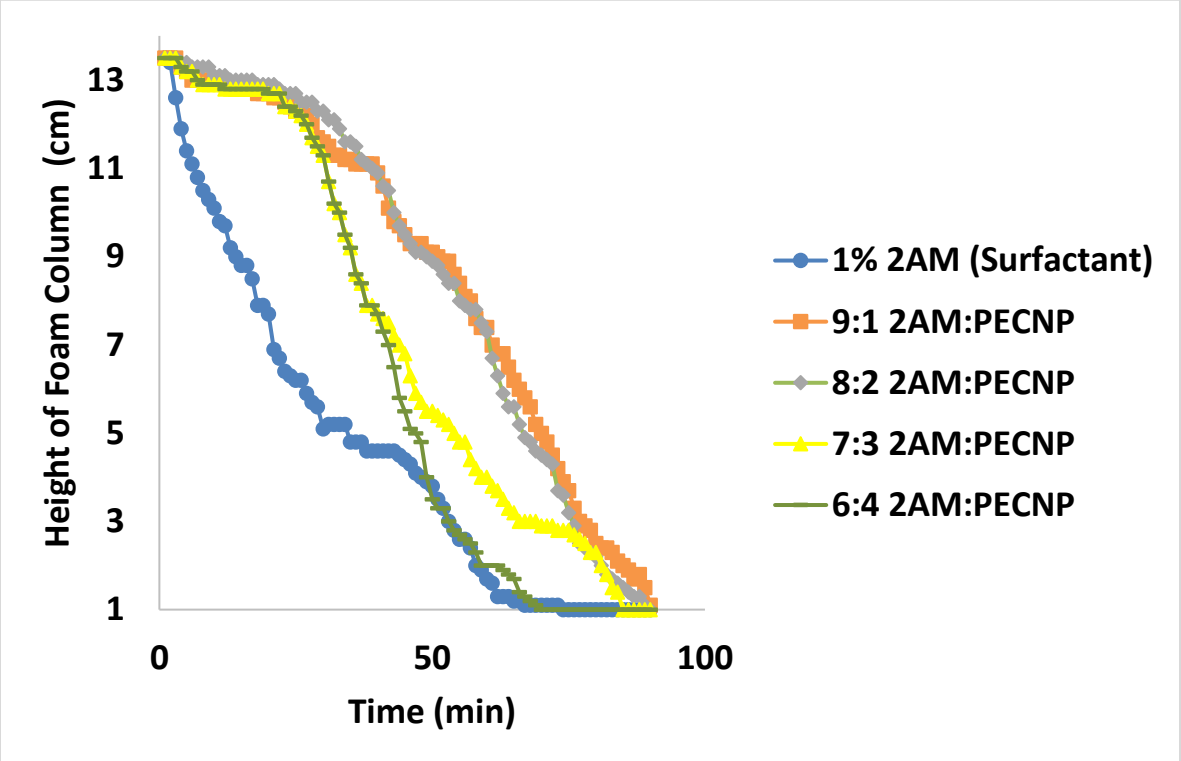

Figure 57. Height of foam column vs time for different surfactant-PECNP systems at 90% foam quality

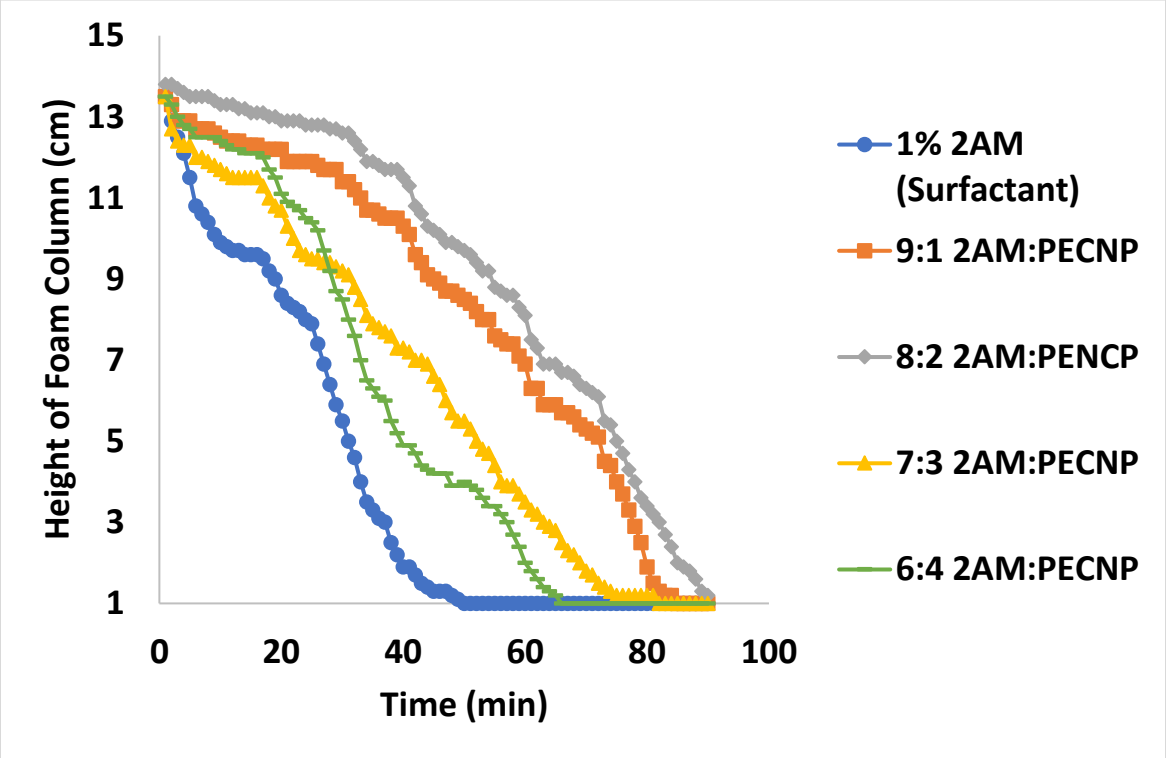

Figure 58. Height of foam column vs time for different surfactant-PECNP systems at 95% foam quality

Effect of foam quality on stability of CO_2 foam in view cell test

Figure 59 presents the influence of foam quality on viscosity of CO_2 foam generated by 8:2 2AM: PECNP as the aqueous phase.

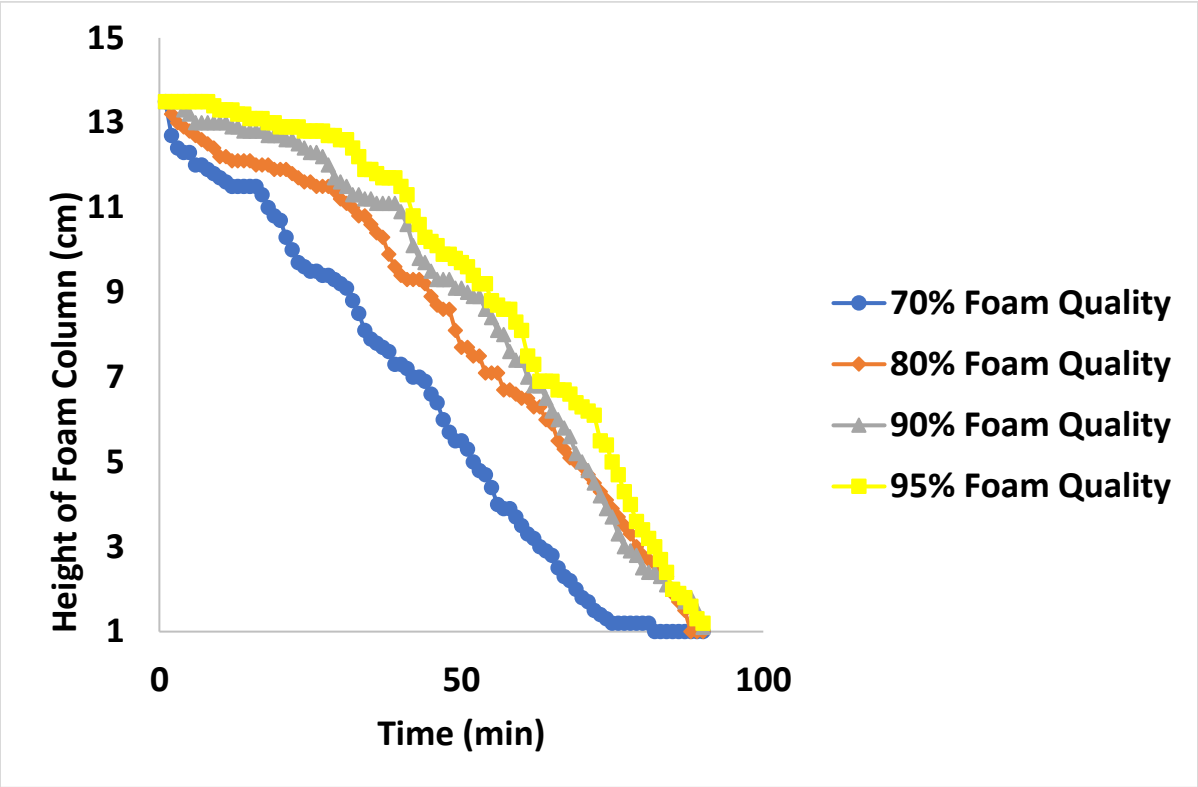

Figure 59. Height of foam column vs time for different foam quality generated by most optimal surfactant-PECNP

It can be observed from Figure 59 that increasing the foam quality improved the stability of the CO_2 foam. Image of the supercritical CO_2 foam generated by optimal surfactant-PECNP system at 45 minutes in isolated view cell are shown in Figure 60 and Figure 61.

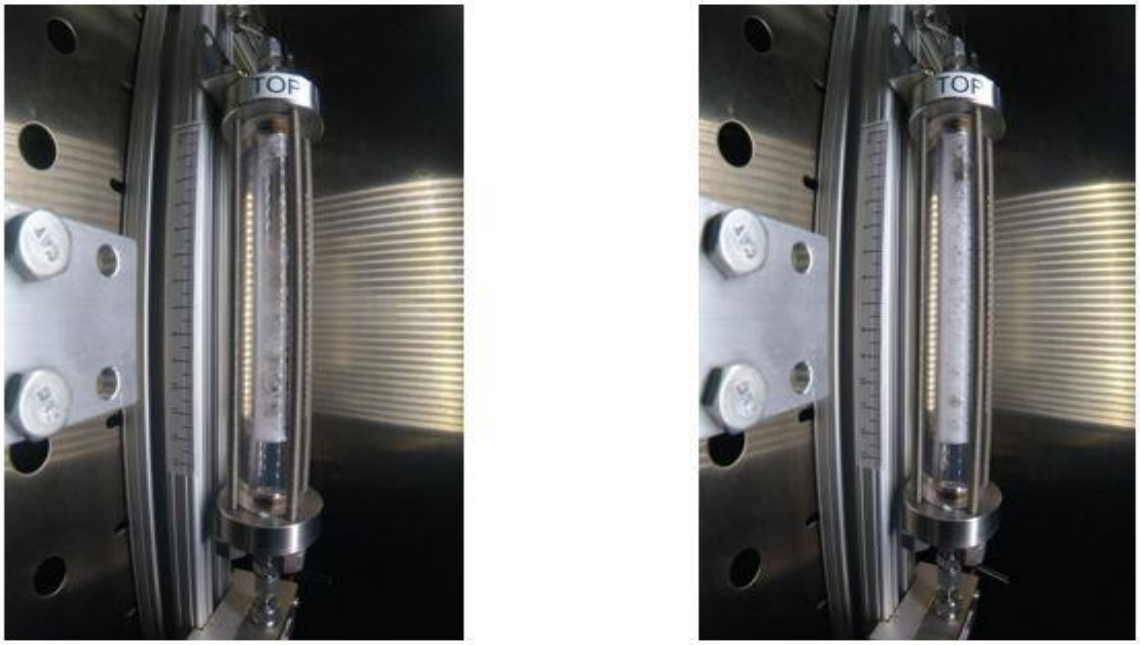

A B

Figure 60. Supercritical CO_2 foam at A) 70% foam quality B) 80% Foam Quality after 45 mins

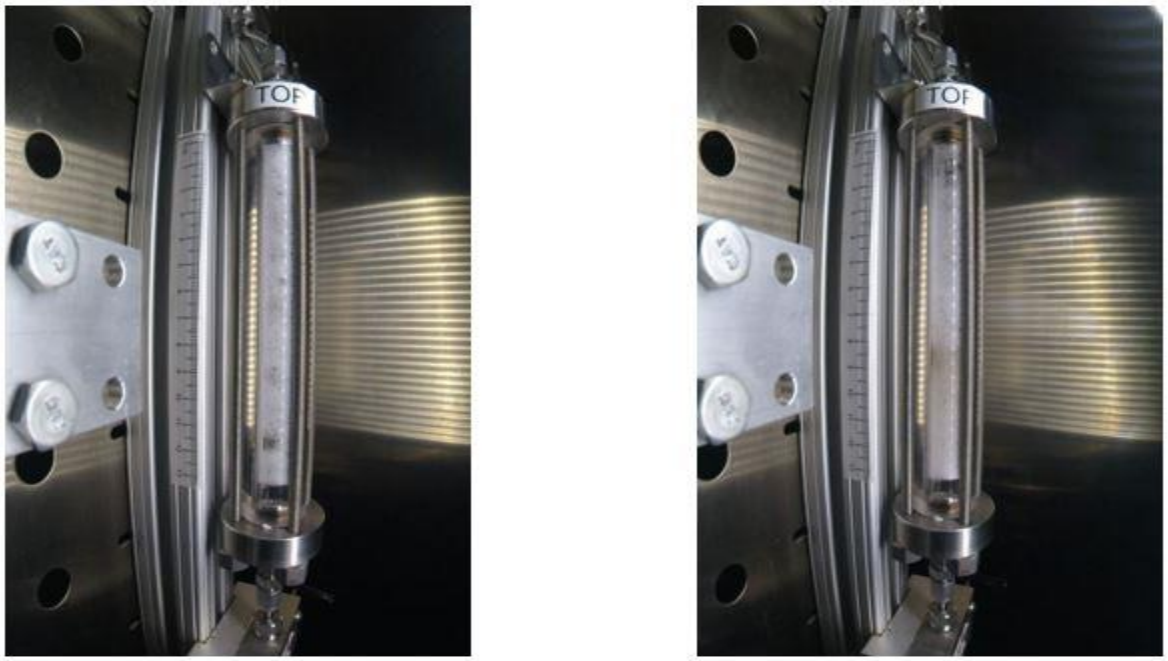

A B

Figure 61. Supercritical CO_2 foam at A) 90% foam quality B) 95% Foam Quality after 45 mins

4.4.2 View Cell Test with Oil

Efficiency of post fracture clean-up affects the well productivity. A successful use of CO_2 foams (70% quality) in Saudi Arabia indicated that, better clean up after the fracturing process resulted in 50% improvement in well productivity (Al-Dhamen, 2015). Interaction of crude oil with CO_2 foam is important for hydraulic fracturing application because it will help us to understand the clean-up process. Though most of the study about clean up efficiency of CO_2 foam was done in sand pack tests, view cell test helps to understand the CO_2 foam interaction with crude oil.

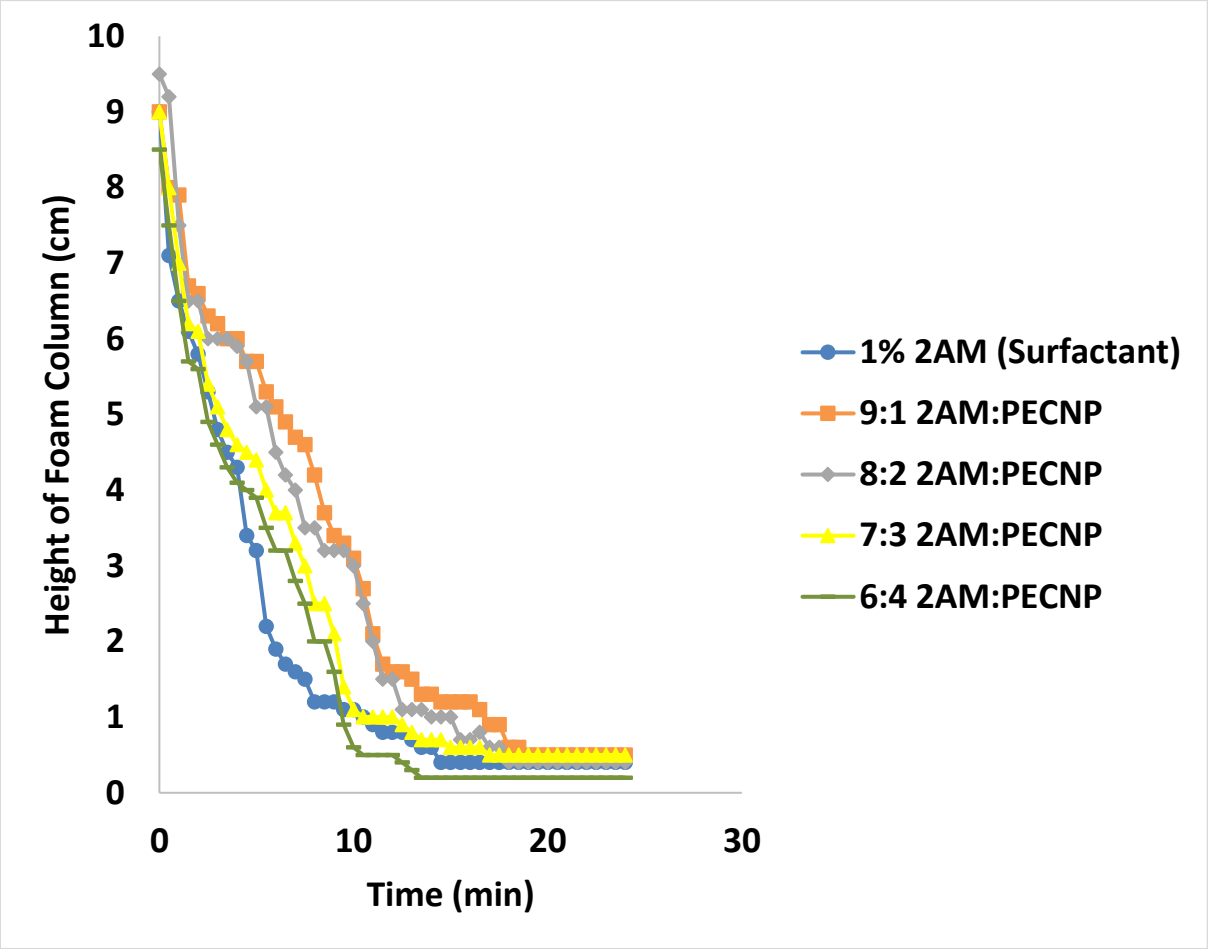

Figure 62. Height of foam column vs time for different surfactant-PECNP systems at 70% foam quality with oil

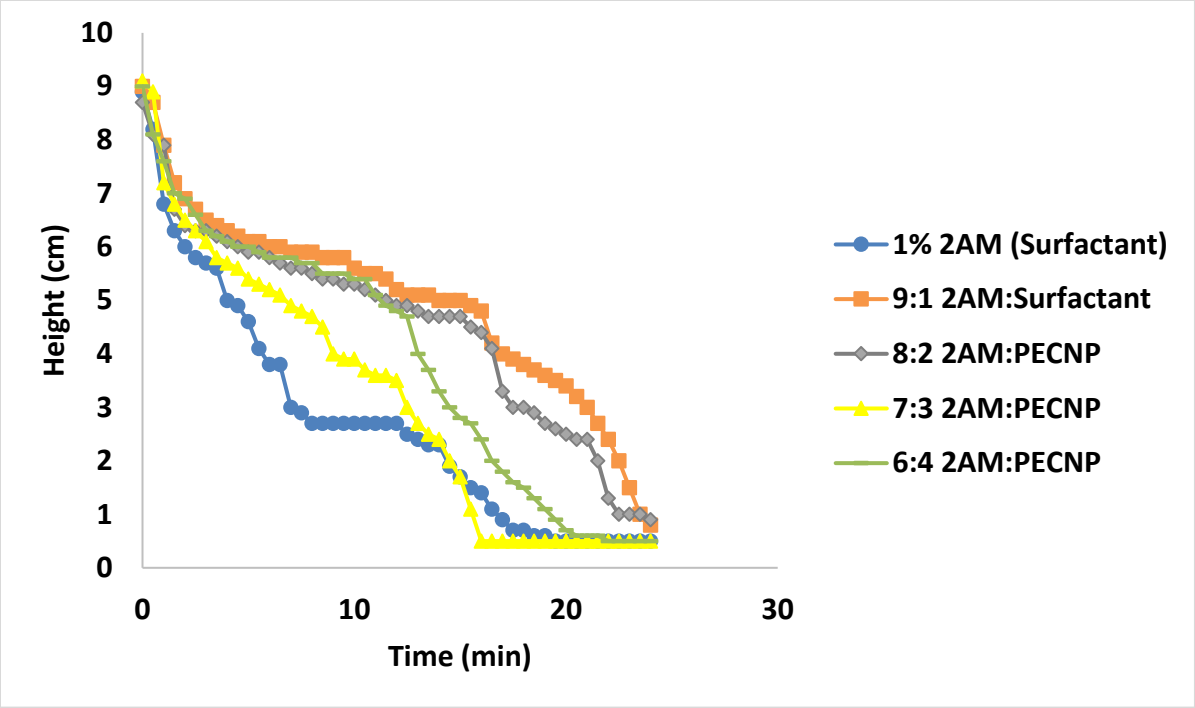

Figure 63. Height of foam column vs time for different surfactant-PECNP systems at 80% foam quality with oil

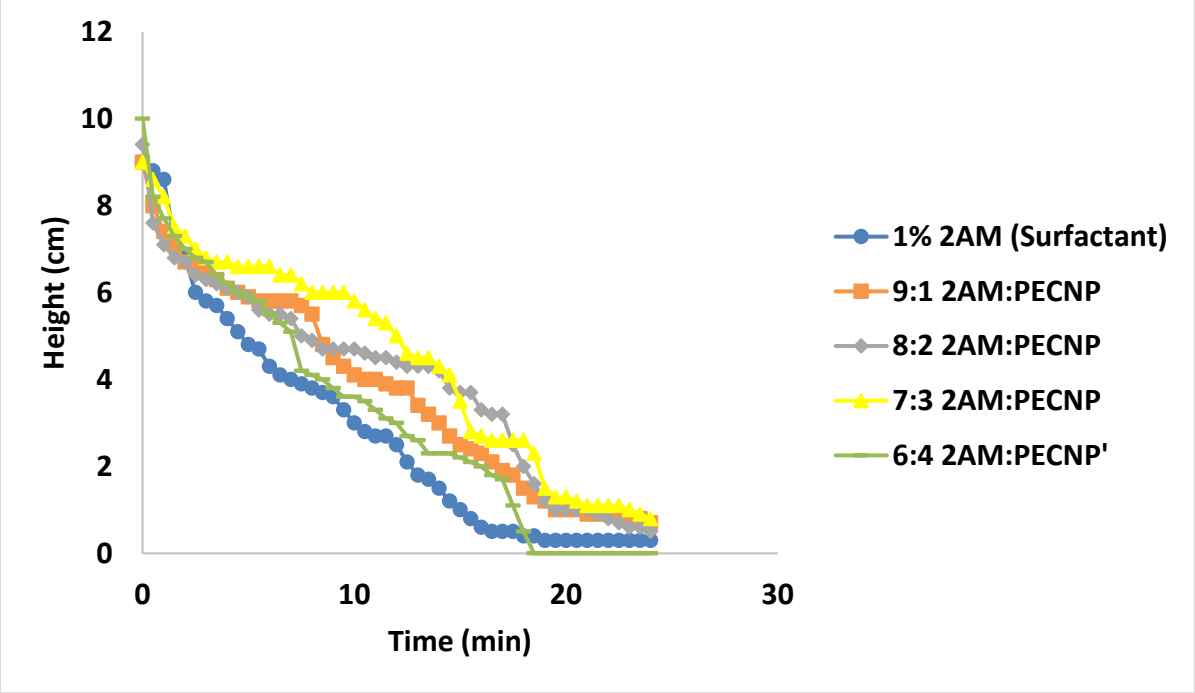

Figure 64. Height of foam column vs time for different surfactant-PECNP systems at 90% foam quality with oil

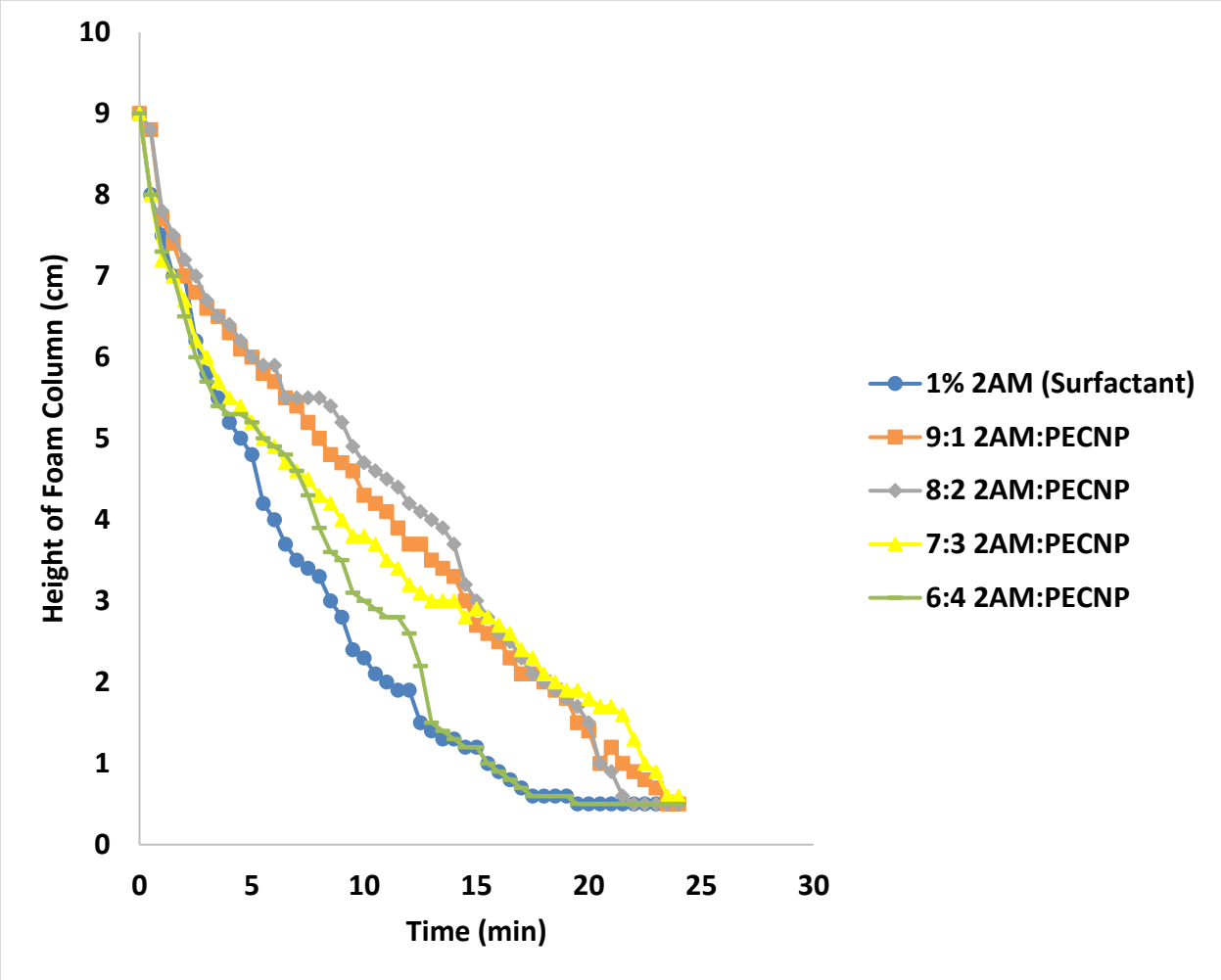

Figure 65. Height of foam column vs time for different surfactant-PECNP systems at 95% foam quality with oil

It can be observed from Figure 62 and Figure 65 that average time it took for the foam to decay in presence of crude oil was just 20 mins compared to 90 mins without crude oil. This means that foam breaks fast in presence of crude oil in all the four foam quality which will result in better cleanup. More detailed study of clean up will be shown in sand pack test.

Image of the supercritical CO_2 foam generated by optimal surfactant-PECNP systems after 5 mins in isolated view cell in the presence of oil are shown in Figure 66 and Figure 67. Note that the foam degraded at the interface for all systems as soon as it reached crude oil.

Figure 66. Supercritical CO_2 foam at A) 70% foam quality B) 80% Foam Quality after 5 mins in the presence of crude oil

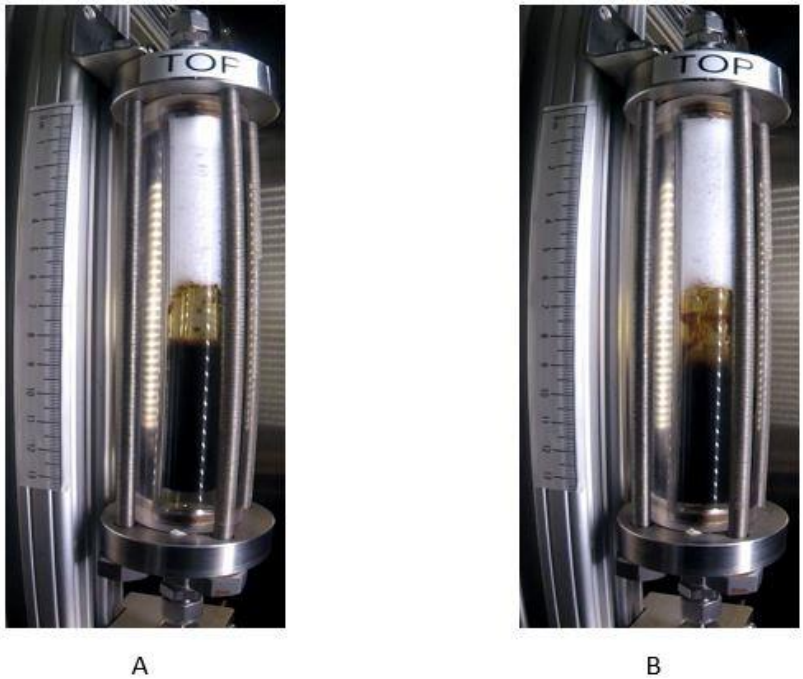

Figure 67. Supercritical CO_2 foam at A) 90% foam quality B) 95% Foam Quality after 5 mins in the presence of crude oil

4.5 Dynamic Fluid Loss Tests

It was found from the rheology and view cell tests that surfactant-PECNP generated CO_2 foam has better rheological properties and stability than foam generated just by surfactant (1% 2AM), and surfactant-PECNP system of 8:2 2AM: PECNP proved to be the most optimal system. High fluid loss of fracturing fluid might lead to capillary pressure shift and formation damage (Penny, 2006) (Economides, 2000). In this section, dynamic fluid loss properties of surfactant-PECNP foam are compared with CO2 foam generated just by surfactant (1% 2AM) to decide whether addition of PECNP to surfactant solution reduces the fluid loss.

4.5.1 Permeability Measurements

A tight sandstone Kentucky Core (K8) was used for the dynamic fluid loss tests. Permeability of the core was measured before and after the fluid loss test. It was observed that there was no change in the permeability of the core. Core flood experiment was conducted with brine (2% NaCl) to measure the permeability of the core. Procedure discussed in chapter 3 was used to perform the permeability measurements. The measurements were performed both before and after the dynamic fluid loss test, and no significant change in core permeability was observed. Using the measured properties summarized in Table 10, porosity of the core was calculated (summarized in Table 11).

Table 10. Measured properties of core K8 used for dynamic fluid loss experiment

Kentucky Core- K8	
Diameter (cm)	2.52
Length (cm)	2.25
Dry weight (g)	25.5
Saturated Weight (g)	26.94

Table 11. Calculated properties of core K8 used for dynamic fluid loss experiments

Kentucky Core- K8	
Pore Volume (cm^3)	1.43
Bulk Volume (cm^3)	11.18
Porosity (%)	12.81

Table 12. Summary of flow rate and pressure data for permeability measurement for the Kentucky core

Flow Rate (ml/ min)	Flow Rate (bbl/day)	Pressure Drop (psi)
0.3	0.009072	625
0.5	0.004536	323.6
1	0.002722	191.1

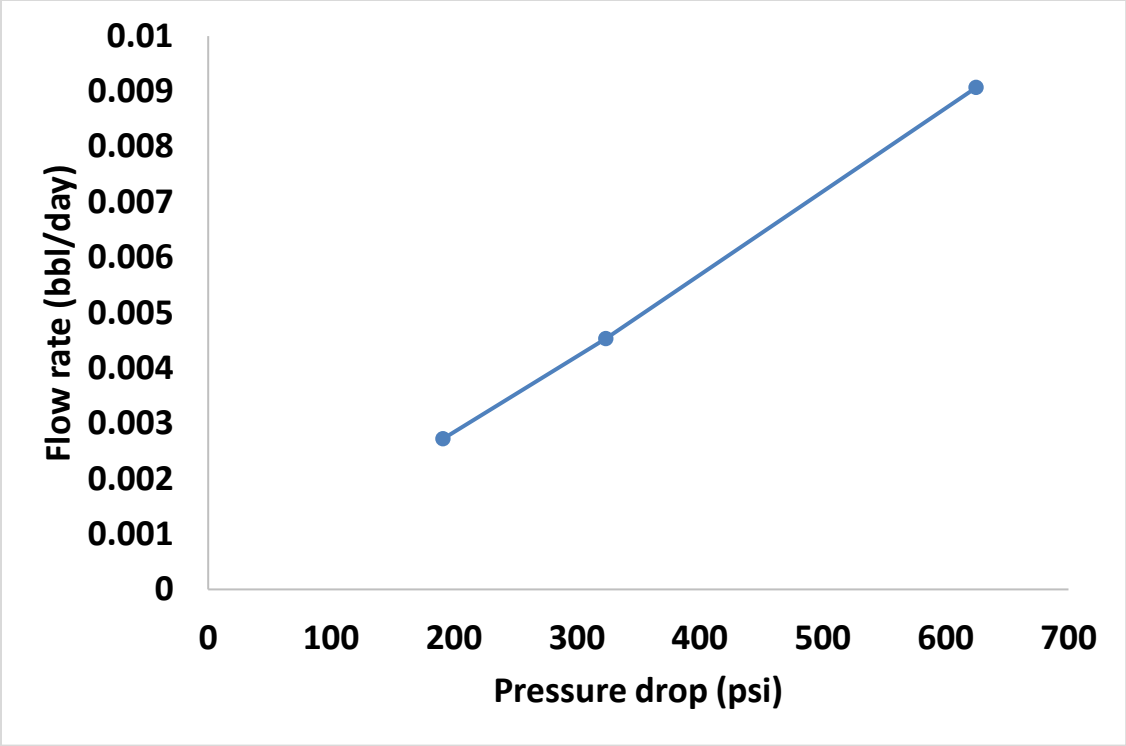

Figure 68. Flow rate vs pressure drop for permeability measurement of Kentucky core

Using the flow rate vs pressure drop data of the core (summarized in Table 12), Figure 68 was plotted. Slope of this curve was used to calculate the permeability of the core, using the Equation 15 below,

Equation 15,

$$q = (-1.127 * 10^{-3} * k * A * \Delta p) / (\mu * L)$$

Where,

q - Flow rate (cm^3/s)

k - Permeability (mD)

A - Area of core (cm^2)

Δp - Pressure drop (atm)

μ - Viscosity of brine (cP)

L - Length of core (cm)

The permeability of the Kentucky core used for the dynamic fluid loss experiment was 0.11 mD.

4.5.2 Dynamic Fluid Loss Measurements

Dynamic fluid loss test was performed with CO_2 foam qualities of 70%, 80%, 90% and 95% generated with surfactant solution (1% 2AM) and surfactant-PECNP ratio of 8:2.The main objective of this test is to find whether addition of PECNP to surfactant solution reduced dynamic fluid loss.

Total fluid loss is the summation of aqueous fluid loss (surfactant or surfactant-PECNP solution) and gaseous phase fluid loss (CO_2). Volume of aqueous fluid loss was measured using standard burette at the exit line and gaseous fluid loss was measured using an Alicat gas analyzer. Alicat gas analyzer measures the volume of CO_2 loss at room temperature and atmospheric pressure. Real gas equation shown in Equation 16 below was used to convert the volume of CO_2 measured by Alicat at room temperature and atmospheric pressure to volume at pressure and temperature of the test and Z factor of 0.51 (Perry, 1997) was used.

Equation 16,

$$PV = ZnRT$$

Then Carter equation shown in Equation 17 below was used to find the fluid loss coefficient:

Equation 17,

$$V_L = C_w * t^{(1/2)} + S_p$$

Where,

V_L: Fluid Loss (cm^3)

C_w: Fluid Loss Coefficient ($cm^3.min^{-1/2}$)

t: Time (min)

S_p: Spurt Loss (cm^3)

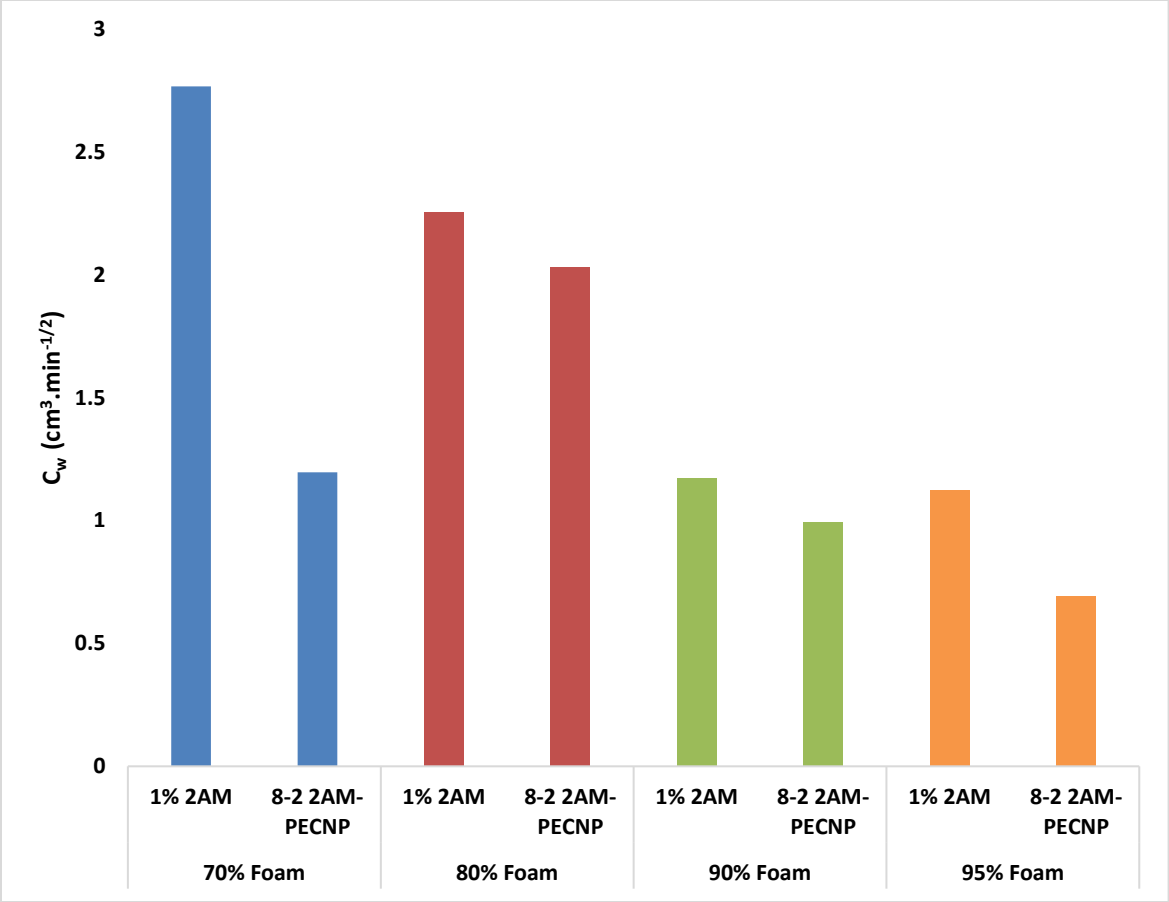

Figure 69. Graph comparing fluid loss coefficient of surfactant and optimal surfactant-PECNP generated CO_2 foam systems for all the four foam qualities

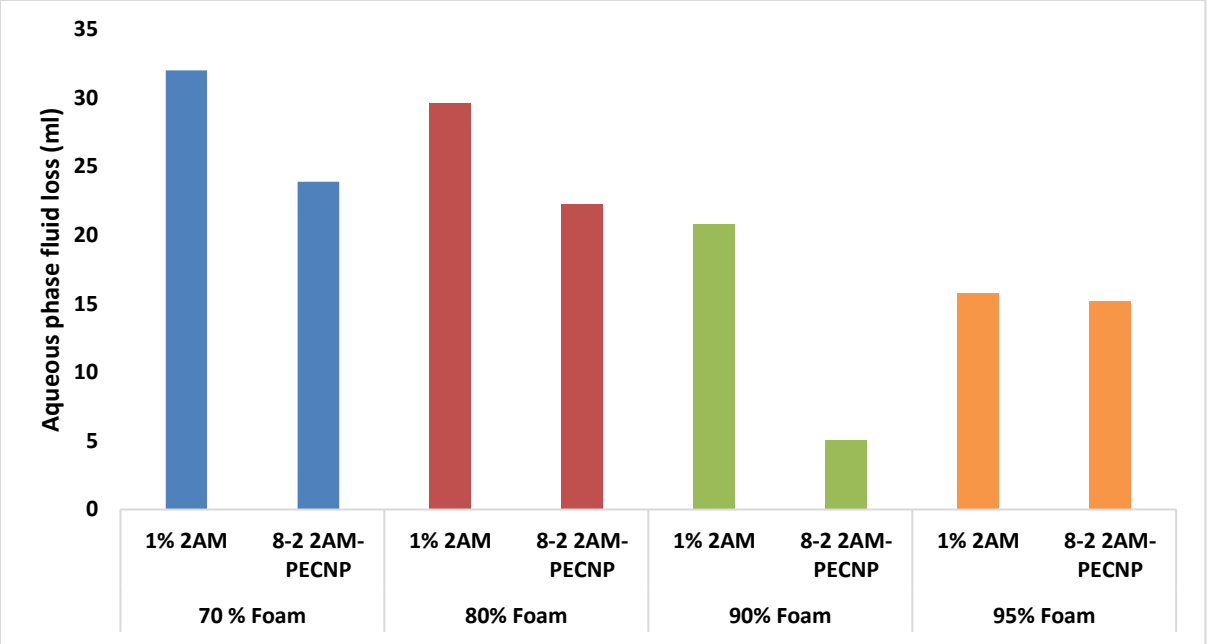

Figure 70. Graph comparing aqueous phase fluid loss of surfactant and optimal surfactant-PECNP generated CO_2 foam system for all the four foam qualities

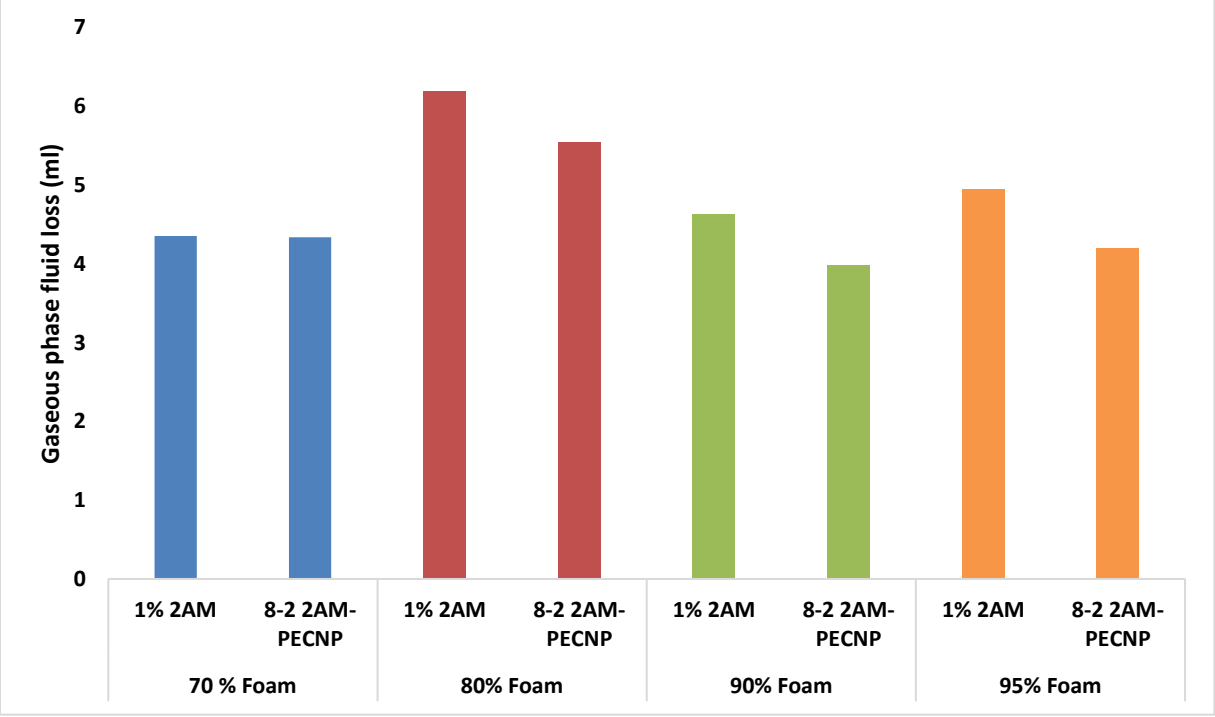

Figure 71. Graph comparing gaseous phase fluid loss (CO_2) of surfactant and optimal surfactant-PECNP generated CO_2 foam system for all the four foam qualities

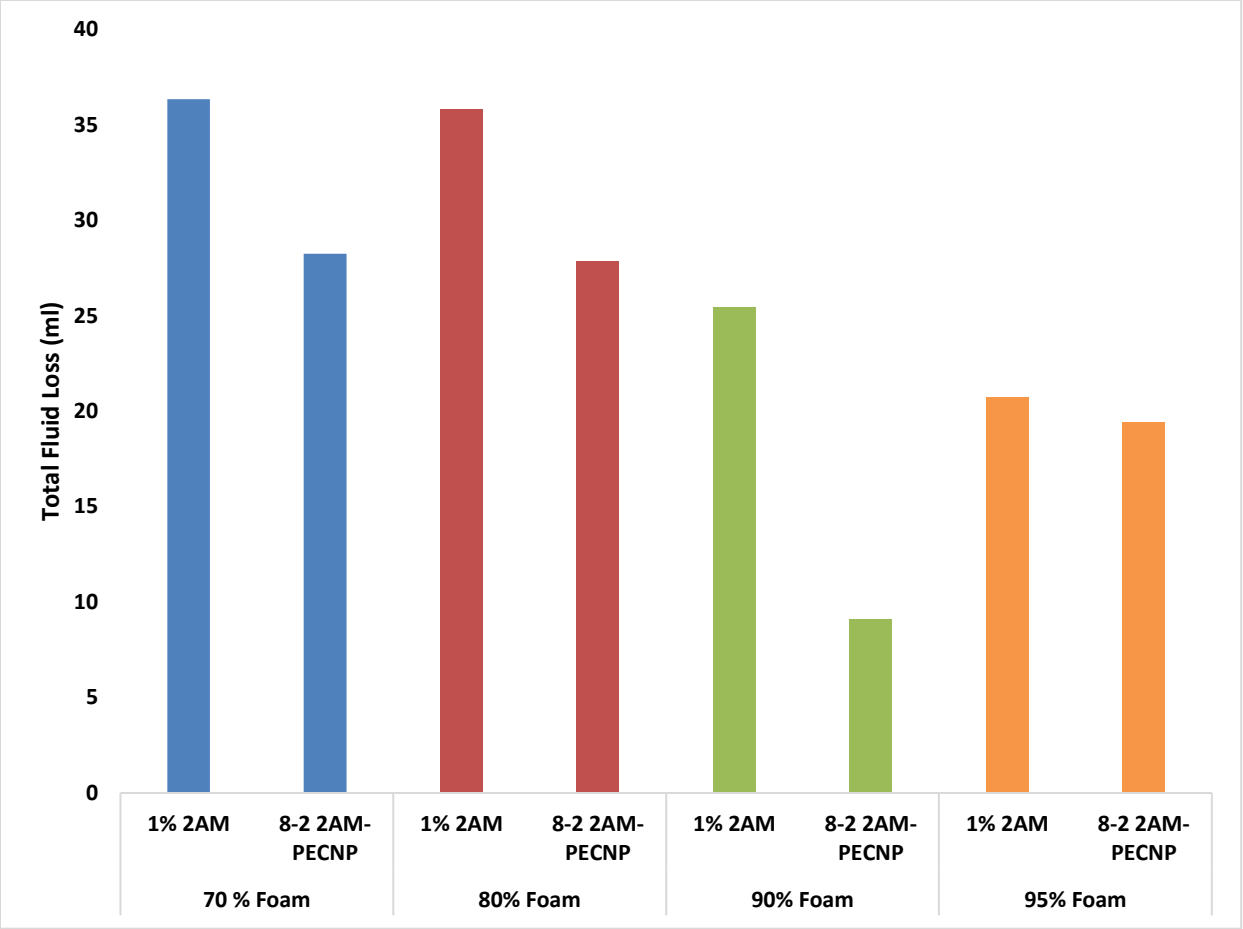

Figure 72. Graph comparing total fluid loss of surfactant and optimal surfactant-PECNP generated CO_2 foam of all the four foam qualities

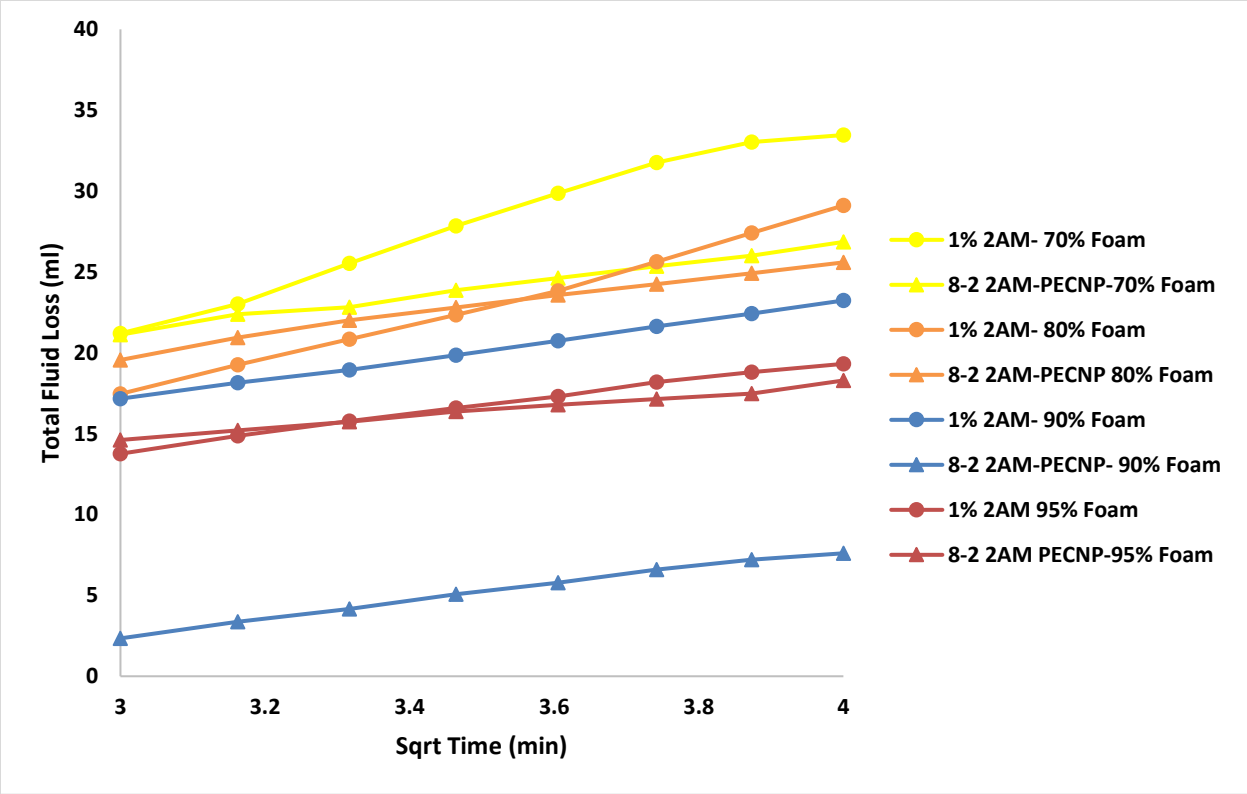

Figure 73. Graph representing the linear part of the total fluid loss vs square root of time curve for surfactant and optimal surfactant-PECNP generated CO_2 foam and various foam qualities

From Figure 69 to Figure 73, it can be observed that both fluid loss of both aqueous phase and gaseous phase are lower for CO_2 foam generated by optimal surfactant-PECNP ratio of 8:2 compared to foam generated only by surfactant (1 wt% 2AM). This resulted in lesser total fluid loss and fluid loss coefficient for CO_2 foam generated by optimal surfactant-PECNP ratio of 8:2 compared to foam generated only by surfactant (1 wt% 2AM).

4.6 Post Fracture Cleanup Study

Sand pack test was performed to analyze the cleanup process of supercritical CO_2 foam as fracturing fluid. Efficiency of cleanup process by CO_2 foam generated by only surfactant (1 wt% 2AM) and most optimal surfactant-PECNP ratio of 8:2 were compared for all the four different foam ratios of 70%, 80%, 90% and 95%.

Detailed procedure to perform the sand pack test was discussed in chapter 3. Before beginning the sand pack experiment, pore volume of the sand pack was measured using UV analysis and mass balance. Then the cleanup experiments was performed.

4.6.1 Pore Volume Measurement

Pore volume of the sand pack was measured both by mass balance and UV analysis. Before pore volume measurement, sand pack dimensions were measured. Then sand pack was loaded with ceramic proppant of 20/40 mesh size and weight of the sand pack loaded with proppant was measured.

Table 13. Summary of the sand pack dimension and weight of proppant loaded in the sand pack

Sand Pack Dimensions	
Length (in)	10.21
Inner Diameter (in)	0.33
Weight of Proppant (g)	35.85

Pore Volume Measurement using Mass Balance:

This is a simple technique of pore volume measurement. Dry weight of sand pack loaded with proppant and weight after saturation was measured. The difference in weight gave weight of brine in the sand pack. Then Equation 5 was used to find the pore volume

Pore Volume of Sand Pack	
Dry Weight (g)	257.99
Saturated Weight (g)	264.98
Pore Volume (cm^3)	6.95

Pore Volume Measurement using UV Analysis

Detailed procedure of pore volume measurement using tracer test was discussed in chapter 3. Tracer followed by RO water was injected into the sand pack at 8 ml/min and 12 ml/min. Equation 9 to Equation 14 were used to plot a graph of area vs volume injected for each flow rate for both tracer and RO water. The point of intersection of the graph was found. Difference in value of point of intersection and dead volume gave the pore volume of sand pack.

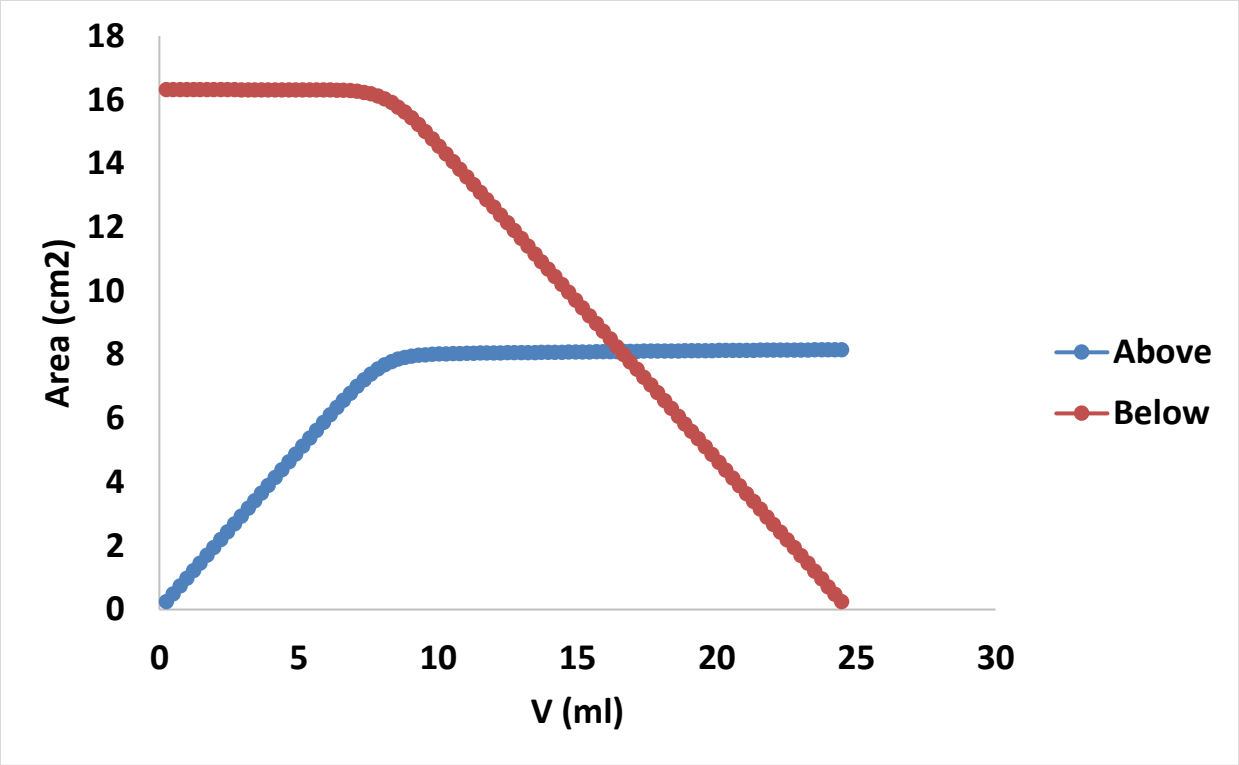

Figure 74. Area vs volume of tracer injected in the sand pack at a flow rate of 8 ml/min

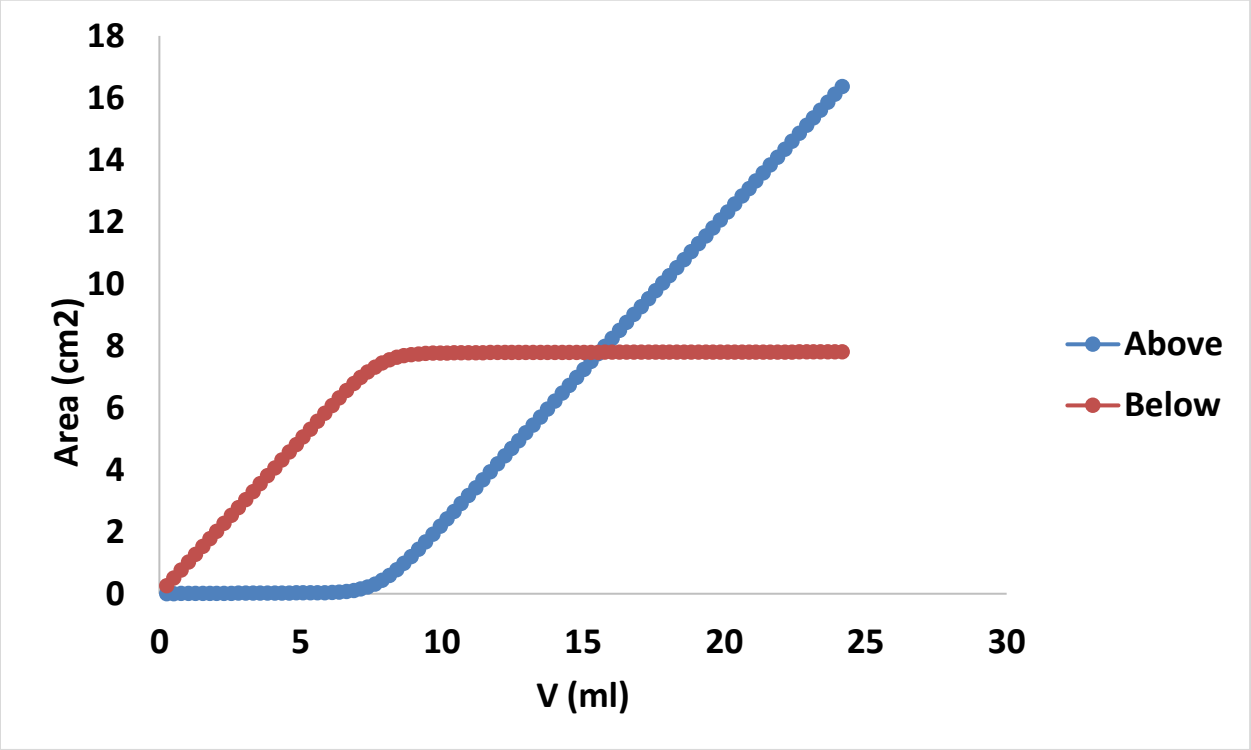

Figure 75. Area vs volume of RO water injected in the sand pack at a flow rate of 8 ml/min

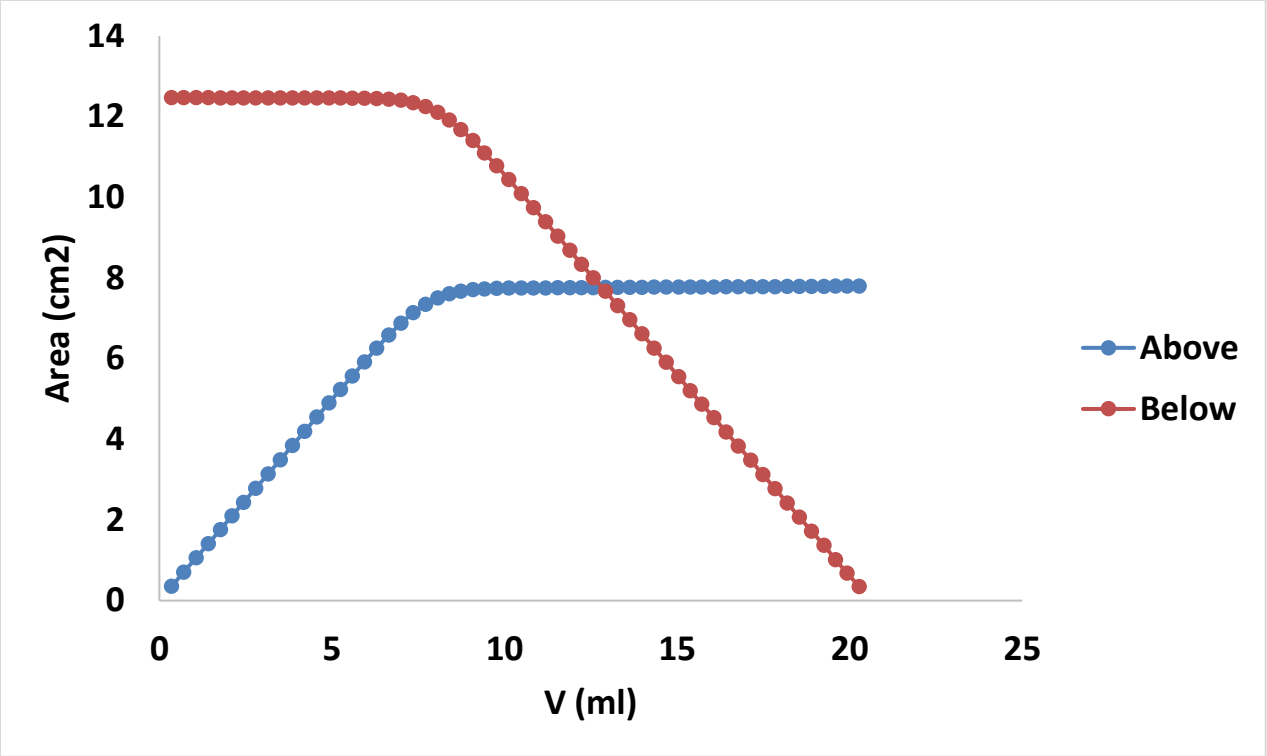

Figure 76. Area vs volume of tracer injected in the sand pack at a flow rate of 12 ml/min

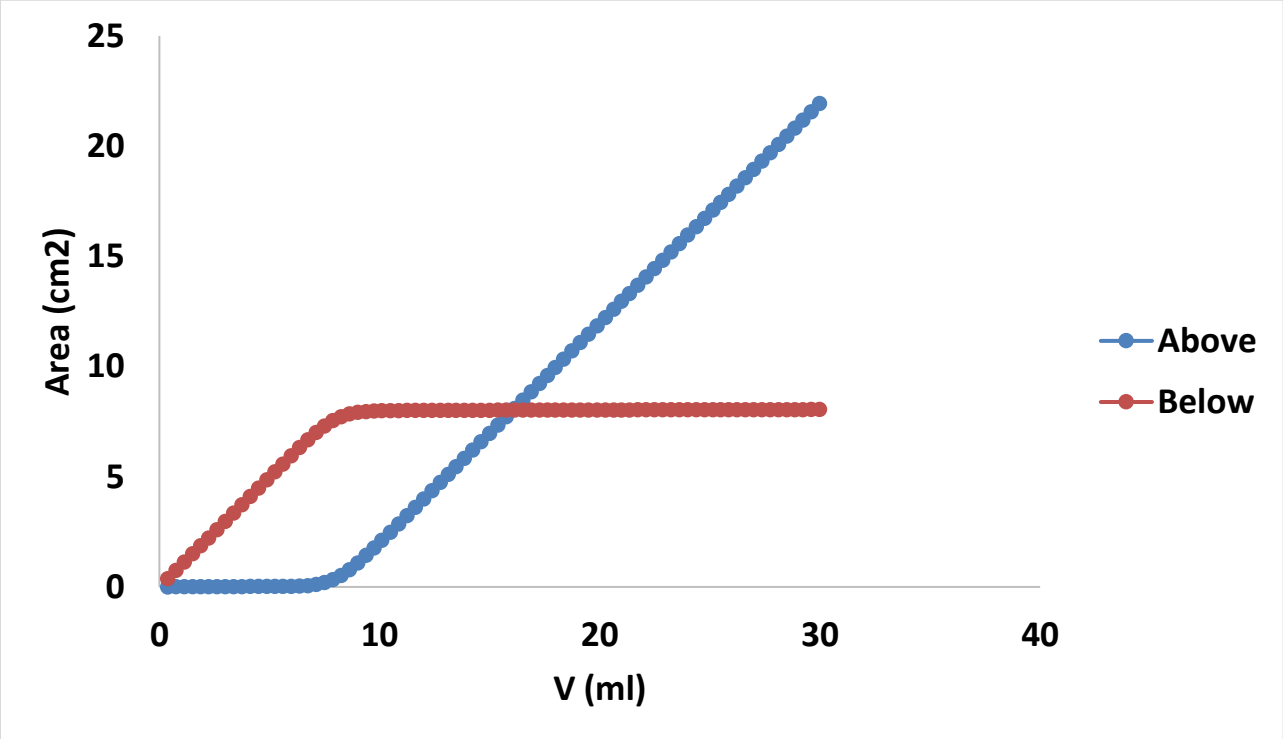

Figure 77. Area vs volume of RO water injected in the sand pack at a flow rate of 12 ml/min

Pore volume calculated from Figure 74 to Figure 77 are summarized in Table 14 below.

Table 14. Summary of pore volume calculated from UV analysis and mass balance

Test	PV	Unit
Tracer- 8ml/min	7.313	cm^3
Tracer- 12ml/min	6.98	cm^3
Mass Balance	6.95	cm^3

Pore volume calculated from mass balance and tracer test at flow rate of 12 ml/min was close. Therefore, pore volume of 6.95 cm^3 was used for all further calculation.

4.6.2 Brine Flood

After pore volume measurements, sand pack loaded with proppant was installed in the foam setup. Detailed procedure to perform the experiment is discussed in chapter 3. Brine flood was performed at a flow rate of 6ml/min, 10 ml/min and 12 ml/min.

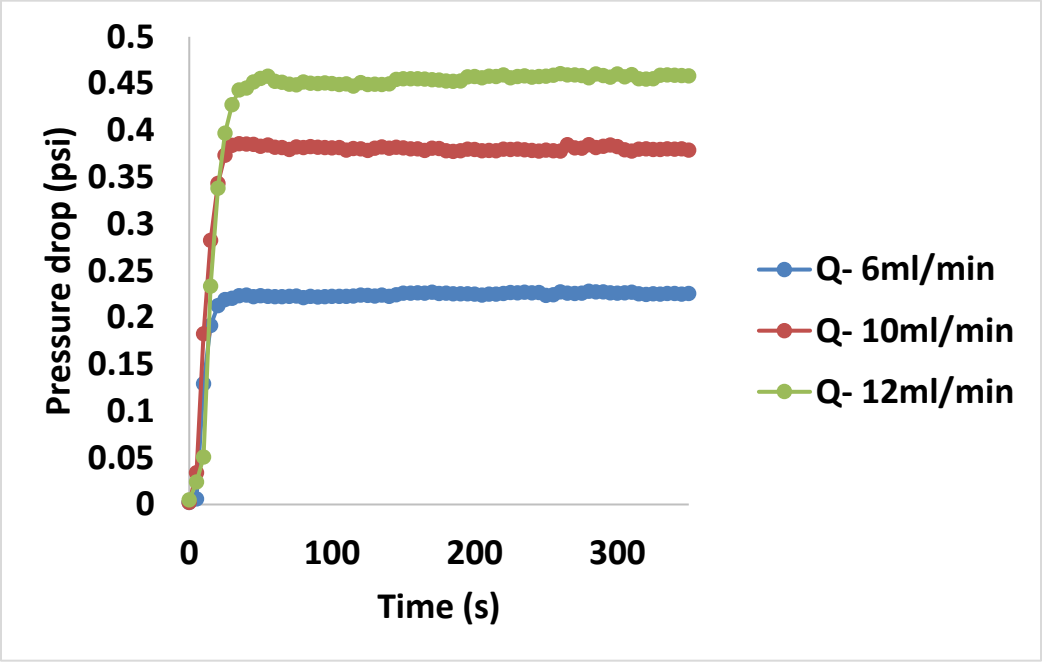

Figure 78. Pressure drop vs time across the sand pack during brine flood at three different flow rates

In case if the pressure drop during brine flood for the respective flow rates was not close to the one shown in Figure 78, it means either the proppants are not properly loaded in the sand pack or there might be a leak in the system.

4.6.2 Foam Flood

Foam flood was performed after the brine flood. CO_2 foam generated by surfactant and most optimal surfactant-PENCP ratio of 8:2 of foam qualities of 70%, 80%, 90% and 95 % were tested.

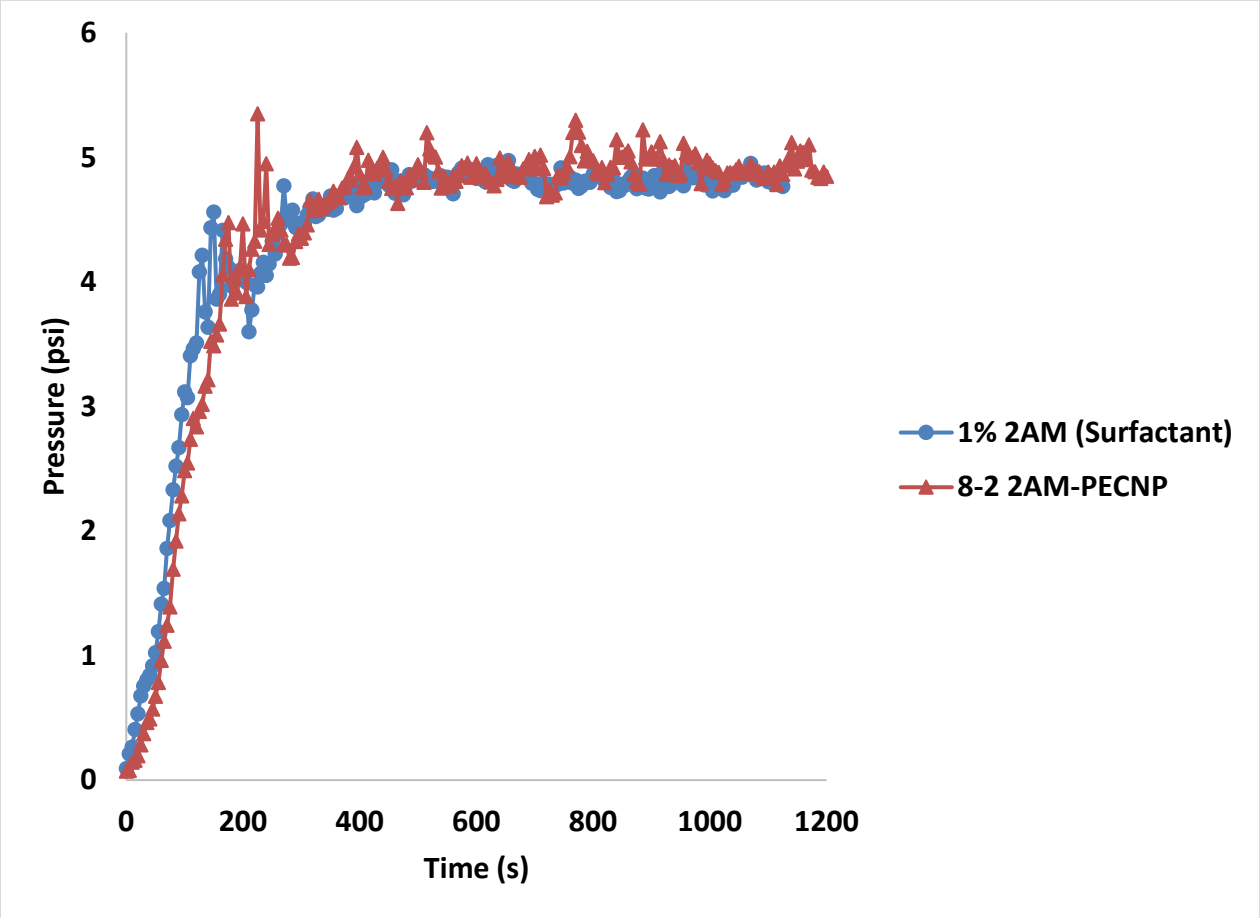

Figure 79. Pressure drop across the sand pack with time for the CO_2 foam generated by surfactant and most optimal ratio of 2AM-PECNP with foam quality of 70%

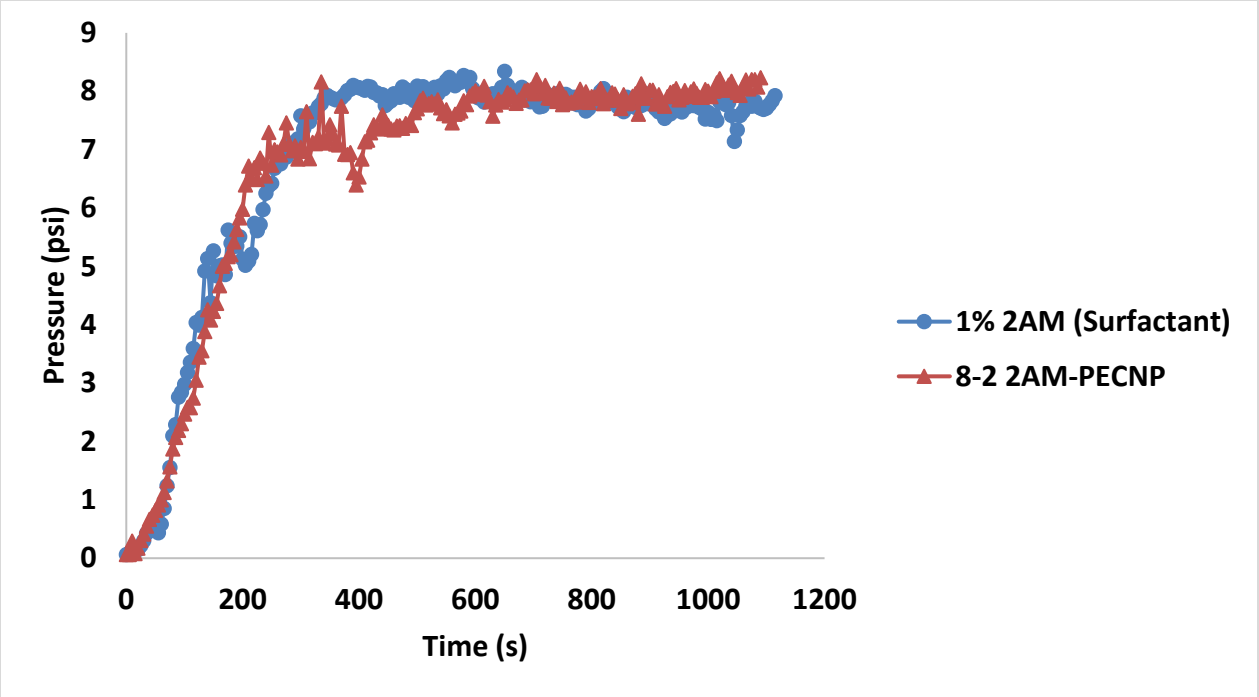

Figure 80. Pressure drop across the sand pack with time for the CO_2 foam generated by surfactant and most optimal ratio of 2AM-PECNP with foam quality of 80%

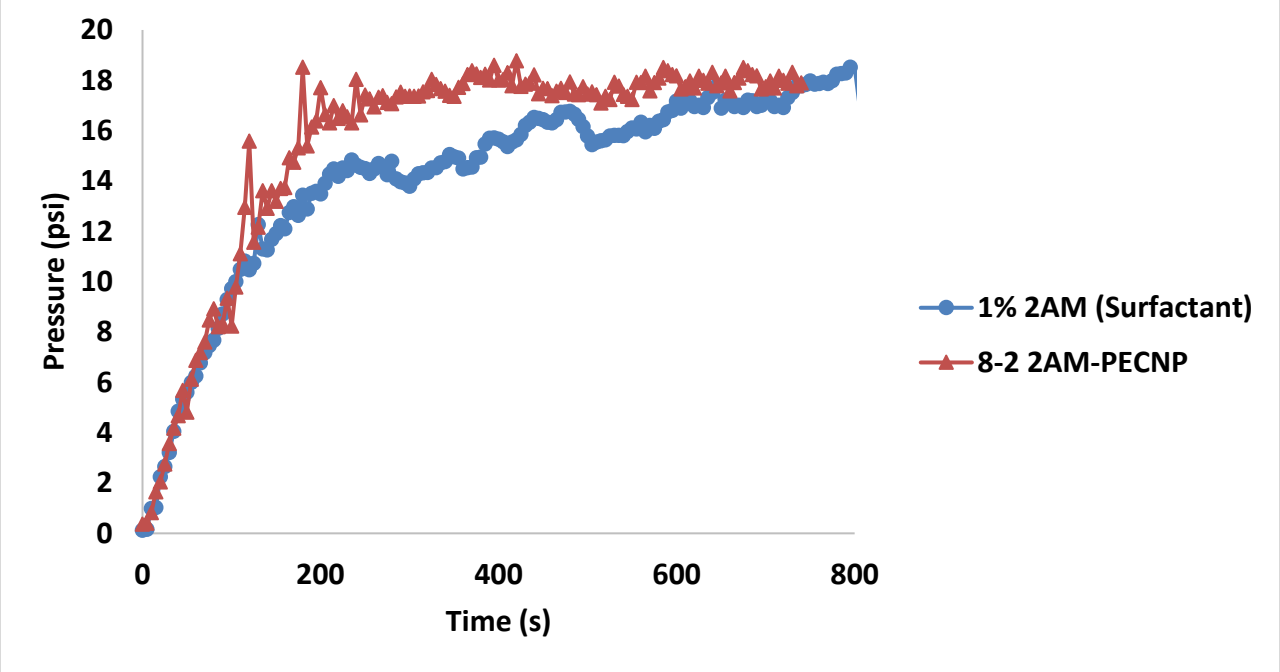

Figure 81. Pressure drop across the sand pack with time for the CO_2 foam generated by surfactant and most optimal ratio of 2AM-PECNP with foam quality of 90%

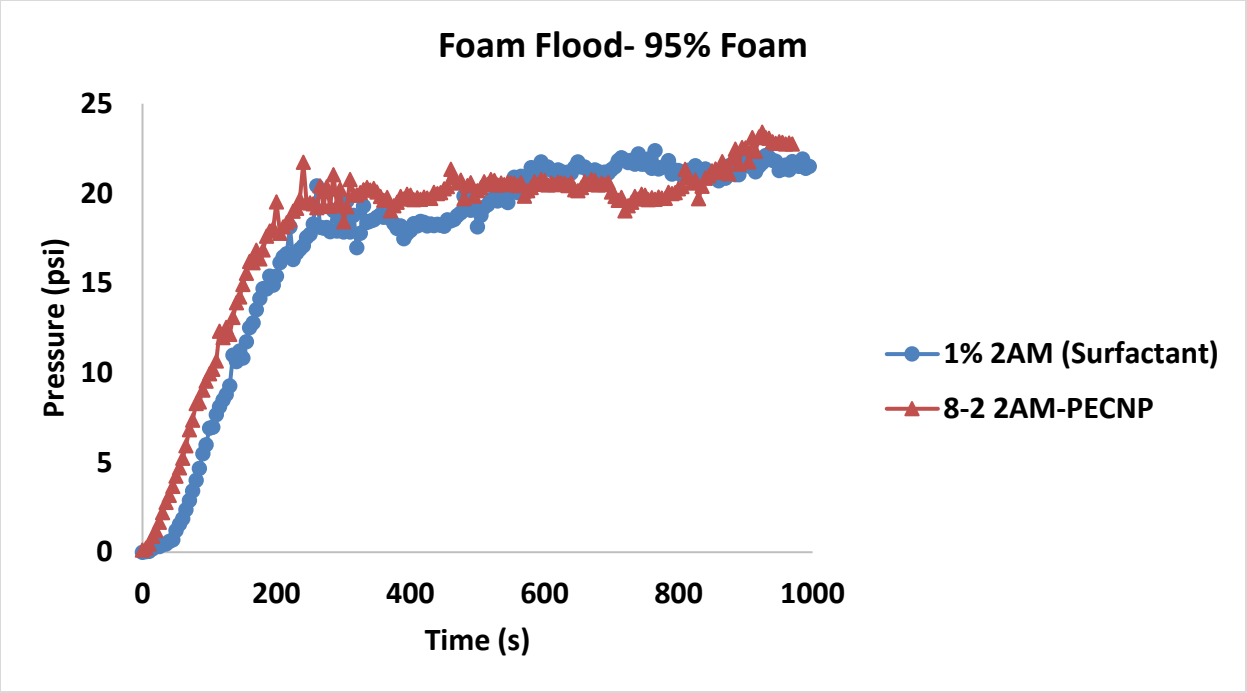

Figure 82. Pressure drop across the sand pack with time for the CO_2 foam generated by surfactant and most optimal ratio of 2AM-PECNP with foam quality of 95%

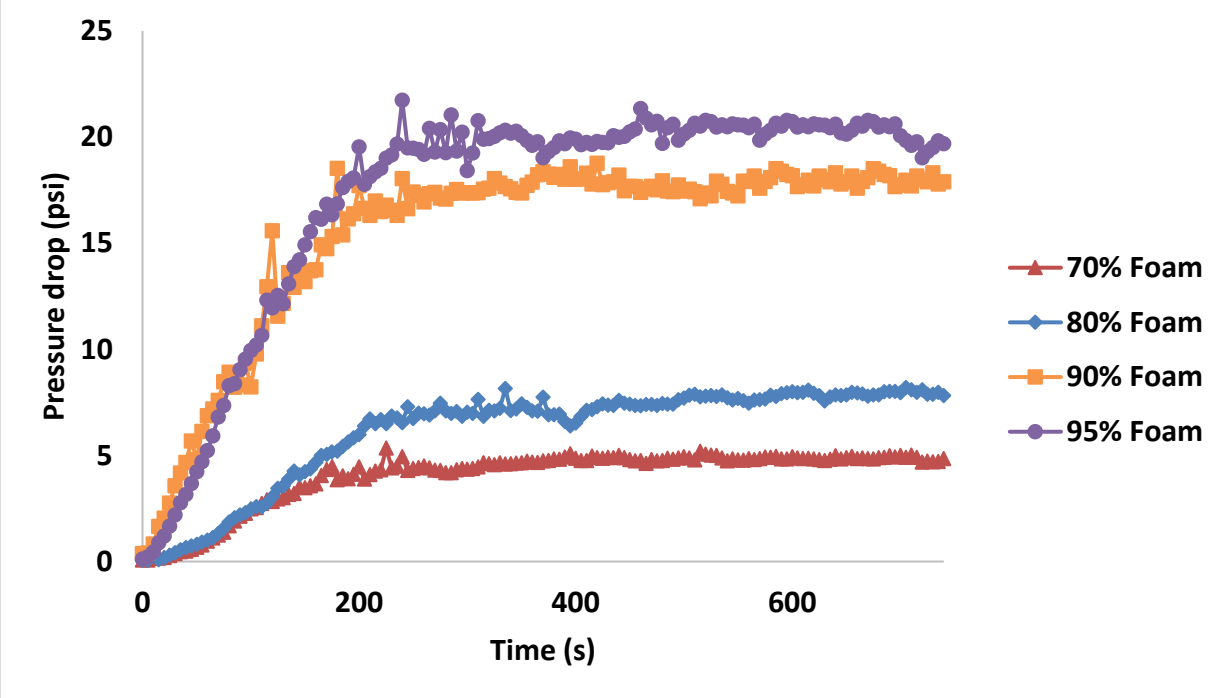

Figure 83. Pressure drop across the sand pack with time for the CO_2 foam generated by most optimal ratio of 2AM-PECNP in each of the four different foam qualities

From Figure 83 it can observed that with increase in foam quality the pressure drop increases, because the viscosity of foam increases with foam quality (shown in Figure 49).

4.6.2 Oil flood after foam flood

After the foam flood, the sand pack with proppants was filled with foam and crude oil was injected to perform oil flood. Injection of crude oil into the sand pack represents the post fracture clean up due to production of hydrocarbon. The aqueous phase in the effluent was collected in a burette during the oil flood. Clean up of the foam generated by surfactant and most optimal surfactant-PECNP was compared with cleanup of just brine (2 wt% NaCl).

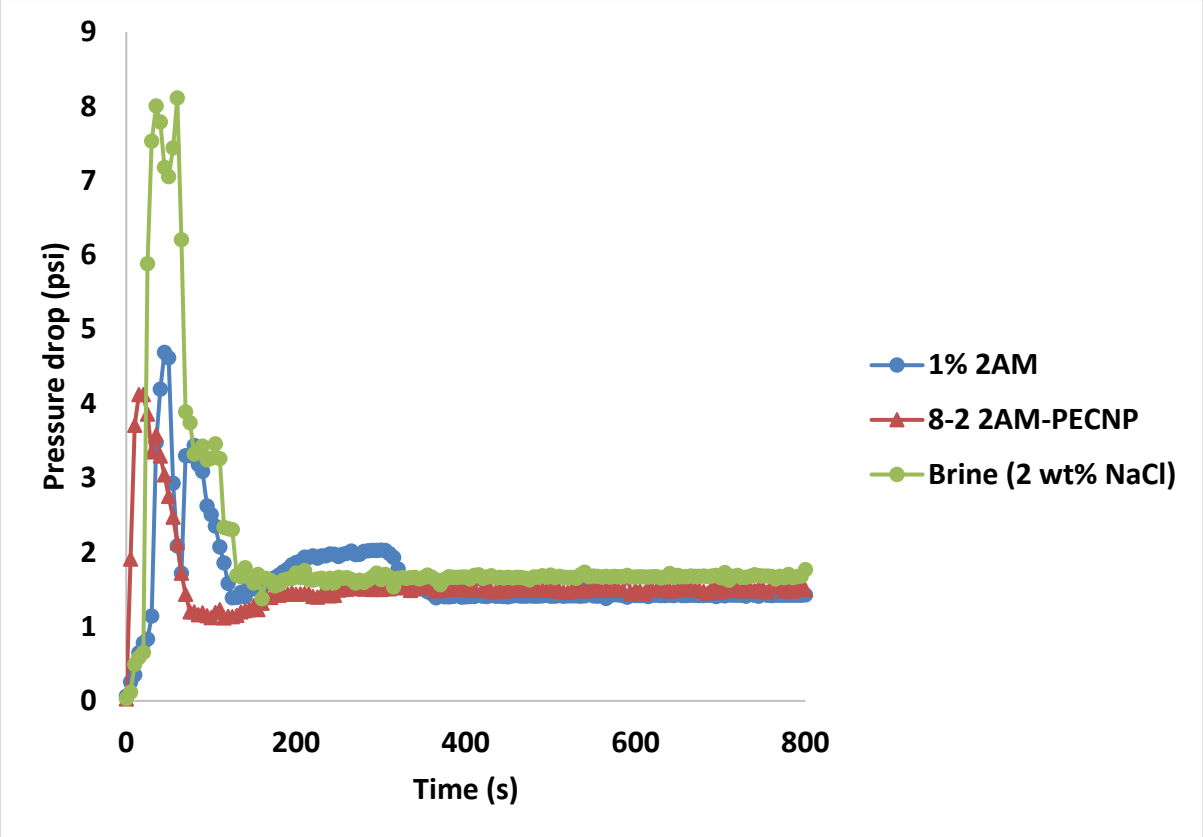

Figure 84. Pressure drop across the sand pack with time for the cleanup of CO_2 foam generated by surfactant and most optimal ratio of 2AM-PECNP with foam quality of 70 % during oil flood

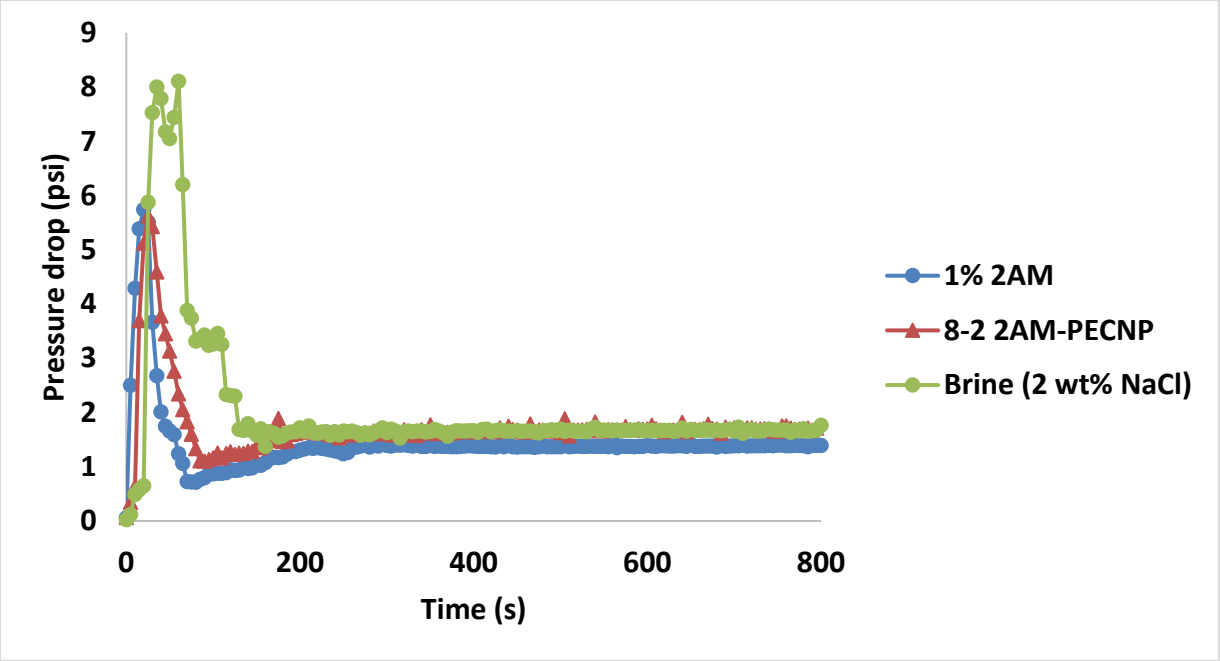

Figure 85. Pressure drop across the sand pack with time for the cleanup of CO_2 foam generated by surfactant and most optimal ratio of 2AM-PECNP with foam quality of 80 % during oil flood

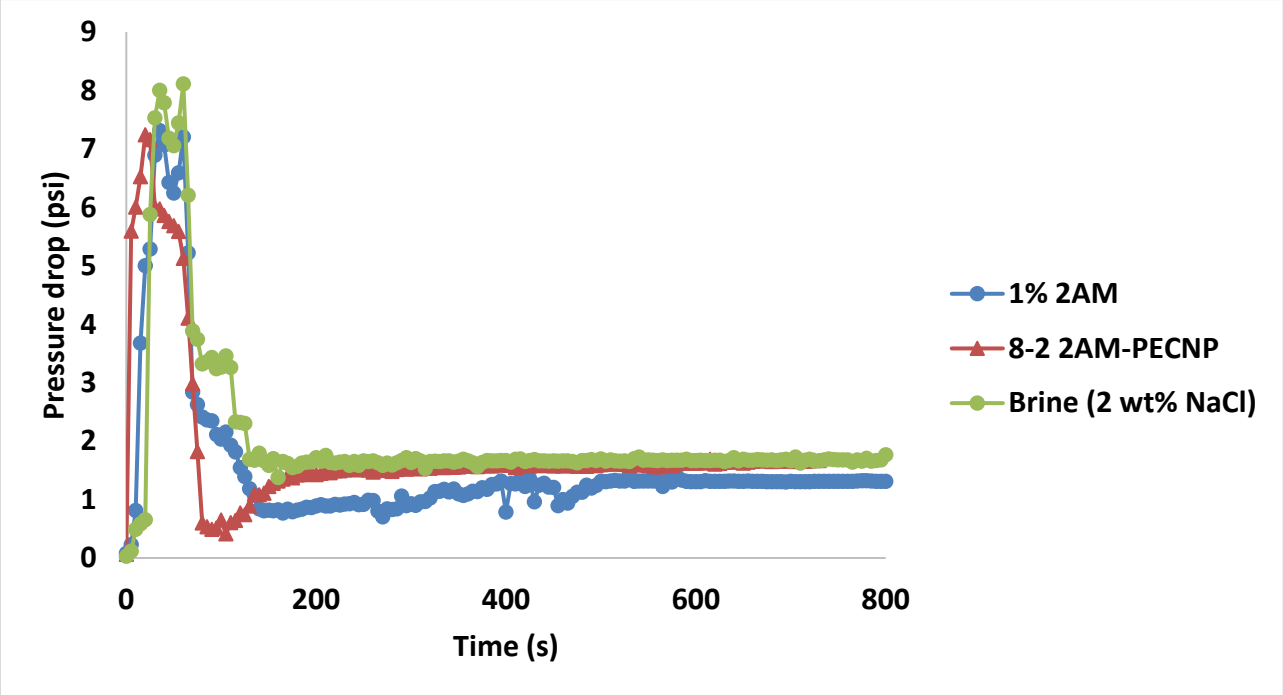

Figure 86. Pressure drop across the sand pack with time for the cleanup of CO_2 foam generated by surfactant and most optimal ratio of 2AM-PECNP with foam quality of 90 % during oil flood

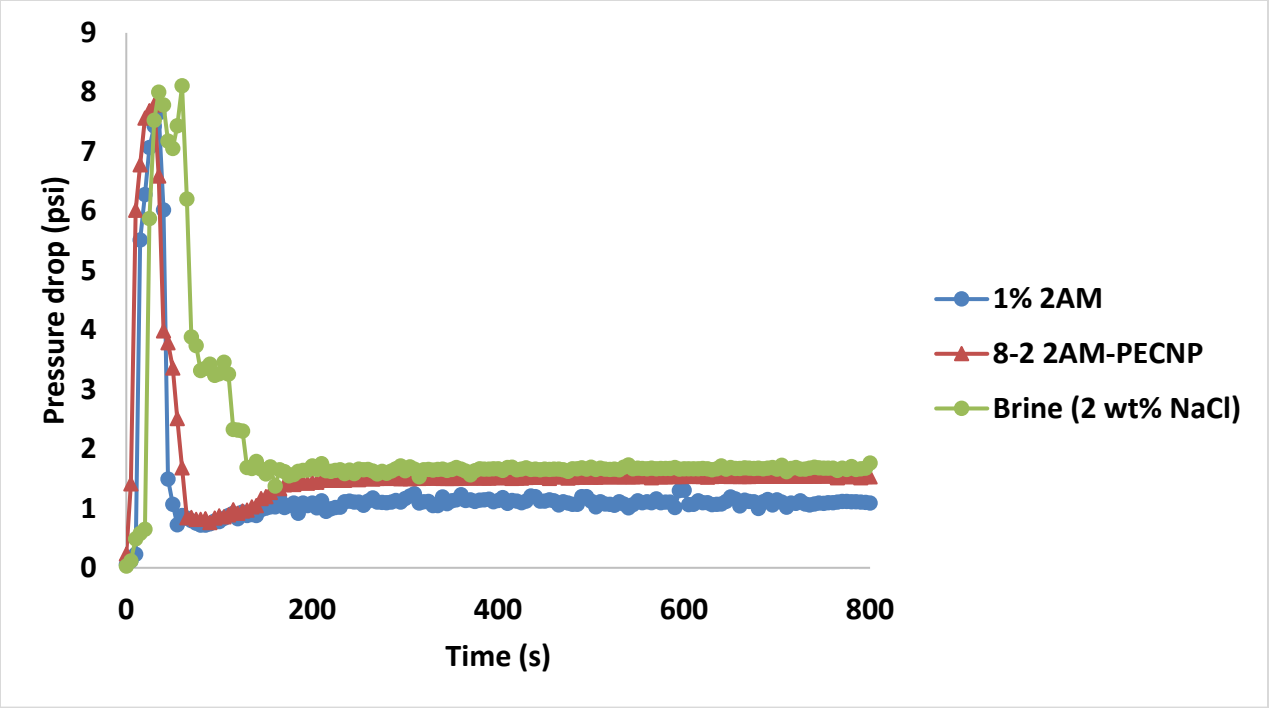

Figure 87. Pressure drop across the sand pack with time for the cleanup of CO_2 foam generated by surfactant and most optimal ratio of 2AM-PECNP with foam quality of 95 % during oil flood

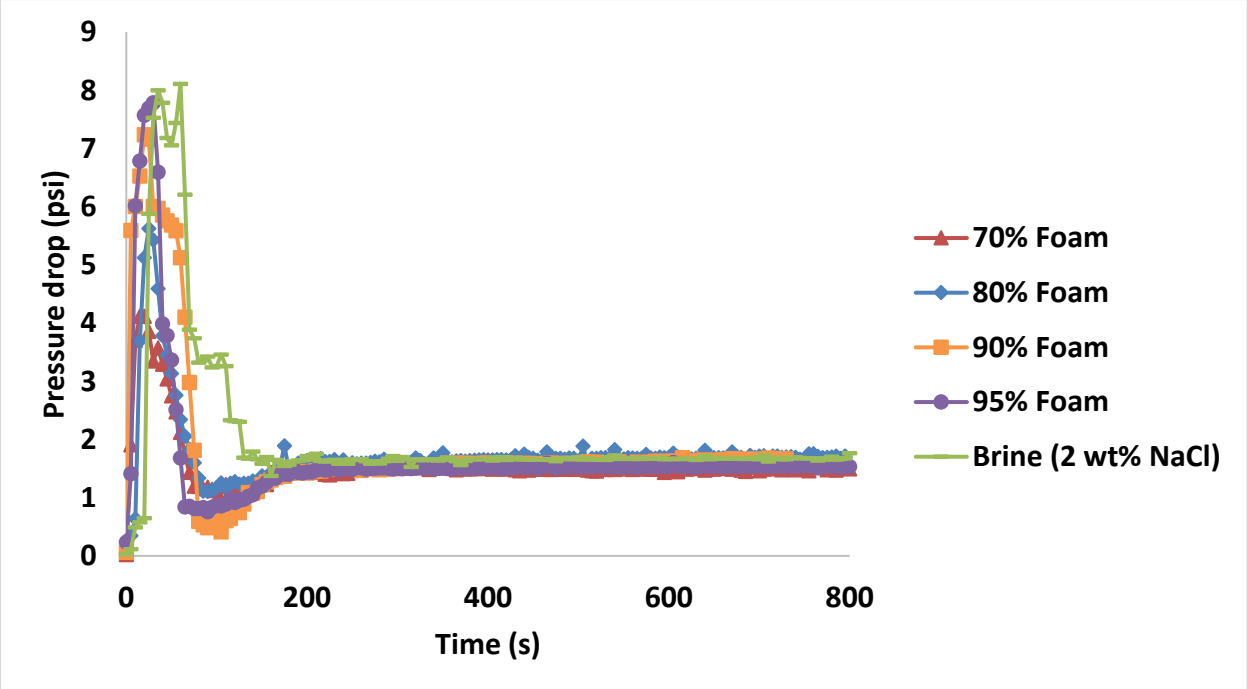

Figure 88. Pressure drop across the sand pack with time for the cleanup of CO_2 foam generated by most optimal ratio of 2AM-PECNP in each of the four different foam qualities during oil flood

From Figure 84 to Figure 88, it can observed that pressure drop for the cleanup of brine is slightly higher than CO_2 foam, which means it's easier for the cleanup of CO_2 foam compared to brine.

Aqueous Phase Recovery after Oil Flood

The effluent of oil flood was collected in a burette and volume of aqueous phase recovered was measured. Maximum volume (V_{max}) of aqueous phase after the foam flood in the sand pack can be calculated using Equation 18, given below,

Equation 18

$$V_{max}\,(ml) = (1- (\text{Foam Quality } (\%)/100))* V_p$$

Surfactant recovery can be calculated using Equation 19 given below,

Equation 19

$$\text{Surfactant Recovery } (\%) = (V/ V_{max})*100$$

where,

V : Volume of aqueous phase (surfactant or surfactant-PECNP solution) collected in burette after the oil flood (ml)

From Figure 89, it is observed that aqueous phase recovery after oil flood for CO_2 foam generated by most optimal surfactant-PECNP ratio is greater than foam generated just by surfactant. This means that flow back of CO_2 foam generated by the most optimal surfactant-PECNP ratio is better than foam generated only by surfactant.

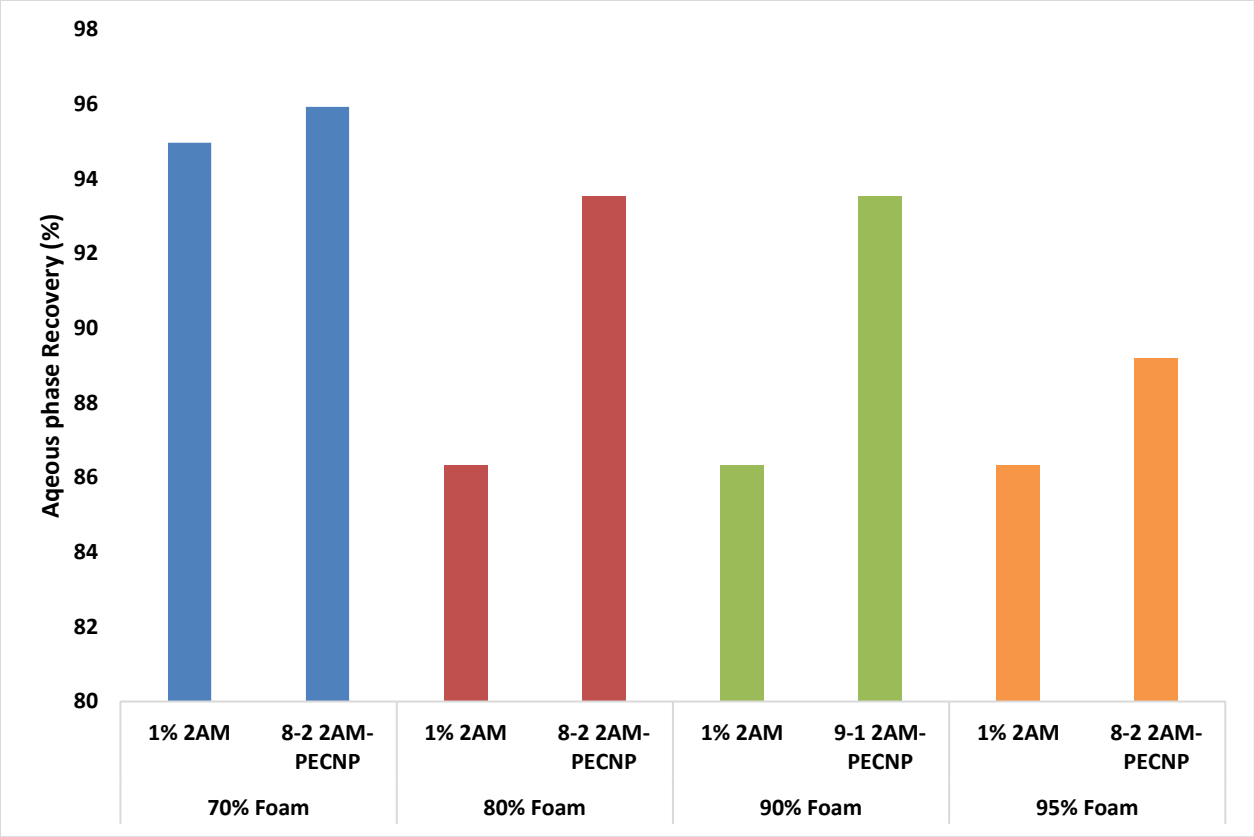

Figure 89. Comparison of aqueous phase recovery (%) after the oil flood between cleanups of CO_2 foam generated by surfactant and most optimal surfactant-PECNP system at all the four different foam qualities

4.6.3 Brine flood after oil flood

After the oil flood, brine flood was performed to recover the oil in the sand pack. Recovered oil was collected in the burette and was used to calculat oil recovery (%) using the equation below,

Equation 20,

Oil recovery (%) = (V_{oc} / V_p) *100

Where,

$V_{oc:}$ Oil collected after brine flood

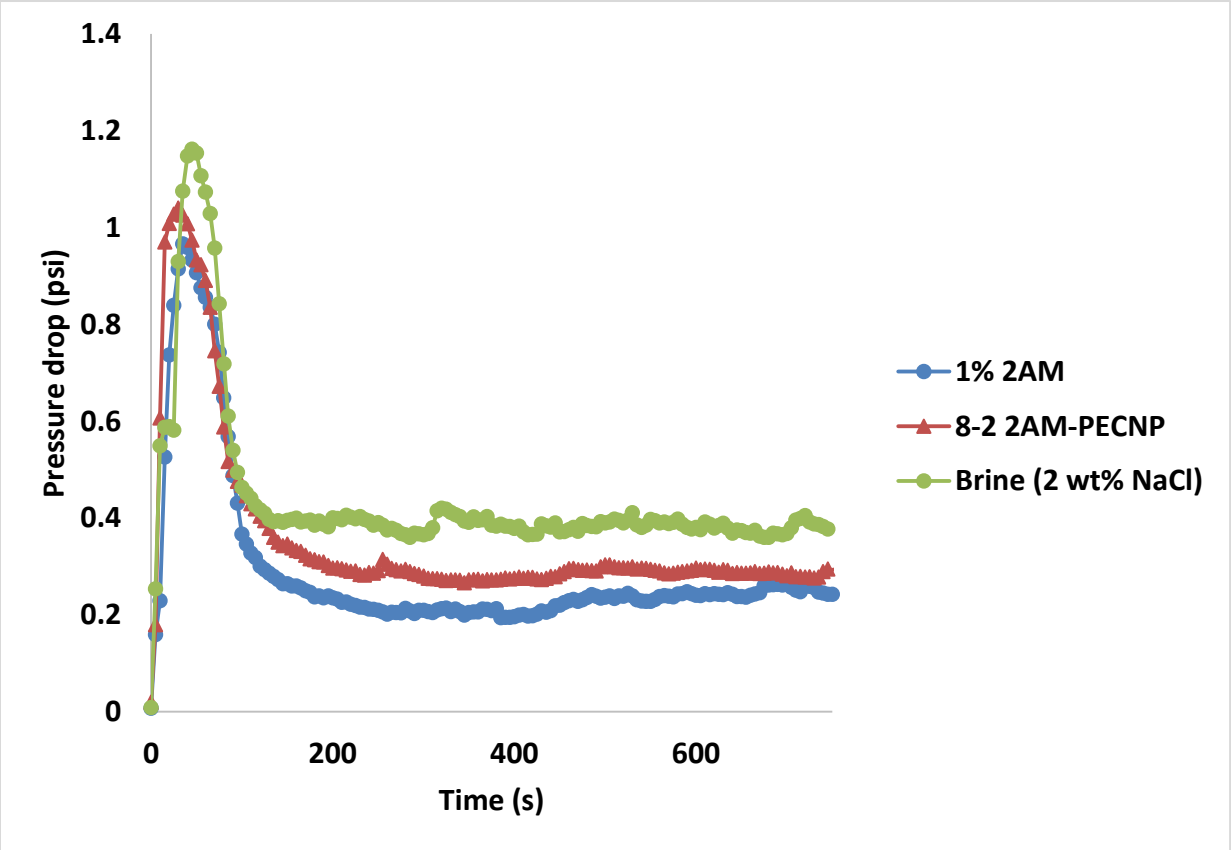

Figure 90. Pressure drop across the sand pack with time in brine flood after oil flood in the cleanup experiment of CO_2 foam generated by surfactant and most optimal ratio of 2AM-PECNP with foam quality of 70 % during oil flood

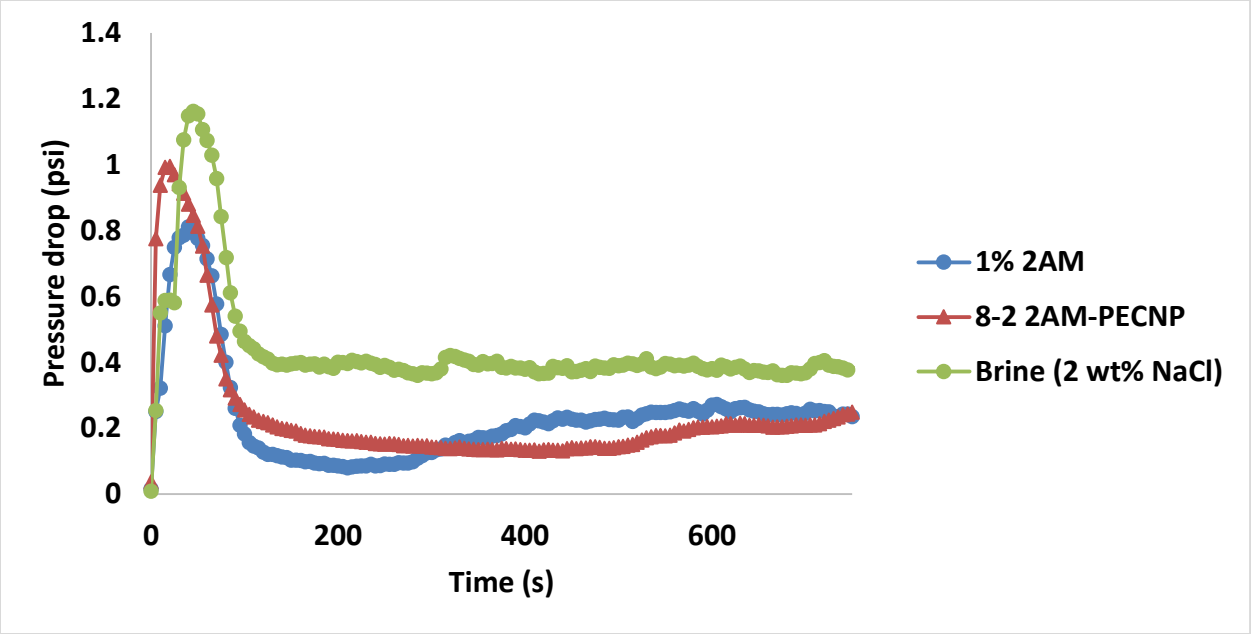

Figure 91. Pressure drop across the sand pack with time in brine flood after oil flood in the cleanup experiment of CO_2 foam generated by surfactant and most optimal ratio of 2AM-PECNP with foam quality of 80 % during oil flood

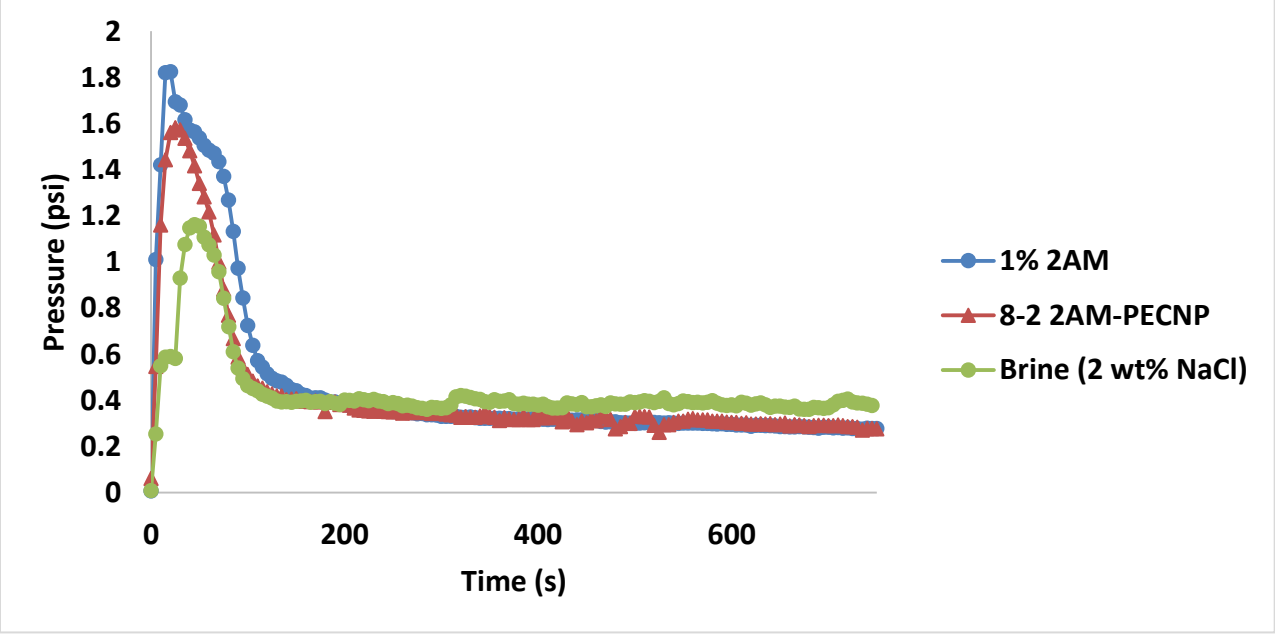

Figure 92. Pressure drop across the sand pack with time in brine flood after oil flood in the cleanup experiment of CO_2 foam generated by surfactant and most optimal ratio of 2AM-PECNP with foam quality of 90 % during oil flood

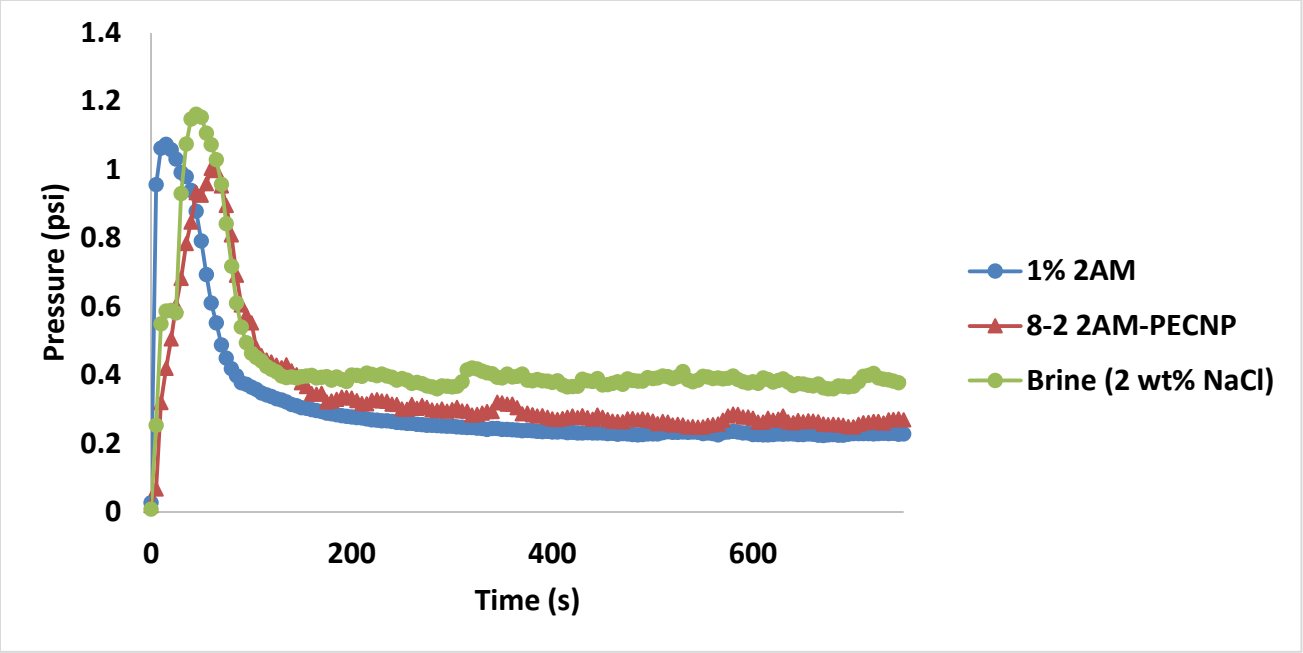

Figure 93. Pressure drop across the sand pack with time in brine flood after oil flood in the cleanup experiment of CO_2 foam generated by surfactant and most optimal ratio of 2AM-PECNP with foam quality of 95 % during oil flood

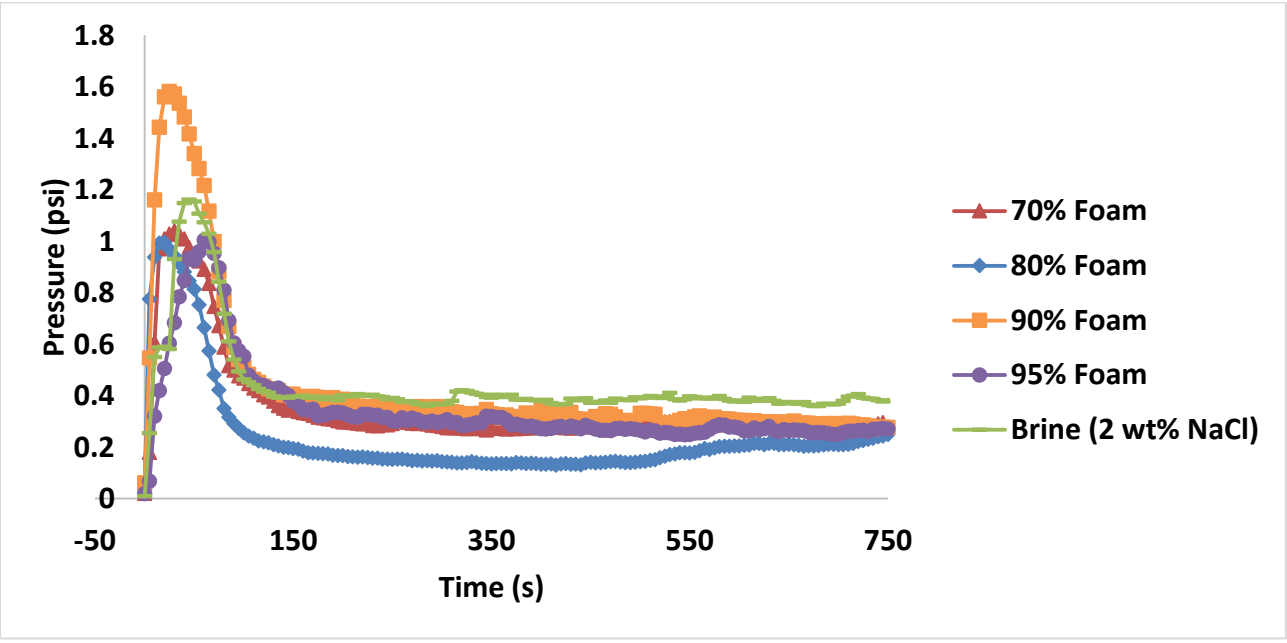

Figure 94. Pressure drop across the sand pack with time in brine flood after oil flood in the cleanup experiment of CO_2 foam generated by most optimal ratio of 2AM-PECNP in each of the four different foam qualities during oil flood

Chapter 5. Conclusions

PECNP formulation was optimized for colloidal stability on the basis of minimizing size and zeta potential. Addition of PECNP to the surfactant solution for generating a more stable supercritical CO_2 foam and effect of foam quality on its rheological properties, stability and durability was investigated. Dynamic fluid loss and post fracture clean up efficiency of $scCO_2$ foam stabilized by addition of PECNP as fracturing fluid was investigated.

1. **Particle size and zeta potential tests:** Different ratios of PEI: DS: 2% NaCl at a range of pH were tested. PECNP formulation of 3: 1: 0.1 of PEI: DS: 2% NaCl with PEI pH of 8.5 proved to be the most favorable ratio based on the particle size and zeta potential test. Addition of PECNP to surfactant solution increased the zeta potential and made the system more stable. Various ratios of surfactant-PECNP were tested to find the most favorable ratio. 2AM: PECNP ratios of 9:1, 8:2, 7:3 and 6:4 were found to be optimized ratios due to higher value of zeta potential. These tests showed that adding PECNP to surfactant solution stabilized the foam lamellae and improved the zeta potential. Aqueous phases used to generate foam in the rheology and view cell tests were prepared with above PECNP formulations and surfactant-PECNP ratios.
2. **Rheometer tests:** The influence of foam quality and effect of PECNP on bulk rheology of $scCO_2$ was observed. Viscosity of foam at constant shear rate of 2000 s^{-1} and flow consistency index values were analyzed to study the effect of PECNP and foam quality on foam rheology. It was observed that adding PECNP to surfactant solution significantly improved the viscosity and flow consistency index of CO_2 foam and increasing the foam quality resulted in better rheological performance of $scCO_2$ foam.

3. **View cell tests:** The influence of foam quality and effect of PECNP on foam durability and stability was studied in this test. In addition, effect of crude oil on foam durability and stability was studied in view cell tests with oil. The test results indicated that adding PECNP to surfactant significantly improved foam stability and durability compared to the foam systems generated using surfactant alone. Moreover, increasing the foam quality improved foam stability and durability. View cell test with oil indicated that presence of oil destabilized the foam lamellae, resulting in rupture of the film and quicker decay of foam compared to foam decay without crude oil. This behavior of foam will improve the post fracture clean-up.
4. **Interfacial Tension Measurements:** Influence of salinity, addition of PECNP to surfactant solution on interfacial tension between air-aqueous phase and $scCO_2$-aqueous phase was studied. The interfacial tension results were similar in both air-aqueous phase and $scCO_2$-aqueous phase systems. Increase in salinity increased the IFT. Addition of surfactant to brine solution significantly reduced the IFT, but the IFT was further reduced with addition of PECNP.
5. **Optimized surfactant-PECNP systems:** Rheometer and view cell tests were not only used to study the rheological properties, stability and durability of $scCO_2$ foam, but was also used as screening tests to find the most optimal surfactant-PENCP system. Based on analyzes of their results, 2AM-PECNP ratio of 8:2 proved to be the most optimal ratio in all the four foam qualities. This surfactant-PENCP ratio was used to prepare the aqueous phase for $scCO_2$ foam tested in dynamic fluid loss and post fracture clean up tests.
6. **Dynamic fluid loss tests:** Addition of optimized PECNP formulation to surfactant solution decreased the fluid loss in all the four foam quality, this resulted to lower fluid loss

coefficient for foam generated using surfactant-PECNP solution than foam generated using only surfactant solution.

7. **Sand Pack tests:** Sand pack tests were performed to study the post fracture clean-up of $scCO_2$ foam and influence of addition of PECNP to surfactant solution. Clean-up of foam was compared with brine (2% NaCl). Based on the pressure drop across the sand pack during the clean-up experiment and volume of aqueous phase collected after injection of crude oil, $scCO_2$ foam as fracturing fluid showed better clean up compared to brine. Moreover, the clean-up further improved by adding optimized PECNP formulation to surfactant solution.

References

Ahmed, U. a. (2016). *Unconventional Oil and Gas Resources: Exploitation and Development.* Taylor Francis Group, Baker Hughes, https://www.crcpress.com/Unconventional-Oil-and-Gas-Resources-Exploitation-and-Development/Ahmed-Meehan/p/book/9781498759403.

Al-Adwani, F. A. (2008). Modeling of an Underbalanced Drilling Operation Utilizing Supercritical Carbon Dioxide. *SPE/IADC Managed Pressure Drilling and Underbalanced Operations Conference and Exhibition.* Abu Dhabi, UAE.

Al-Dhamen, M. S. (2015). *Increased Well Productivity from the Use of Carbon Dioxide to Foam Fracturing Fluids During a Refracturing Treatment in Saudi Arabia.* SPE Latin American and Caribbean Petroleum Engineering Conference, Quito, Ecuador, 18-20 November. SPE-177112-MS: Society of Petroleum Engineers.

Amstrong, K. R. (1996). *Advanced Fracturing Fluid Improve Well Economics.* Oil Field Review.

Anandan, R. J. (2017). Polyelectrolyte Complex Stabilized CO2 Foam Systems for Hydraulic Fracturing Application . *SPE Liquids-Rich Basins Conference- North America held in Midland, TX, USA, 13-14 September 2017.* SPE.

Ansarizadeh, M. D. (2015). *Carbon Dioxide- Challenges and Opportunities.* Oilfield Review.

Antoci, J. C. (2001). Crosslinked Methanol: Analysis of a Successful Experience in Fracturing Gas Wells. *SPE Latin American and Caribbean Petroleum Engineering Conference.* Buenos Aires, Argentina.

Ayoub, J. R. (2006). New Findings in Fracture Cleanup Change Industry Perceptions. *SPE International Symposium and Exhibition on Formation damage Control,.* Lafayette, LA.

Barati. (2010). *Fracturing Fluid Cleanp by Controlled Release of Enzymes from Polyelectrolyte Complex nanoparticles.* University of Kansas, Lawrence,.

Barati, R. H. (2009). Fracture Impact of Yield Stress and Fracture-Face Damage on Production with a Three Phase 2D Model. *SPE Production and Operations Journal, 24(2): 336-345*.

Barati., R. a. (2014). A Review of the Polymeric Fracturing Fluid Systems Used for Hydraulic Fracturing of Oil and Gas Wells. *Journal of Applied Polymer Science*.

Bell, C. E. (1993). Effective diverting in horizontal wells in the Austin Chalk. *Society of Petroleum Engineers conference paper. Archived 5 October 2013 at the Wayback Machine.*

Benson, S. M. (2010). *Carbon Capture and Sequestration (CCS) 101.* Stanford, California.

Bently, C. (2012). *Deformed carbonatite dikes in Cambrian slate, Yoho National Park, British Columbia.* http://blogs.agu.org/mountainbeltway/2012/07/31/deformed-carbonatite-dikes-in-cambrian-slate-yoho-national-park-british-columbia/.

Blauch, M. M. (2009). Marcellus Shale post frac flowback waters- where is all the salt coming from and what are the implication ? *SPE Regional Meeting.* Charleston.

Blauer, R. E. (1974). Formation Fracturing with Foam. *Fall Meeting of the Society of Petroleum Engineers of AIME, 6-9 October, Houston, Texas. https://doi.org/10.2118/5003-MS.* SPE.

Bose, C. C. (2014). *Dual Application of Polyelectrolyte Complex Nanoparticles as Enzyme Breaker Carriers and Fluid Loss Additives for Fracturing Fluids.* Society of Petroleum Engineers. doi:10.2118/171571-MS.

Burke, L. a. (2011). Improved Hydraulic Fracture Performance with Energized Fluids: A Montney Example. *Recovery-2011 CSPG CSEG CWLS Convention.*

Cawiezel, K. a. (1987). Rheological Properties of Foam Fracturing Fluids Under Downhole Conditions. *SPE Production Operations Symposium, 8-10 March, Oklahoma City, Oklahoma.* SPE.

Chancellor, R. (1977). *Mesaverde hydraulic fracture stimulation, northern Piceance Basin – progress report,*. Exploration Frontiers of the Central and Southern Rockies (Denver: Rocky Mountain Association of Geologists, 1977) 285–291.

Charlez, P. A. (1997). *Rock Mechanics: Petroleum Applications.* Paris: Editions Technip. p. 239. ISBN 9782710805861. Retrieved 2012-05-14.

Dawson, K. M. (2013). *Evaluating Characteristics of Source, Flowback and Produced Water for Effective Treatment.* http://assets.cmp.bh.mxmcloud.com/system/96599d804d94403e9215de5516d322ef/pdfs/pdf/SPWM-Nov-Dec-BakerHughes.pdf.

Detlef, M. (1989). *Hydraulic Proppant Fracturing and Gravel Packing.* Elsevier. pp. 173–174; 202. ISBN 9780444873521.

Dispersion Process. (2005). Retrieved from http://www.inkline.gr/inkjet/newtech/tech/dispersion/

Economides, M. a. (2000). *Reservoir Stimulation, third edition.* Wiley, New York and Chichester.

Eftekhari, A. A. (2015). Foam stabilized by Fly-Ash nanoparticles for Enhanced Oil Recovery. *SPE Kuwait oil and gas show and conference, Kuwait.*

Enick, R. M. (2012). *Mobility and Conformance Control for Carbon Dioxide Enhanced Oil Recovery (CO2-EOR) via Thickners, Foams, and Gels- A Detailed Literature Review of 40 years of Research.* U.S. Department of Energy.

Enzien, M. Y. (2011). Improved Microbian Control Programs for Hydraulic Fracturing Fluids used during Unconventional Shale Gas Exploration and Production. *SPE International Syposium on Oilfield Chemistry.* The Woodlands, Texas.

EPA. (2011). *Draft Plan to Study the Potential Impacts of Hydraulic Fracturing on Drinking Water Resources.* https://yosemite.epa.gov/sab/sabproduct.nsf/0/D3483AB445AE61418525775900603E79/$File/Draft+Plan+to+Study+the+Potential+Impacts+of+Hydraulic+Fracturing+on+Drinking+Water+Resources-February+2011.pdf.

Esmaili, S. K. (2012). Forecasting, Sensitivity and Economic Analysis of Hydrocarbon Production from Shale Plays Using Artificial Intelligence & Data Mining. *SPE Canadian Unconventional Resources Conference, 30 October-1 November, Calgary, Alberta, Canada.* SPE.

Fast, C. R., & Holman G, B. a. (1977). *"The application of massive hydraulic fracturing to the tight Muddy 'J' Formation, Wattenberg Field, Colorado.* Exploration Frontiers of the Central and Southern Rockies (Denver: Rocky Mountain Association of Geologists, 1977) 293–300.

Fix, J. E., & Frantz Jr, J. L. (1991). Application of Microseismic Technology in a Devonian Shale Well in the Appalachian Basin. *SPE Eastern Regional Meeting.* Lexington, KY.

Fontaine, J. J. (2008). Design, Exceution and Evaluation of a typical Marcellus Shale Slickwater Stimulation: A Case History. *SPE Eastern Regional joint meeting.* Pittsburgh, PA.

Friehauf, K. a. (2009). Fluid Selection for Energized Hydraulic Fractures. *SPE Annual Technical Conference and Exhibition, 4-7 October, New Orleans, Louisiana. SPE-124361-MS. https://doi.org/10.2118/124361-MS.*

Friehauf, K. E. (2009). Application of a New Compositional Model for Hydraulic Fracturing With Energized Fluids: A South Texas Case Study. *SPE Hydraulic Fracturing Technology Conference, 19-21 January, The Woodlands, Texas.* SPE.

Gandossi, L. a. (2013). *An overview of hydraulic fracturing and other formation stimulation technologies for shale gas production.* EUR 26347: Joint Research Centre Science Hub, European Commision.

Gao, Y. (2014). *Fundamental Studies of Refined Polyelectrolyte/Surfactant Nanoparticles-Bulk and Interfacial properties.* niversity of Kansas, Lawrence.

Gdanski, R. D. (2010). Returns Matching Reveals New Tools for Reservoir Evaluation. *SPE Tight Gas Completioins Conference.* San Antonio, Texas.

Gennes, D. a. (1979). *Scaling Concepts in Polymer Physics.* Cornell University Press. ISBN 0-8014-1203-X.

Gill, R. (2010). *Igneous rocks and processes: a practical guide.* John Wiley and Sons. p. 102. ISBN 978-1-4443-3065-6. Retrieved 5 November 2011.

Grundmann, S. R. (1983). Foam Stimulation . *Journal of Petroleum Technology SPE-9754-PA.*

Gupta, A. P. (2005). Feasibility of Supercritical Carbon Dioxide as a Drilling Fluid for Deep Underbalanced Drilling Operation. *SPE Annual Technical Conference and Exhibition. Dallas, Texas, Society of Petroleum Engineers.*

Harris, P. C. (1988). Fracturing-Fluid Additives. *Journal of Petroleum Technology, vol. SPE Distinguished Author Series,.*

Hayakawa, K. a. (1982). *Journal of Physical Chemistry, pp. 86(19): p. 3866-3870..*

He, K. Y. (2015). Minimizing Surfactant Adsorption Using Polyelectrolyte Based Sacrificial Agent: a Way to Optimize Surfactant Performance in Unconventional Formations . *SPE*

International Symposium on Oilfield Chemistry, 13-15 April, The Woodlands, Texas, USA. SPE-173750-MS. https://doi.org/10.2118/173750-MS.

Hoeman, K. K. (2011). Method for Identification and Analysis of Polysaccharide based Hydraluic fracture Flowback Fluids. *SPE International Symposium on OIlfield Chemistry.* Woodlands, TX.

Houston, N. B. (2009). Fracture Stimulation in the Marcellus Shale-Lessons Learned in Fluid Selection and Excecution. *SPE Regional Meeting.* Charleston.

Howard, G. C. (1957). *Optimum Fluid Characteristics for Fracturing Extension.* Drilling and Production Practice.

Hughes, B., & Malone, S. a. (2015). *Explore a Fracturing Operation- Virtually.* https://www.fractracker.org/resources/oil-and-gas-101/explore/.

Hunter, R. (1988). *Zeta Potential in Colloid Science: Principles and Application.* San Diego, California.: ACADEMIC PRESS INC.

Hunter, R. (1988). *Zeta Potential in Colloid Science: Principles and Application.* San Diego, California.: ACADEMIC PRESS INC.

Israelachvili, J. (1991). *Intermolecular and Surface Forces, Second Edition: With Applications to Colloidal and Biological Systems (Colloid Science). 2nd ed,.* London: Academic Press: London Second ed.,.

Jenkins, A. D., Kratochvíl, P., Stepto, R. F., & Suter, U. W. (1996). *"Glossary of basic terms in polymer science (IUPAC Recommendations 1996)".* Pure and Applied Chemistry. 68 (12). doi:10.1351/pac199668122287.

Jenkins, C. a. (2008). Coalbed and Shale Gas Reservoirs. *SPE JPT.*

Kalyanaraman, N. A. (2015). Stability Improvement of CO2 Foam for Enhanced Oil Recovery Applications Using Polyelectrolytes and Polyelectrolyte Complex Nanoparticle. *Presented at SPE Asia Pacific Enhanced oil Recovery Conference, Kuala Lumpur, Malaysia, 11-13 August 2015*, SPE-174650-MS.

Kalyani, R. (2013). *"Awakening the Slumbering Giant: How Horizontal Drilling Technology Brought the Endangered Species Act to Bear on Hydraulic Fracturin.* Case Western Reserve Law Review. 63 (4). Archived from the original (PDF) on 2014-03-26. Retrieved 2016-09-18.

King, G. E. (2012). Hydraulic Fracturing 101: What every representative, environmentalist, regulator, reporter, investor, university researcher, neighbor and engineer should know about estimating frac risk and improving frac performance in unconventional gas and oil wells. *SPE Hydraulic fracturing technolohyu conference* . Woodland, Texas, USA: SPE.

Klitzing, R. E. (1997). Forces in foam films containing polyelectrolyte and surfactant. *Science Direct. https://doi.org/10.1016/S0927-7757(98)00307-0*.

Koetz, J. a. (2006). *Polyelectrolytes and Nanoparticles,.* Springer Laboratory Manuals in Polymer Science.

Koetz, J. S. (2001). Self assembled polyelectrolyte systems. *Elseiver, Progress in Polymer Science pp. 1199-1232, .*

Kohshour, I. O. (2016). *Examination of Water Management Challenges and Solutions in Resource Development- Could Waterless Fracturing Techologies Work? .* Unconventional Resources Technology Conference held in San Antonio, Texas, USA, 1-3 August 2016. URTeC: 2461040.

Kristen, N. a. (2010). Effect of polyelectrolyte/surfactant combinations on the stability. *Soft Matter, Royal Society of Chemistry DOI: 10.1039/b917297a*.

Lapitsky, Y., & Kaler, M. P. (2007). *Journal of Physical Chemistry pp. 111(29), p. 8379-8387*.

Laubach, S. E., Reed, R. M., Olson, J. E., Lander, R. H., & Bonnell, L. M. (2004). "Coevolution of crack-seal texture and fracture porosity in sedimentary rocks: cathodoluminescence observations of regional fractures. *Journal of Structural Geology. Elsevier. 26 (5): 967–982. Bibcode:2004JSG....26..967L. doi:10.1016/j.jsg.2003.08.019. Retrieved 5 November 2011*.

Law, B. a. (1993). *Gas in tight reservoirs-an emerging major source of energy.* The Future of Energy Gasses, US Geological Survey, Professional Paper 1570, p.233-252.

Li, D. (2013). *Towards rational design of polyelectrolyte-surfactant complexes: Thermodynamics, Microstructure and property.* University of Delaware.

Linde. (2013). *Benefits of Energized Solutions in Fracturing.* Murray Hill, New Jersey: Linde North America, Inc.

Lipid. (2012). *"Bubbles, Bubbles, Everywhere, But Not a Drop to Drink".* The Lipid Chronicles. Retrieved 1 August 2012.

Makhanov, K. D. (2012). An Experimental Study of Spontaneous Imbibition in Horn River Shales. *SPE Canadian Unconventional Resources Conference, 30 October-1 November, Calgary, Alberta, Canada.* SPE.

Manning, G. S. (1979). *Counterion Binding in Polyelectrolyte Theory.* Rutgers University, NJ, USA.

Manthei, G., Eisenblätter, J., & Kamlot, P. (2003). *Stress measurement in salt mines using a special hydraulic fracturing borehole tool.* In Natau, Fecker & Pimentel. Geotechnical

Measurements and Modelling (PDF). pp. 355–360. ISBN 90-5809-603-3. Retrieved 6 March 2012.

McGowen, J. a. (1996). In Fracturing-Fluid Leakoff under Dynamic Conditions, Part1: Development of a Realistic Laboratory Testing Procedure. *SPE ATC.* Denver, U.S.A.

Moayedi, H. A. (2011). Zeta potential of Organic soil in Presence of Calcium Chloride, Cement and Polyvinyl Alcohol. *International Journal of ELECTROCHEMICAL SCIENCE; http://www.electrochemsci.org/papers/vol6/6104493.pdf*.

Montgomery, C. (2013). *Fracturing Fluids.* Free Article.

Montgomery, C. T. (2010). Hydraulic fracturing. History of an enduring technology. *Online. Society of Petroleum Engineers: 26–41. Archived from the original (PDF) on 2011-09-27. Retrieved 13 May 2012.*

Narsimhan, G. a. (1986). *Hydrodynamics, enrichment, and collapse in foams.*

Navarette, R. C. (1996). Dynamic Fluid Loss in Hydraulic Fracturing under Realistic Shear Conditions in High-Permeability Rocks. *SPE Production and Facilities.*

Navarette, R., & Cawiezel, K. E. (1996). *Dynamic Fluid Loss in Hydraulic Fracturing under Realistic Shear Conditions in High-Permeability Rocks.* SPE Production and Facilities.

Nazari, N. T. (2017). CO2 Foam Stability Improvement Using Polyelectrolyte Complex Nanoparticles Prepared in Produced Water. *Energies- Special Issue of Nanotechnology for Oil and Gas Application. http://www.mdpi.com/1996-1073/10/4/516.*

Neill, G. H. (1964). *Field and Laboratory Results of Carbon Dioxide and Nitrogen in Well Stimulation.*

Nguyen, P. F. (2014). Nanoparticle Stabilized CO2 in Water Foam for Mobility Control in Enhanced Oil Recovery via Microfluidic Method. . *SPE Heavy Oil Conference-Canada, 10-12 June, Calgary, Alberta, Canada. SPE-170167-MS.* SPE.

Novosad, J. a. (1990). *Micro-visualization of foam interactions with a crude oil.* Colloids and Surfaces, no. 46, pp. 21-43,.

Parekh, B. a. (2004). Cleanup of Water Blocks in Depleted Low-Permeability Reservoirs. *SPE Annual Technical Conference and Exhibition.* Houston, Texas.

Penny, G. D. (2006). Field Study of Completion Fluids to Enhance Gas Production in the Barnett Shale. *SPE Gas Technology Symposium, 15-17 May, Calgary, Alberta, Canada.* SPE.

Perry, R. G. (1997). *Perry's Chemical Engineering Handbook.* Table 2-167. Seventh Edition. Mcgraw Hill. ISBN 0-07-049841-5.

Petkova, R. S. (2012). "Foaming and foam stability for mixed polymer-surfactant solutions: effects of surfactant type and polymer charge,". *Langmuir, ACS Publications, pp. 4996-5009.*

Products, A. (2013). *Enhanced Unconventional Oil and Gas Production with Nitrogen Fracturing.* Air Products.

Roodhart, L. P. (1985). Fracturing Fluids: Fluid-Loss Measurement under Dynamic Conditions. *Society of Petroleum Engineers Journal*.

Rosen, M. &. (2012). *Surfactants and Interfacial Phenomena.* (4th ed.). Hoboken, New Jersey: John Wiley & Sons. p. 1. ISBN 1-118-22902-9.

Rossen W. R., R. K. (1996). *Chapter 11: Foams in Enhanced Oil Recovery," in Foams: Theory, Measurements and Applications, New York, Marcel Dekker Inc,, pp. 413-465.*

Samuel, M. C. (1999). *Polymer free fluid for fracturing Application. Paper SPE 59478.* Drilling and Completion Journal.

Schramm, L. L. (1994). *FOAMS, Fundamentals and Applications in the Petroleum Industry.* Washington D.C:: Advances in Chemistry Series.

Schramm, L. L. (2000). *Foams: Fundamentals and Applications in the Petroleum Industry.* Cambridge, United Kingdom: Cambridge University Press.

Sharma, M. a. (2013, September 26, 2013). Impact of Liquid Loading in Hydraulic Fractures on Well Productivity. Society of Petroleum Engineers. *SPE Hydraulic Fracturing Technology Conference, 4-6 February, The Woodlands, Texas, USA. SPE-163837-MS.* SPE.

Sven, H. (2000). *heoretical and experimental investigations of the high-pressure phase equilibrium behavior of fluid mixtures for the expansion of the PSRK group contribution equation of state.* Carl-von-Ossietzky Universität Oldenburg. ISBN 3-8265-7829-5.

Talebian, S. H. (2013). Foam assissted CO2- EOR; Concepts, Challenges and Applications. *SPE EOR conference.* Kuala Lumpur, Malaysia.

Taylor R, S., & Lestz, R. S. (2006). Liquid Petroleum Gas Fracturing Fluids for Unconventional Gas Reservoirs. *Canadian International Petroleum Conference.* Calgary, Alberta.

Tiyaboonchai, W. (2003). *Development of a New Nanoparticle Delivery Vehicle Based on an Aqueous Polymer System: Polyethylenimine and Dextran Sulfate.* The University of Kansas, Lawrence.

Vitthal, S. a. (1996). In Fracturing Fluid Leakoff under Dynamic Conditions, Part 2: Effect of Shear Rate, Permeability, and Pressure. *SPE Annual Technical Conference,*. Denver, U.S.A.

Wang, H. G. (2012). A Feasibility Analysis on Shale Gas Exploitation with Supercritical Carbon Dioxide. *Energy Sources, Part A: Recovery, Utilization, and Environmental Effects*.

Waree T, J., & Middaugh, R. C. (2003). Insulin Containing Polyethylenimine-Dextran Sulfate Nanoparticles. *International Journal of Pharmaceutics, pp. 139-151,*.

Warpinski, N. W. (2007). *Development of an Advanced Hydraulic Fracture Mapping System.* Final Report for US Department of Energy.

water, P. (2009). *Produced water treatment facility*. Retrieved from http://www.wateronline.com/solution/produced-water-treatment

Williams, B. G. (1979). *Acidizing Fundamentals.* 55. New York: SPE/AIME. Retrieved from PetroWiki - Society of Petroleum Engineers: http://petrowiki.org/Acid_fracturing

Woodroof, R., & Asadi, M. a. (2003). Monitoring Fracturing Fluid flowback and optimizing fluid cleanup using frac tracers. *SPE European Fomation Damage Conference.* The Hague, Netherlands.

Yost II, A. B. (1993). *CO2/Sand Fracturing in Devonian Shales. SPE Eastern Regional Meeting.* Pittsburgh, Pennsylvania.

Yost, A. (1994). Analysis of Production Response to CO_2/Sand Fracturing: A Case Study. *SPE Eastern Regional Meeting, 8-10 November, Charleston, West Virginia. SPE-29191-MS. https://doi.org/10.2118/29191-MS.*

Yu, J. A. (2012). Foam Mobility Control for Nanoparticle-Stabilized Supercritical CO2 Foam. *SPE Improved Oil Recovery Symposium, 14-18 April, Tulsa, Oklahoma, USA. SPE-153336-MS. https://doi.org/10.2118/153336-MS.*

Yu, J. L. (2012). Generation of Nanoparticle-Stabilized Supercritical CO2 Foams. *Carbon Management Technology Conference, 7-9 February, Orlando, Florida, USA. CMTC-150849-MS. https://doi.org/10.7122/150849-MS.*

Appendix

This section provides graphs of the ramp tests conducted for various foam qualities used to calculate flow consistency index (K) and flow behavior index (n).

Ramp Test

In this test, shear sweep from 2000 s^{-1} to 100 s^{-1} and again back from 100 s^{-1} to 2000 s^{-1} was performed on different foam systems. Using viscosity and shear rate values, a log-log graph was plotted. Using Ostwald-de Waele equation (power law model), K and n was found. Figure 95 to Figure 98 show the log-log plot of viscosity vs shear rate for different surfactant-PECNP systems of 70%, 80%, 90% and 95% foam quality.

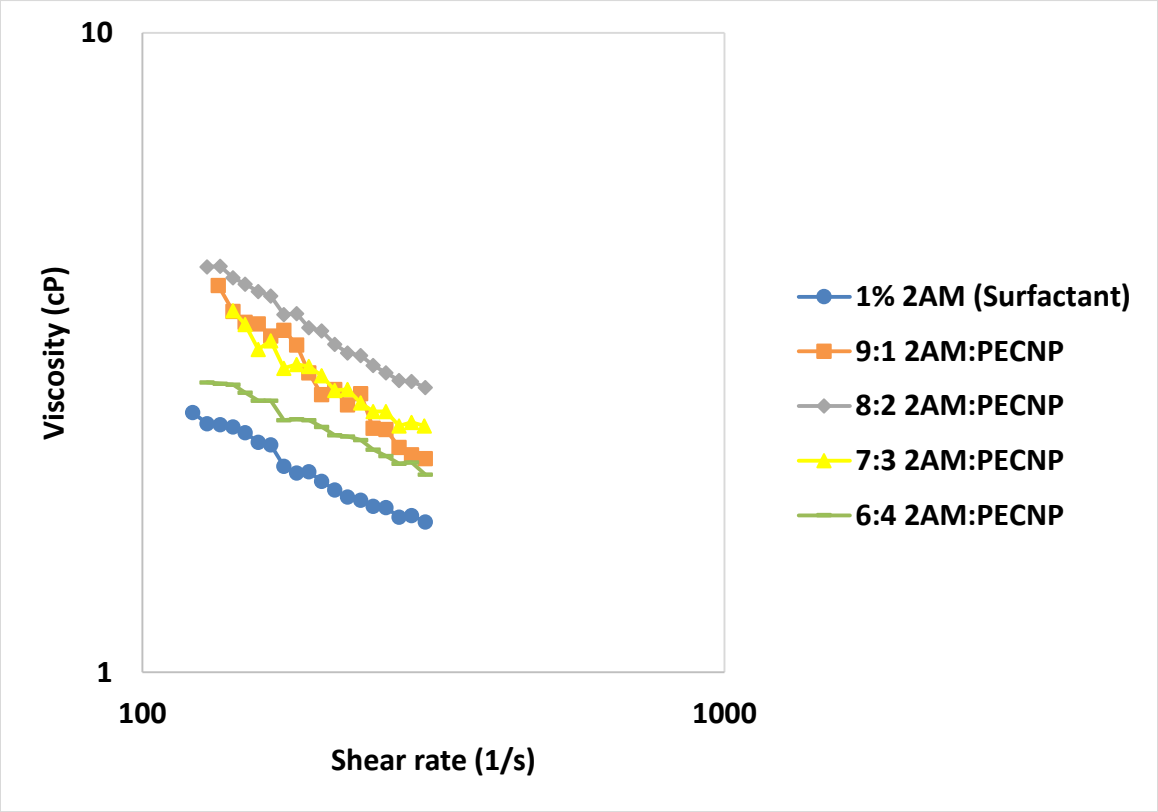

Figure 95. Log-log plot of viscosity vs shear rate for different surfactant-PECNP systems at 70% foam quality

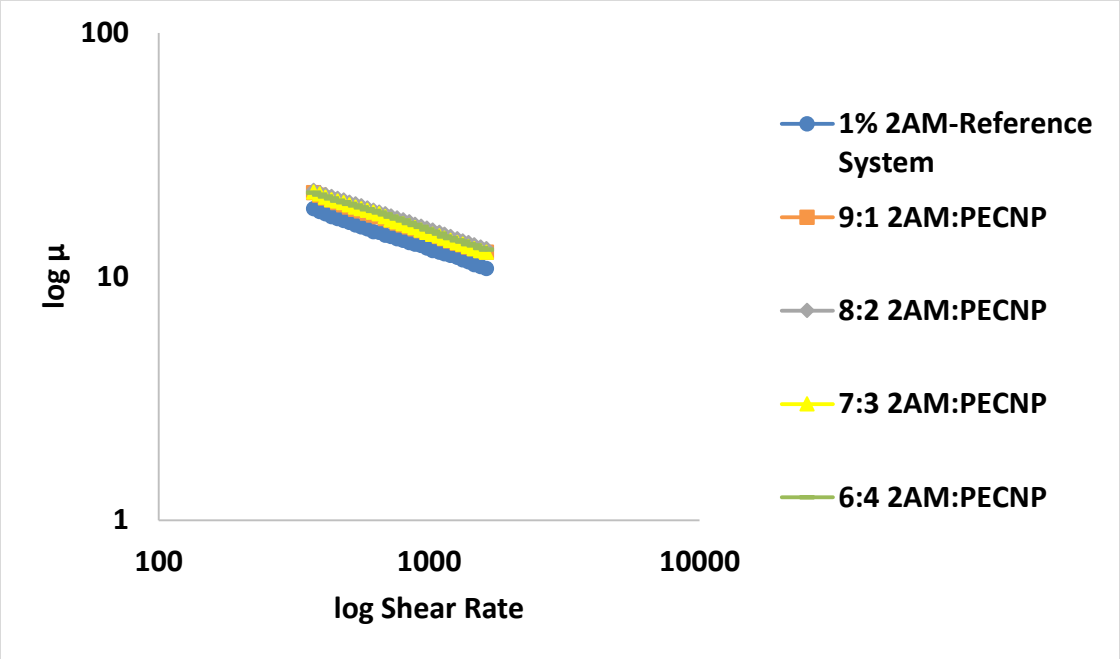

Figure 96. Log-log plot of viscosity vs shear rate for different surfactant-PECNP systems at 80% foam quality

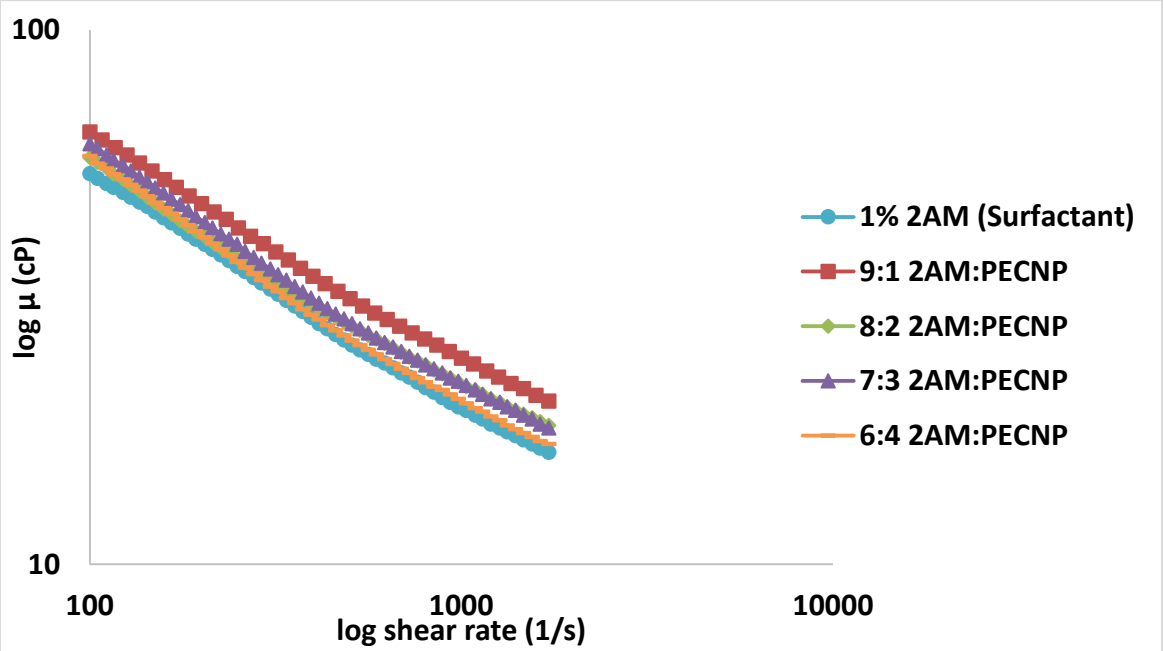

Figure 97. Log-log plot of viscosity vs shear rate for different surfactant-PECNP systems at 90% foam quality

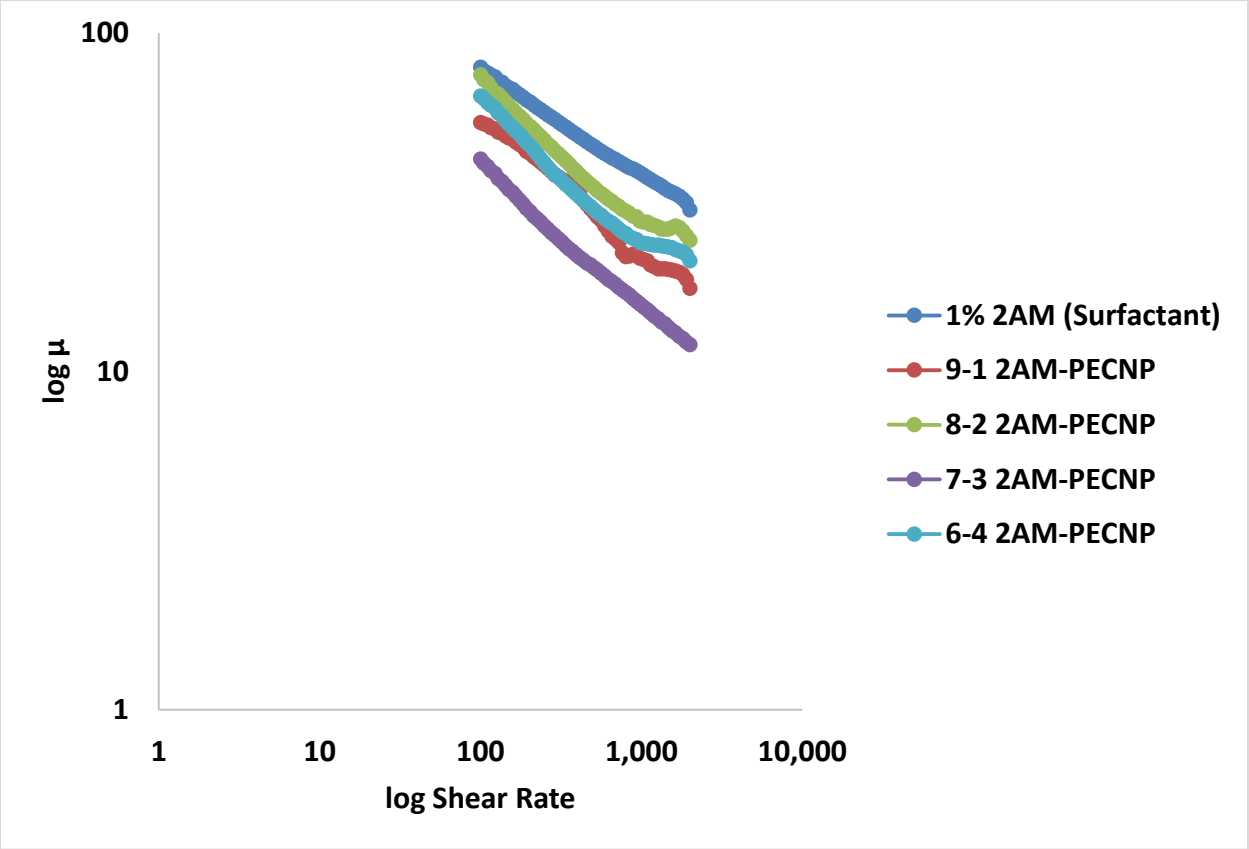

Figure 98. Log-log plot of viscosity vs shear rate for different surfactant-PECNP systems at 95% foam quality